Baryogenesis and gravity waves from a first-order electroweak phase transition

Benoit Laurent

Supervised by James M. Cline

Department of Physics

McGill University, Montréal

April 2021

A thesis submitted to McGill University in partial fulfillment

of the requirements of the degree of Masters of Science

© Benoit Laurent 2021

Contents

List of tables . . . iii

List of figures . . . iv

Acknowledgements . . . v

Contribution of the author . . . vi

Abstract . . . vii

Résumé . . . viii

1 Introduction **1**

1.1 First-order phase transition and bubble nucleation . . . 3

1.1.1 Classification of phase transitions . . . 3

1.1.2 Bubble nucleation . . . 5

1.1.3 Z_2-symmetric singlet scalar extension . . . 7

1.2 Baryon asymmetry . . . 9

1.2.1 Sakharov's conditions . . . 10

1.2.2 B violation in the Standard Model . . . 12

1.2.3 Electroweak baryogenesis . . . 15

2 Fluid equations for fast-moving electroweak bubble walls **19**

2.1 Introduction . . . 19

2.2 Old formalism (OF) . . . 21

2.3 Improved fluid equations (NF) . . . 22

2.4 Solutions for a Standard Model-like plasma . . . 24

2.5 Consequences for wall friction . . . 28

2.6 Conclusion . . . 30

2.A v-dependence of the $C_v^{m,n}$ and $D_v^{m,n}$ functions . . . 31

2.B Evaluation of the collision rates . . . 32

3 Baryogenesis and gravity waves from a UV-completed electroweak phase transition **40**

3.1 Introduction 41

3.2 Z_2-symmetric singlet model 43

3.2.1 Laboratory constraints 45

3.2.2 Explicit breaking of Z_2 symmetry 50

3.3 Phase Transition and Bubble Nucleation 52

3.4 Wall velocity and shape 54

3.4.1 Transport equations for fluid perturbations 57

3.5 Cosmological signatures 59

3.5.1 Gravitational Waves 59

3.5.2 Baryogenesis 62

3.6 Monte Carlo results 63

3.6.1 Deflagration versus detonation solutions 65

3.6.2 Baryogenesis and gravity wave production 68

3.6.3 Dependence on λ_s and Λ 70

3.6.4 Theoretical uncertainties 71

3.6.5 Comparison of the GW signal with previous studies 75

3.7 Conclusion 75

3.A Effective Potential 77

3.B Relativistic fluid equation 80

3.C Gravitational Wave Production 83

4 Conclusions **92**

List of Tables

2.1 Relevant processes for the top quark and W bosons and their corresponding scattering amplitude in the leading log approximation. 34

3.1 Examples of tunneling action S_3/T in various approximations. 53

3.2 Statistics from the scans. 72

List of Figures

1.1 Examples of first and second-order phase transitions. 4

1.2 Instanton solution. 6

1.3 Two-step phase transition. 9

1.4 Summary of the processes involved in EWBG. 18

2.1 Solutions for the perturbations of the W and t fluids and friction term. . . . 25

2.2 Comparison of the friction term in the two formalisms. 29

3.1 Feynman diagrams for decay of the singlet s. 47

3.2 Experimental limits form ATLAS and CMS and lower bounds on Λ. 48

3.3 Constraints on η_1 and η_2, diphoton resonances searches and serches for vector-like quarks. 49

3.4 Moments of the Higgs EOM. 56

3.5 Scan of the parameter space. 65

3.6 Pressure on the wall and velocity and temperature in front of the wall. . . . 66

3.7 Shape and velocity of the deflagration solutions. 67

3.8 GW spectrum. 68

3.9 Relation between the $\mathrm{SNR}_{\mathrm{max}}$ and the baryon asymmetry and the wall velocity. 70

3.10 Error on the wall velocity and width. 74

Acknowledgements

This thesis would not have been possible without the continuous support of many people around me. I would first like to thank my collaborators A. Friedlander, D.-M. He, K. Kainulainen and D. Tucker-Smith for their precious contribution to Chapter 3. I am most grateful to my supervisor, Jim Cline, for his great advice and uninterrupted assistance during my Master's degree. His attention to detail and deep physical insights have greatly enhanced the scientific quality of this work.

Je voudrais également remercier mes amis et ma famille, particulièrement mes parents Marjolaine et Michel, qui m'ont toujours supporté et encouragé inconditionnellement à poursuivre mes études. Finalement, je remercie ma compagne de vie, Viviane, qui ne se fatigue jamais de m'entendre parler de physique, même si elle ne comprend pas toujours tout, et qui est toujours là pour moi.

This work was funded in part by the Fonds de Recherche du Québec - Nature et Technologies (FRQNT) and the Natural Sciences and Engineering Research Council of Canada (NSERC).

Contribution of the author

This thesis is based on original research carried out with collaborators James M. Cline, Avi Friedlander, Dong-Ming He, Kimmo Kainulainen and David Tucker-Smith, and is presented here with their permission.

- I wrote entirely the introductory sections and created all the figures appearing in them, unless explicitly stated.
- Chapter 2 was published as Ref. [1]. I derived the improved fluid equations based on the approach in Refs. [2, 3], I computed entirely the collision integrals for the top and W fluids and I computed the solutions for the top, W and background perturbations. I wrote most of Sections 2.3, 2.4, 2.5, 2.A and 2.B and created all the figures in the article.
- Chapter 3 was published as Ref. [4]. I wrote the code to solve the Boltzmann equation, determine the wall velocity and shape and compute the GW spectrum. I performed the scans of the parameter space, did the analysis of the theoretical uncertainties and obtained all the results presented in Section 3.6. I wrote most of Sections 3.4, 3.5.1, 3.6, 3.A, 3.B and 3.C and created all the figures in these sections.

Abstract

Although the electroweak phase transition is predicted to be a smooth crossover in the Standard Model, it can be made first-order by a simple new physics input. This type of cosmological phase transition is particularly interesting since it provides a mechanism for electroweak baryogenesis, which could explain the origin of the baryon asymmetry of the Universe. Furthermore, first-order phase transitions produce a stochastic background of gravitational waves that future space-based detectors could probe. These two observable quantities depend closely on the shape and terminal velocity of the electroweak bubble wall, which are highly nontrivial to compute. Moreover, the fluid equations previously used in the literature to describe them suffer from unphysical artifacts that make them unreliable for supersonic walls. For these reasons, previous studies usually considered the wall's shape and velocity as free parameters, and fixed them to some arbitrary values.

In this thesis, I study the Z_2-symmetric singlet scalar extension of the Standard Model, making the electroweak phase transition first-order. To accurately predict the baryon asymmetry and gravitational waves spectrum produced by the phase transition, I derive an improved set of fluid equations which is accurate for all wall velocities. I use these to compute the wall's shape and velocity from first principles instead of treating them as free parameters. I then perform a scan of the parameter space to study the properties of this model. I find that a large fraction of the parameter space can yield a baryon asymmetry that agrees with observations. However, only a small fraction can produce detectable gravitational waves. Contrary to the standard lore, I find that these two quantities are positively correlated; however, no models were found with both successful baryogenesis and detectable gravitational waves.

Résumé

Bien que la transition de phase électrofaible soit prédite comme étant continue dans le Modèle Standard, elle peut devenir de premier ordre avec de simples additions de nouvelles physiques. Ce type de transition de phase cosmologique est particulièrement intéressant puisqu'il fournit un mécanisme pour la baryogénèse électrofaible, qui pourrait expliquer l'origine de l'asymétrie baryonique de l'Univers. De plus, les transitions de phase de premier ordre produisent un fond stochastique d'ondes gravitationnelles qui pourrait être exploré par de futurs détecteurs spatiaux. Ces deux quantités observables dépendent sensiblement sur la forme et la vitesse terminale du mur de la bulle électrofaible, qui sont hautement non triviales à calculer. De plus, les équations du fluide auparavant utilisées pour les décrire ne sont pas valables pour les murs supersoniques. Pour ces raisons, les précédentes études se contentaient généralement de traiter la forme et la vitesse du mur comme des paramètres libres, et leur donnaient des valeurs arbitraires.

Dans ce mémoire, j'étudie une extension du Modèle Standard avec un nouveau champ scalaire singlet symétrique sous Z_2, qui rend la transition de phase électrofaible de premier ordre. Pour prédire de manière fiable l'asymétrie baryonique et le spectre d'ondes gravitationnelles produits par la transition de phase, je dérive des équations du fluide améliorées qui sont valables pour toutes les vitesses du mur. J'utilise ces équations pour calculer la forme et la vitesse terminale du mur à partir de principes fondamentaux, plutôt que de les traiter comme des paramètres libres. Ensuite, je fais un scan de l'espace des paramètres pour étudier les propriétés de ce modèle. Je trouve qu'une grande fraction de l'espace des paramètres permet d'obtenir une asymétrie baryonique en accord avec la valeur observée. Par contre, seulement une petite fraction peut produire des ondes gravitationnelles détectables. Contrairement à ce qui était cru auparavant, mes résultats montrent que ces deux quantités sont corrélées positivement; par contre, aucun modèle avec à la fois une baryogénèse réussie et des ondes gravitationnelles détectables n'a été trouvé.

Chapter 1

Introduction

Symmetries offer a deep insight into the fundamental physical laws that govern the Universe. Many physical phenomena, as incomprehensible as they first may seem, can be beautifully and elegantly explained by the various symmetries of the world. As much as they have been a powerful predictive tool in theoretical physics, they can sometimes be a double-edged sword. A completely symmetric Universe would be too restrictive to allow for all the complexity observed in nature. The mere fact that we exist points to the existence of an asymmetry between matter and antimatter, and the world as we know it would be drastically different without the breaking of the electroweak symmetry at low energy. The real world turns out to be better described by a subtle interplay between symmetries and their breaking.

An interesting feature of symmetry breakings is that they can produce strong cosmological signals, especially if they happened through a first-order phase transition. In some cases, these signals could have remained until today; their detection would therefore provide a better comprehension of the laws of physics at high energy. The goal of this thesis is to study the production of two such signals during the electroweak phase transition (EWPT): the baryon asymmetry of the Universe (BAU) and a stochastic background of gravitational waves (GW). The motivation for the former is the observation that matter is much more abundant than antimatter, while the latter is motivated by the prospect of several upcoming space-based GW detectors, such as LISA [5].

The production of the BAU and GW during the EWPT have already been studied extensively within several standard model (SM) extensions [6–20]. These models are particularly attractive because they generally require new physics at the electroweak scale, which is already being probed by several experiments. They are therefore much more likely to be testable than other baryogenesis or GW production scenarios that involve higher energy scales. Previously, the calculation of the electroweak bubble wall's shape and velocity was generally avoided because they are highly nontrivial to compute; they were typically considered as free parameters and fixed to some arbitrary values. However, these quantities have an important effect on the predicted BAU and GW spectrum; hence it is not justifiable to neglect them.

One of this thesis's main contributions is that all the observable quantities are completely determined from the free parameters of the model considered. In Chapter 2 (published as Ref. [1]), we begin with a review of the fluid equations derived in Ref. [2] previously used to compute the wall's velocity and shape. We argue that these equations suffer from unphysical artifacts that make them unreliable for supersonic walls. We then propose an improved set of equations, well-behaved for all velocities, and compare the two formalisms. In Chapter 3 (published as Ref. [4]), we perform a scan of the parameter space of the Z_2-symmetric singlet scalar extension of the SM. We use our improved fluid equations to compute the wall's velocity and shape, which allow for a complete prediction of the BAU and GW spectrum produced during the EWPT.

Before getting into the main subject of this thesis, I review some useful concepts not covered in the two articles presented below. In the first introductory section, I explain the notions of first-order phase transition and bubble nucleation. I then describe the baryon asymmetry and the mechanisms involved in baryogenesis.

1.1 First-order phase transition and bubble nucleation

Phase transitions (PT) occur when the preferred ground state of a system changes at different temperatures. They are often accompanied by a symmetry breaking, resulting in a qualitative modification of the system's behaviour. In this thesis, we are mainly interested in the EWPT, where the SM's gauge symmetry group $\mathrm{SU}(3)_c \times \mathrm{SU}(2)_L \times \mathrm{U}(1)_Y$ gets broken to its subgroup $\mathrm{SU}(3)_c \times \mathrm{U}(1)_{EM}$ by the Higgs boson's non-vanishing vacuum expectation value (VEV)

$$v \equiv \langle h \rangle \neq 0. \tag{1.1}$$

We start this section by presenting the main types of PT and the differences between them. We then specialize to the case of first-order PT and describe the concept of *bubble nucleation*. Finally, we introduce a simple extension to the SM which makes the EWPT first order.

1.1.1 Classification of phase transitions

Phase transitions can be classified according to the lowest discontinuous derivative of the free energy with respect to some thermodynamic variable (see for example Refs. [21, 22]). Within this classification scheme, a PT with $d^{(n)}\mathcal{F}/dX^{(n)}$ as its lowest discontinuous derivative is labeled a nth-order PT. The most common kinds are first-order (e.g. the solid/liquid/gas transitions of various fluids) and second-order (e.g. the ferromagnetism/paramagnetism transition) phase transitions. If all the derivatives are continuous, the PT is a smooth crossover.

A simple toy model that yields a second-order PT is given by the real scalar field ϕ with the potential

$$V(\phi, T) = \frac{1}{2}(cT^2 - m^2)\phi^2 + \frac{\lambda}{4}\phi^4, \tag{1.2}$$

with $c, m^2, \lambda > 0$. This is the usual $\lambda\phi^4$ model, but with a negative squared mass and the leading thermal contribution $\sim T^2\phi^2$. One can easily see that the vacuum structure of this

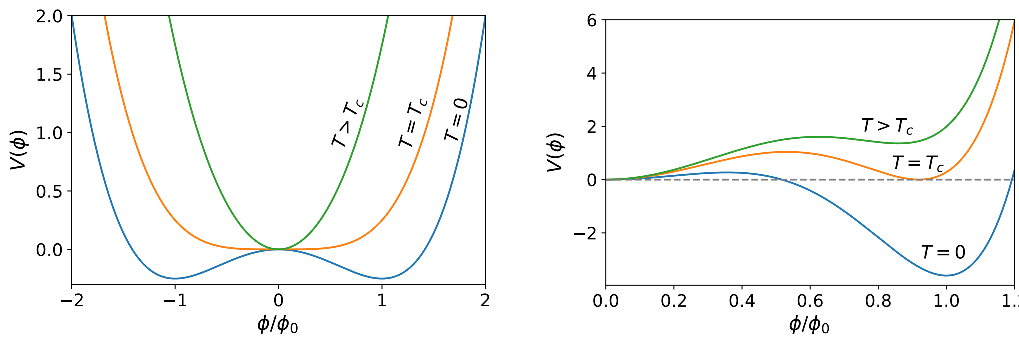

(a) (b)

Figure 1.1: Example of potential V for a (a) second-order and (b) first-order PT with $T = 0$, $T = T_c$ and $T > T_c$. ϕ_0 is the VEV evaluated at $T = 0$.

potential (i.e. its minima) depends on the temperature. At high temperature ($T > m/\sqrt{c}$), there is only one minimum at $\phi = 0$, while below that temperature, there are two equivalent vacua at $\phi = \pm\sqrt{(m^2 - cT^2)/\lambda} \equiv \pm v$. The temperature at which the transition happens is called the critical temperature:

$$T_c = \frac{m}{\sqrt{c}}. \tag{1.3}$$

The potential (1.2) for different temperatures is illustrated in Fig. 1.1 (a). Since there is no energy barrier between the high-temperature vacuum at $\phi = 0$ and the two low-temperature vacua at $\phi = \pm v$, the field goes smoothly from one minimum to the other as the temperature decreases below T_c. Therefore, the PT happens everywhere in space simultaneously, when the temperature T_c is reached.

To obtain a first-order PT, one needs two nonequivalent vacua separated by an energy barrier to coexist for some range of temperature. An example of such a potential is shown in Fig. 1.1 (b). At high temperature, the minimum at $\phi = 0$ is the *true vacuum*, i.e. the potential's global minimum which is the most stable solution. The field is therefore trapped at $\phi = 0$. As the temperature decreases, the second minimum's depth at $\phi \neq 0$ decreases until the critical temperature T_c is reached, where both minima are degenerate. Below T_c, the minimum at $\phi \neq 0$ becomes the true vacuum. But since the energy barrier between the two vacua remains, the field cannot transition smoothly towards the true vacuum, and it stays in the metastable minimum at $\phi = 0$ for some time. Because of the energy barrier, the PT can only happen through quantum tunnelling or thermal fluctuations, which are random processes described in the next subsection. For this reason, the PT occurs only in small regions of space at first. Then, these *bubbles* containing the new phase expand until they collide and fill the whole Universe. The nucleation of these bubbles happens at a temperature T_n, which is defined as the temperature where the probability of having one bubble per Hubble volume is of order ~ 1.

1.1.2 Bubble nucleation

We now derive the nucleation rate of bubbles containing the new phase in a first-order PT. As previously stated, these bubbles proceed through quantum tunnelling or thermal fluctuations, which can both be quantitatively described by an instanton solution interpolating between the false and true vacua. In practice, most of the interesting PTs happen at high temperatures, where thermal fluctuations are much more efficient than quantum tunnelling; hence we only describe the former here. One can show with a semi-classical calculation that the nucleation rate per unit volume for this process is given by [23]

$$\Gamma = T^4 \left(\frac{S_3}{2\pi T} \right)^{3/2} e^{-S_3/T}, \tag{1.4}$$

where S_3 is the O(3)-symmetric Euclidean action

$$S_3(T) = 4\pi \int dr\, r^2 \left[\frac{1}{2} \left(\frac{d\phi_i}{dr} \right)^2 + V(\phi_i, T) \right], \tag{1.5}$$

and we now allow the potential to depend on N independent real scalars ϕ_i, with $i = 1, \cdots, N$. In the semi-classical approximation, the fields $\phi_i(r)$ take their classical configuration which can be obtained by minimizing the action S_3, yielding the equations of motion (EOMs)

$$\frac{d^2\phi_i}{dr^2} + \frac{2}{r}\frac{d\phi_i}{dr} = \frac{\partial V}{\partial \phi_i}, \quad i = 1, \cdots, N. \tag{1.6}$$

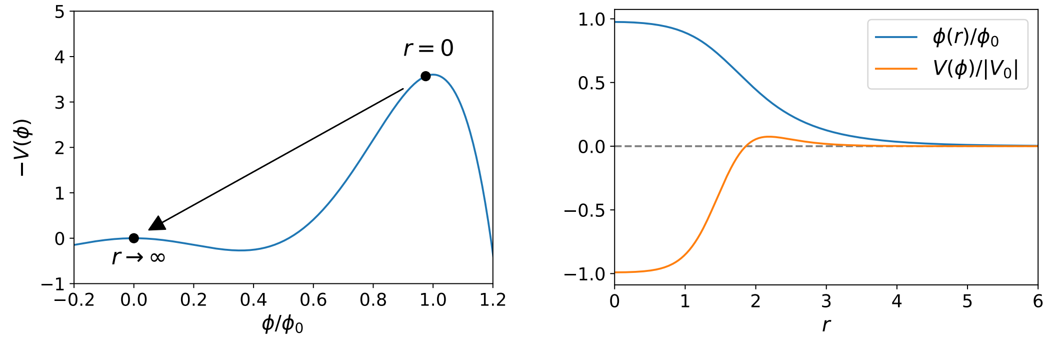

(a) (b)

Figure 1.2: Instanton solution for the model presented in Fig. 1.1 (b) at $T = 0$. (a): Boundary conditions in the inverted potential $-V(\phi)$; (b): Instanton configuration $\phi(r)$ and potential energy $V(\phi)$. Again, ϕ_0 is the field's VEV evaluated at $T = 0$ and $V_0 = V(\phi_0)$. The instanton solution was computed with the package CosmoTransitions [24].

Since the instanton solution must interpolate between the two vacua, one also needs to require that the fields at $r \to \infty$ are in the false vacuum ϕ_i^{false} and that the solution is smooth at the center of the bubble $r = 0$. This leads, respectively, to the boundary conditions

$$\phi_i(r \to \infty) = \phi_i^{\text{false}} \quad \text{and} \quad \left.\frac{d\phi_i}{dr}\right|_{r=0} = 0. \tag{1.7}$$

We note that the EOMs (1.6) are equivalent to the classical motion of a particle in N dimensions with coordinates $\phi_i(r)$ and time r in an inverted potential $-V(\phi_i)$ with a time-dependent friction force $2\dot{\phi}_i/r$. With the boundary conditions (1.7), the trajectory corresponds to a particle starting with no velocity close to the potential's global maximum (previously the true vacuum), rolling downhill from there and stabilizing at the top of the local maximum at ϕ_i^{false} after an infinite time. This situation is illustrated in Fig. 1.2 for the exemplary potential at $T = 0$ presented in Fig. 1.1 (b). The exact position of the particle at $r = 0$ is *a priori* unknown, but it can be determined by requiring that it does not undershoot or overshoot the local maximum ϕ_i^{false} at $r \to \infty$.

We can now use Eq. (1.4) to compute the nucleation temperature T_n. As previously mentioned, it is defined as the temperature where Γ is comparable to the Hubble rate per

Hubble volume

$$\frac{H}{V_H} = \frac{H}{\frac{4}{3}\pi(1/H)^3} = \frac{3}{4\pi}H^4.$$

The Hubble rate H in the radiation-dominated era is given by

$$H(T) = \left(\frac{8\pi^3}{90}g_*(T)\right)^{1/2}\frac{T^2}{M_p}, \tag{1.8}$$

with $M_p \approx 1.22 \times 10^{19}$ GeV the Planck mass and $g_*(T)$ the effective number of degrees of freedom at temperature T ($g_* \approx 100$ for $T \sim 100$ GeV). T_n can then be determined by solving the equation

$$\begin{aligned} \Gamma(T_n) &\approx \frac{H(T_n)}{V_H(T_n)} \\ \Rightarrow e^{-S_3(T_n)/T_n} &\approx \frac{3}{4\pi}\left(\frac{H(T_n)}{T_n}\right)^4\left(\frac{2\pi T_n}{S_3(T_n)}\right)^{3/2}. \end{aligned} \tag{1.9}$$

1.1.3 Z_2-symmetric singlet scalar extension

Lattice studies have shown that the EWPT is a smooth crossover in the SM [25–27]. We therefore need some new physics input beyond the SM to get a first-order EWPT, which is required to predict a baryon asymmetry and a strong GW signal. Fortunately, it is not difficult to do so with the addition of modest particle content. In this thesis, we consider the Z_2-symmetric singlet scalar extension of the SM [28–37], which couples a new real scalar field s to the Higgs boson.

The tree-level potential for the scalar sector in that extension is given by

$$V(h,s) = \frac{\mu_h^2}{2}h^2 + \frac{\lambda_h}{4}h^4 + \frac{\mu_s^2}{2}s^2 + \frac{\lambda_s}{4}s^4 + \frac{\lambda_{hs}}{4}h^2s^2, \tag{1.10}$$

where h is the Higgs field in the unitary gauge. Provided that $\mu_h^2, \mu_s^2 < 0$ and $\lambda_h, \lambda_s, \lambda_{hs} > 0$, this zero-temperature potential has four distinct minima, all separated by an energy barrier, at

$$(h, s) = (\pm|\mu_h|/\sqrt{\lambda_h}, 0) \equiv (\pm v_0, 0) \quad \text{and}$$
$$(h, s) = (0, \pm|\mu_s|/\sqrt{\lambda_s}) \equiv (0, \pm w_0).$$

Since we are today in the Higgs vacuum at $(v_0, 0)$, the two parameters μ_h^2 and λ_h can be related to the measured values of the Higgs VEV $v_0 \approx 246$ GeV and mass $m_h \approx 125$ GeV through the relations $m_h^2 = -2\mu_h^2$ and $v_0^2 = -\mu_h^2/\lambda_h$. The s mass is then given by $m_s^2 = \mu_s^2 + \lambda_{hs} v_0^2/2$. This model is therefore completely determined by the three free parameters m_s, λ_s and λ_{hs}. The latter controls the height of the energy barrier between the minima, with a larger value corresponding to a higher barrier, and thus a stronger PT. A motivation for imposing the Z_2 symmetry for the singlet field is that it considerably reduces the number of allowed operators, making this model more predictable.

To make quantitative predictions, one needs to add quantum and thermal corrections to the potential (1.10), which are described in Appendix 3.A. For the purpose of the present analysis, it is sufficient to consider only the leading thermal contributions, which are proportional to h^2T^2 and s^2T^2. Above respective temperatures $T_c^{(h)}$ and $T_c^{(s)}$, the effective couplings of the h^2 and s^2 terms become positive; hence the minima at $(\pm v_T, 0)$ and $(0, \pm w_T)$ disappear, respectively. For $T > T_c^{(h)}, T_c^{(s)}$, only one minimum remains at the origin.

An interesting case is that where $T_c^{(s)} > T_c^{(h)}$: the singlet's Z_2 symmetry first breaks at $T = T_c^{(s)}$, but since we impose that the Higgs vacuum is the true vacuum at $T = 0$, there must be a critical temperature $T_c < T_c^{(h)}$ where both the s and h minima are equally deep. Below T_c, the s minimum becomes metastable and a first-order PT from $(0, w_T)$ to $(v_T, 0)$ can occur, breaking the electroweak symmetry and restoring the singlet's Z_2 symmetry. As for any first-order PT, the second step does not happen directly at T_c, but at the nucleation temperature T_n, which can be determined by solving Eq. (1.9). This two-step PT is illustrated in Fig. 1.3. In practice, the details of the first step are not important since the singlet field does not couple directly to the SM particles; one only needs to make sure that $T_c^{(s)} > T_c^{(h)}$ to get the right symmetry breaking pattern.

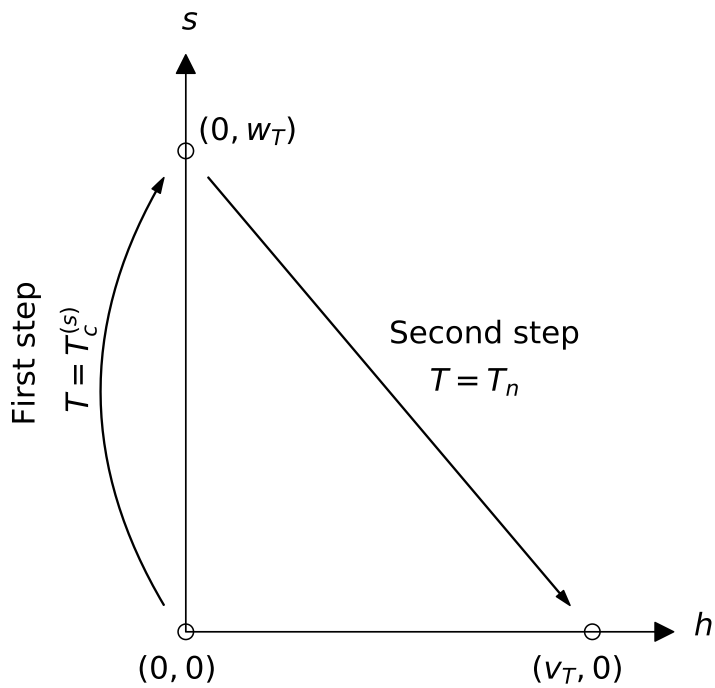

Figure 1.3: Two-step phase transition in the Z_2-symmetric singlet scalar extension. First, the s field gets a VEV at $T = T_c^{(s)}$; then the fields go from $(0, w_T)$ to $(v_T, 0)$ through a first-order PT at $T = T_n$.

1.2 Baryon asymmetry

The *Planck* measurements of the cosmic microwave background anisotropies determine the value of the baryon density of the Universe as [38]

$$\Omega_b h^2 = 0.02237 \pm 0.00015, \tag{1.11}$$

with h being the reduced Hubble constant. A more appropriate quantity to study the BAU is the baryon-to-photon ratio η_b, defined as

$$\eta_b \equiv \frac{n_B - n_{\bar{B}}}{n_\gamma}, \tag{1.12}$$

where n_B, $n_{\bar{B}}$ and n_γ are the number densities of baryons, antibaryons and photons, respectively. It can be related to the baryon density through the relation [39]

$$\eta_b = 2.74 \times 10^{-8} \Omega_b h^2 = (6.13 \pm 0.04) \times 10^{-10}. \tag{1.13}$$

It is well known that this asymmetry cannot be explained by the SM alone [40]. This has motivated the development of several baryogenesis scenario involving various SM extensions. Some of the most popular are leptogenesis [41–44], Affleck-Dine baryogenesis [45] and electroweak baryogenesis (EWBG) [6–9]. We describe here the latter, starting with Sakharov's conditions, which are necessary conditions common to all scenarios that are required for successful baryogenesis. We then describe the sources of B violation already present in the SM and explain the general principles behind EWBG.

1.2.1 Sakharov's conditions

The idea of baryogenesis is attributed to the Russian physicist Andrei Sakharov, who first identified three necessary conditions to dynamically generate a net baryon number to explain the observed BAU. These conditions are [46]

1. B violation
2. Deviation from thermal equilibrium
3. C and CP violation

The following arguments for each of the three conditions are based on Ref. [40]. The first one is quite obvious: if one wants to build up a net amount of baryons, B must not be a conserved quantity. The second condition is also easy to understand. Let us consider a general B violating process

$$X \to Y + B.$$

If the Universe is in thermal equilibrium, the rate of that process $\Gamma(X \to Y + B)$ is, by definition, equal to the rate of the inverse process:

$$\Gamma(X \to Y + B) = \Gamma(Y + B \to X).$$

The net B variation is then

$$\frac{dn_B}{dt} \propto \Gamma(X \to Y + B) - \Gamma(Y + B \to X) = 0.$$

A similar argument can be used to justify the requirement of C violation. If C is conserved, the rate for the production of baryons is by definition the same as the rate for the production of antibaryons. So again, the net B variation is

$$\frac{dn_B}{dt} \propto \Gamma(X \to Y + B) - \Gamma(\bar{X} \to \bar{Y} + \bar{B}) = 0.$$

The condition of CP violation is a bit more subtle. Consider a process generating a left or right-handed quark which violates C but conserves CP

$$X \to Y + q_{L/R}. \tag{1.14}$$

C and CP act on quarks according to

$$C : q_{L/R} \to \bar{q}_{L/R}$$
$$CP : q_{L/R} \to \bar{q}_{R/L}$$

Since the process (1.14) violates C, one obtains

$$\Gamma(X \to Y + q_{L/R}) \neq \Gamma(\bar{X} \to \bar{Y} + \bar{q}_{L/R}).$$

However, conservation of CP implies

$$\Gamma(X \to Y + q_{L/R}) = \Gamma(\bar{X} \to \bar{Y} + \bar{q}_{R/L}),$$

which ensures that the total rates of quark and antiquark production are equal:

$$\Gamma(X \to Y + q_L) + \Gamma(X \to Y + q_R) = \Gamma(\bar{X} \to \bar{Y} + \bar{q}_R) + \Gamma(\bar{X} \to \bar{Y} + \bar{q}_L).$$

The net B production is then

$$\frac{dn_B}{dt} \propto \Gamma(X \to Y + q_L) + \Gamma(X \to Y + q_R) - \Gamma(\bar{X} \to \bar{Y} - \bar{q}_R) - \Gamma(\bar{X} \to \bar{Y} + \bar{q}_L) = 0.$$

1.2.2 B violation in the Standard Model

Although the baryon number is classically conserved in the SM, 't Hooft showed in 1976 that B is violated by the triangle anomaly through a nonperturbative process [47]. In the presence of background $\mathrm{SU}(2)_L$ gauge fields W, one can show that the anomalous divergence of the baryon current J_B^μ is

$$\partial_\mu J_B^\mu = \frac{Ng^2}{32\pi^2}\epsilon^{\mu\nu\rho\lambda}W^a_{\mu\nu}W^a_{\rho\lambda}, \tag{1.15}$$

where $W^a_{\mu\nu}$ is the $\mathrm{SU}(2)_L$ field strength and $N = 3$ is the number of families. To gain some intuition with the topological properties of the right-hand-side, we can first work out the simpler problem corresponding to the U(1) group in two Euclidean dimensions, as done by Coleman in Ref. [48].

Physical field configurations must have a finite action. This implies that the field must be in a vacuum configuration at infinity, which corresponds to $F^{\mu\nu} = 0$, with $F^{\mu\nu}$ the U(1) strength field. Under a gauge transformation, the corresponding gauge field A^μ transforms like

$$A^\mu \to A^\mu + g\partial^\mu g^{-1}, \tag{1.16}$$

with $g(x) \in \mathrm{U}(1)$. Therefore, a vacuum can have a non-vanishing pure gauge configuration

$$A^\mu = g\partial^\mu g^{-1}, \tag{1.17}$$

which is completely determined by the arbitrary U(1) group element $g(x)$. To study the topological structure of these vacua, let us gauge transform Eq. (1.17) with another group element $h(x) \in \mathrm{U}(1)$. One can easily see that this has the same effect as the transformation

$$g(x) \to h(x)g(x). \tag{1.18}$$

One could therefore try to choose $h = g^{-1}$ to make the field A^μ vanish everywhere. However, this choice is not always possible. Unlike $g(x)$, which is only defined at the spatial boundary $r \to \infty$, $h(x)$ must be a continuous function everywhere in space, including at the origin. This implies that at $r = 0$, h must be independent of the angular variable θ, i.e. a constant. The function everywhere else in space can then be obtained by a continuous deformation of this constant, which means that $h(x)$ is topologically equivalent to the identity transformation. Therefore, one can only gauge transform into a topologically equivalent vacuum configuration, i.e. a configuration that can be obtained from a continuous deformation.

This implies that there can be several different (but physically equivalent) vacuum configurations of the gauge field A^μ. Since $g(x)$ is a map from the boundary of the two-dimensional Euclidean space (which is the usual circle S^1) to the gauge group $\mathrm{U}(1) \cong S^1$, these configurations are given by the homotopy classes of $S^1 \to S^1$, which correspond to all the topologically different ways one can wrap a circle around another circle. These are isomorphic to $\mathbb{Z}$ since the first circle must wind an integer number of times around the other. All the gauge group functions $g(x)$ are therefore topologically equivalent to an element of the set

$$g_\nu(\theta) = e^{i\nu\theta}, \tag{1.19}$$

with $\nu \in \mathbb{Z}$ the winding number, which corresponds to the number of times the gauge group U(1) winds around the spatial boundary S^1.

We can now return to the more relevant case of the $\mathrm{SU}(2)_L$ gauge group in four-dimensional Euclidean space, which is again discussed in Ref. [48]. The previous derivation still applies, but now, the vacuum gauge field configuration is a map from $\partial\mathbb{R}^4 \cong S^3$ to the gauge group $\mathrm{SU}(2)_L \cong S^3$. Again, the homotopy classes of $S^3 \to S^3$ are isomorphic to $\mathbb{Z}$, so there is an infinite number of different vacua labelled by a winding number $\nu \in \mathbb{Z}$. One can show that ν can be written in terms of the field strength $W^{\mu\nu}$ as

$$\nu = \int dx^4 \frac{g^2}{32\pi^2} \epsilon^{\mu\nu\rho\lambda} W^a_{\mu\nu} W^a_{\rho\lambda} = \frac{1}{N} \int dx^4 \partial_\mu J^\mu_B. \tag{1.20}$$

In Ref. [47], 't Hooft showed that transitions from one vacuum to another are possible through instanton solutions. From Eq. (1.20), one can see that such a transition violates B by $N = 3$ units. During this process, the field must go through non-vacuum configurations where Eq. (1.20) is not an integer. These field configurations have a higher energy than the vacua, and the energy barrier between each vacuum is [49]

$$E_{\mathrm{sph}} \approx \frac{4M_W}{\alpha_W}, \tag{1.21}$$

where M_W is the W boson's mass and $\alpha_W = g^2/(4\pi) \approx 1/30$. 't Hooft showed that the rate of this transition at $T = 0$ is of order $e^{-16\pi^2/g^2} \sim 10^{-160}$, which is so small that it should not have happened once in the Universe's lifetime. But, at temperatures higher than the electroweak phase transition, the gauge bosons become massless and the energy barrier between the vacua vanishes. These transitions at finite temperature are called *sphalerons*, meaning "ready to fall" in Greek. With no energy barrier to tunnel through, the sphaleron's rate is only suppressed by powers of g, instead of exponentially, like the $T = 0$ process.

Lattice studies have shown that this rate is [50]

$$\frac{\Gamma}{V} = (1.05 \pm 0.08) \times 10^{-6}\, T^4. \tag{1.22}$$

The sphaleron is in thermal equilibrium as long as $\Gamma/H > 1$, with the Hubble rate $H \sim T^2/M_\mathrm{p}$. Choosing a typical volume $V \sim 1/T^3$, this condition is satisfied for

$$T < 1.05 \times 10^{-6} M_\mathrm{p} \sim 10^{13}\ \mathrm{GeV}, \tag{1.23}$$

which is far above the electroweak scale. After the electroweak phase transition, although the vacua become separated by a nonvanishing energy barrier E_sph, the transition from one vacuum to another may still be possible through thermal fluctuations which are more efficient than quantum tunnelling at the electroweak scale. Ref. [51] has shown that the sphaleron remains efficient after the symmetry breaking if

$$\frac{v_n}{T_n} < 1.1, \tag{1.24}$$

where T_n is the nucleation temperature and v_n is the Higgs VEV just after the phase transition. We will explain below why this must be avoided for EWBG to be successful. It should be noted that the bound (1.24) is somewhat arbitrary and is model-dependent. An improved estimate can be found in Ref. [52], but we verify in Chapter 3 that it does not have a large impact on our results. This sphaleron bound is also gauge and scale dependent; Ref. [53] has elaborated a gauge-independent criterion at the cost of neglecting resummation at leading order. We therefore use the simple estimate (1.24) in this thesis.

1.2.3 Electroweak baryogenesis

We now describe how the three Sakharov's conditions can be satisfied by the EWBG scenario [7, 8]. Let us start with the third condition: C and CP violation. CP violating processes have been observed in the decay of neutral kaons [54], B mesons [55] and D mesons [56]. This CP violation is explained in the SM by the complex parametrization of the CKM matrix, which mixes the quarks of different generations through the electroweak interaction. However, it is generally accepted that the SM's CP violation is insufficient for the purposes of EWBG [40]. Nevertheless, it is straightforward to find natural extensions to the SM that provide such a source of CP violation.

In the simple Z_2-symmetric singlet scalar extension presented in Subsection 1.1.3, the following dimension-5 operator, which yields an imaginary contribution to the top quark mass [57], can provide the required CP violation[1]

$$V_{BG} = \frac{y_t}{\sqrt{2}} h \bar{t}_L \left(1 + i\frac{s}{\Lambda}\right) t_R + \text{H.c.} \tag{1.25}$$

where y_t is the top Yukawa coupling and $\Lambda \gtrsim 500$ GeV is some energy scale above the electroweak scale. We note that different types of CP-violating source like mixing terms between different species can lead to resonant enhancement which can yield efficient baryogenesis (see for example Ref. [58]). To see that the operator in Eq. (1.25) violates CP, one can first rewrite it as

$$V_{BG} = m(z)\bar{t}e^{i\theta(z)\gamma^5}t = -m(z)t^{\intercal}e^{i\theta(z)\gamma^5}\gamma^0 t^*, \tag{1.26}$$

where we transposed to obtain the second equation (which do not change its value since V_{BG} is a real number), the minus sign comes from the fact that the two Grassmann numbers t and t^* anticommute, and

$$m(z) = \frac{y_t}{\sqrt{2}} h(z) \sqrt{1 + \left(\frac{s(z)}{\Lambda}\right)^2},$$
$$\theta(z) = \arctan\left(\frac{s(z)}{\Lambda}\right).$$

The two fields h and s are chargeless real scalar fields, so they both transform trivially under

[1] C is already maximally violated by the electroweak interaction.

CP. For fermionic fields:

$$CP: \quad \psi \to i\gamma^2\gamma^0\psi^*, \tag{1.27}$$

which implies

$$\begin{aligned} CP: \quad V_{BG} \to &- m(z)(i\gamma^2\gamma^0 t^*)^\intercal e^{i\theta(z)\gamma^5}\gamma^0(i\gamma^2\gamma^0 t^*)^* \\ =&m(z)t^\dagger\gamma^0\gamma^2 e^{i\theta(z)\gamma^5}\gamma^0\gamma^2\gamma^0 t \\ =&m(z)\bar{t}e^{-i\theta(z)\gamma^5}t \end{aligned} \tag{1.28}$$

where we used $(\gamma^2)^* = -\gamma^2$, $(\gamma^2)^\intercal = \gamma^2$, $(\gamma^0)^* = (\gamma^0)^\intercal = \gamma^0$ and $e^{i\theta\gamma^5}\gamma^\mu = \gamma^\mu e^{-i\theta\gamma^5}$. Hence, the phase picks up a minus sign during the CP transformation. And since $\theta(z)$ depends on z, the phase cannot be removed by a field redefinition. V_{BG} is therefore a CP violating term.

The second condition that EWBG must satisfy is the loss of thermal equilibrium. This can be obtained with a first-order phase transition, where the rapidly varying scalar fields in the bubble wall drive the plasma around it out of equilibrium. As seen in Subsection 1.1.3, the simple addition of a Z_2-symmetric singlet scalar coupling to the Higgs is enough to create a potential barrier between the true and false minima, which makes the electroweak phase transition first order. In Chapter 2, we will derive the transport equations needed to describe the CP-even modes' departure from equilibrium. Similar transport equations for the CP-odd modes have already been derived in Ref. [3].

Finally, no new physics input is required to satisfy the B-violation condition since the baryon number is already violated in the SM by the sphaleron process described in Subsection 1.2.2. One only needs to make sure that the sphaleron is efficient in front of the wall (which is always the case since the $\mathrm{SU}(2)_L$ symmetry is not yet broken there), but inefficient behind the wall. According to Eq. (1.24), this leads to the condition

$$\frac{v_n}{T_n} > 1.1. \tag{1.29}$$

The processes involved in EWBG are summarized in Fig. 1.4. At first, the CP-violating interaction (1.25), coupled to the loss of thermal equilibrium in the wall, generates a chiral

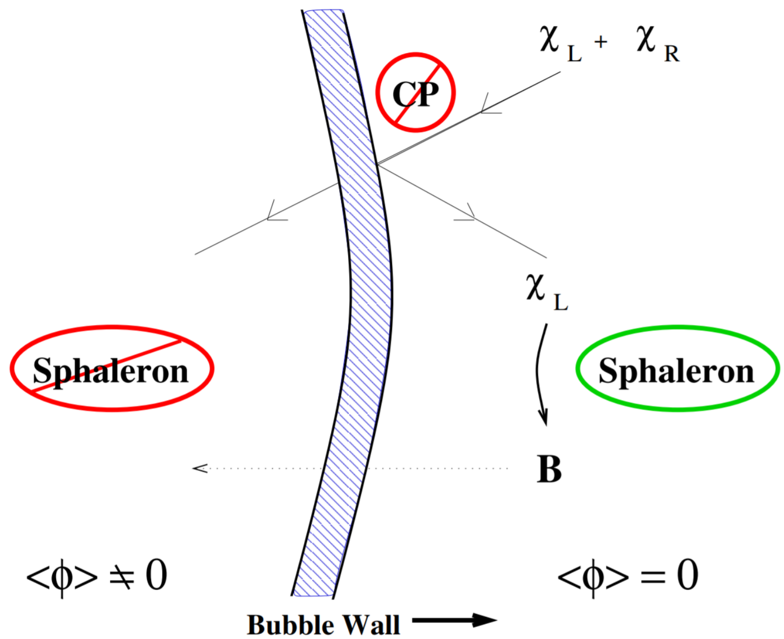

Figure 1.4: Summary of the processes involved in EWBG. Image originally used in Ref. [59].

asymmetry that diffuses, in part, in front of the wall. Then, this CP asymmetry is converted into a B asymmetry by the sphaleron, which is in thermal equilibrium. This B asymmetry finally diffuses behind the wall. Since the sphaleron is inefficient after the symmetry breaking (as long as Eq. (1.29) is satisfied), the B asymmetry gets frozen out and stays unchanged, forming the BAU that we observe today.

Chapter 2

Fluid equations for fast-moving electroweak bubble walls

Work published with James M. Cline as Ref. [1].

Abstract

The cosmological electroweak phase transition can be strongly first order in extended particle physics models. To accurately predict the speed and shape of the bubble walls during such a transition, Boltzmann equations for the CP-even fluid perturbations must be solved. We point out that the equations usually adopted lead to unphysical behavior of the perturbations, for walls traveling close to or above the speed of sound in the plasma. This is an artifact that can be overcome by more carefully truncating the full Boltzmann equation. We present an improved set of fluid equations, suitable for studying the dynamics of both subsonic and supersonic walls, of interest for gravitational wave production and electroweak baryogenesis.

2.1 Introduction

The electroweak phase transition in the early universe is known to be a smooth-crossover within the standard model (SM), given the measured value of the Higgs boson mass [25, 60]. The addition of new particles coupling to the Higgs can turn it into a strongly first order phase transition, proceeding by the nucleation of bubbles of the true, electroweak symmetry breaking vacuum, in the initially symmetric plasma. This possibility has been widely studied because of its potential for providing electroweak baryogenesis (EWBG) [40, 59, 61], and gravity waves that might be observable in the upcoming LISA experiment [62, 63].

An important parameter for the efficiency of baryon or gravitational wave production is the terminal speed v of the bubble walls, with baryogenesis generally favoring slower walls, while faster walls tend to produce stronger gravity wave signals. To determine v and other relevant properties of the bubble wall, within a given particle physics model, one must self-consistently solve for the perturbations to the fluid induced by the wall; these are needed to determine the frictional force acting on the wall, that brings it to a state of steady expansion.

In previous literature on this subject, quantitative study of fast-moving walls has been hampered by an apparent singularity of the fluid equations occurring at the sound speed $c_s = 1/\sqrt{3}$, that we will explicitly demonstrate below. This makes a microscopic calculation of the friction in such cases problematic, motivating phenomenological estimates for the friction [64–67], or else leaving aside supersonic walls altogether [68]. Complementary approaches have been used to study the ultrarelativistic limit [69–71]; in this work we are primarily interested in velocities $v \gtrsim c_s$ rather than $v \cong 1$. We argue that the apparent sound barrier is an artifact of a particular truncation of the Boltzmann equations for the fluid perturbations, and that sensible solutions exist for wall speeds up to $v = 1$ by making a better choice.

A similar observation was recently made in ref. [3] in the context of the CP-odd fluid perturbations that are needed to compute the source terms for EWBG, but the analogous study for the CP-even perturbations, relevant to determining the bubble wall properties, has not been done. It requires more work because the perturbation in the local temperature $\delta\tau = \delta T/T$ (not needed for the EWBG source terms) must now be included in the network. The optimal way of doing this turns out to be somewhat subtle, as we will discuss.

We start by reviewing the standard approach in section 2.2 and the pathology of the perturbations it predicts for supersonic walls. We derive improved fluid equations in section 2.3, and in section 2.4 the solutions of the old and new formalisms are compared for a typical background wall profile, as a function of the wall velocity v. These results are used in section 2.5 to compute the predictions for the friction term in the Higgs field equation of motion, that determines the bubble wall shape and speed. There we highlight the problems with the old approach and their absence in the new one. Conclusions are given in section 2.6. Formulas for the coefficients of the new fluid equations are presented in Appendix 2.A, and the results of refined estimates for the collision terms are explained in Appendix 2.B.

2.2 Old formalism (OF)

We begin by recapitulating the method that has been used in previous literature for computing the plasma perturbations [2, 65, 68, 72–75]. These are the deviations of the distribution function f for a given particle away from its equilibrium form, that have been parametrized as [2, 72, 76]

$$f = \frac{1}{e^X \pm 1} = \frac{1}{e^{\beta\gamma(E - vp_z) - \delta X} \pm 1},$$
$$\delta X(z) = \mu + \beta\gamma[\delta\tau(E - vp_z) + u(p_z - vE)]$$

where $\beta = 1/T$, $\gamma = 1/\sqrt{1-v^2}$ and the equilibrium part, with $\delta X = 0$, is expressed in the rest frame of the bubble wall, taken to be planar and moving to the left. μ is the dimensionless chemical potential (in units of temperature) and u is the velocity perturbation. The wall frame is convenient for expressing the Boltzmann equation since the solutions in this frame are stationary,

$$\mathbf{L}[f] = \left(\frac{p_z}{E}\partial_z - \frac{(m^2)'}{2E}\partial_{p_z}\right)(f_v + \delta f) \cong -\mathcal{C}[f] \tag{2.1}$$

where $\delta f = -(df_v/dX)\,\delta X \equiv -f_v'\,\delta X$ is the perturbation, $(m^2)' = dm^2/dz$ for a particle whose mass depends on the background Higgs field $h(z)$ (and possibly other fields like a singlet scalar) in the wall, and f_v is the equilibrium distribution in the wall frame.

To approximately solve eq. (2.1), three moments are taken, by integrating over momenta $\int d^3p$ with the respective weight factors [2] 1, $\gamma(p_z - vE)$ and $\gamma(E - vp_z)$, giving three coupled ordinary differential equations for the perturbations $q \equiv (\mu, u, \delta\tau)^\intercal$, that can be written in the 3×3 matrix form

$$A_v q' + \Gamma q = S \tag{2.2}$$

with a rate matrix Γ from the moments of the collision term $\mathcal{C}$ and a source $S \sim v\beta^2(m^2)'$ from the Liouville operator $\mathbf{L}$ in (2.1) acting on f_v.

The A_v matrix depends on v in such a way that $A_v^{-1}\Gamma$ becomes singular at $v = c_s$, and has only positive eigenvalues for $v > c_s$. By constructing a Green's function to solve eq. (2.2) [3], one can see that this implies that the perturbations q must strictly vanish in front of the wall for $v > c_s$. Ref. [3] has argued that this kind of behavior is unphysical, since the fluid equations (2.2) describe particle diffusion, which is a physically distinct process from the propagation of sound waves. There is no reason why diffusion should be suddenly quenched in the vicinity of a supersonic wall, since some fraction of particles in front of the wall can still travel fast enough to get ahead of it.

2.3 Improved fluid equations (NF)

In this section we propose a new formalism (NF) for the fluid equations, motivated by the recent paper [3]. In that work, the problem of artificial suppression of diffusion for supersonic walls was overcome, following a long-established method of dealing with the velocity perturbation u [77–79]. The adoption of a specific form for u is known to lead to unphysical results, that can be avoided by instead writing the perturbations in the form

$$f = f_v - f_v'\,\delta\bar{X} + \delta f_u \tag{2.3}$$

[2] In the fluid frame these are simply 1, p_z and E.

[3] Strictly speaking, this method only works when the z-dependence of $A_v^{-1}\Gamma$ can be ignored on either side of the wall, but the same conclusion is borne out by a full numerical solution.

where now $\delta\bar{X}$ omits the velocity perturbation u, which is instead encoded through δf_u in such a way that

$$u \propto \int d^3p \, \frac{p_z}{E} \, \delta f_u \quad \text{and} \quad \int d^3p \, \delta f_u = 0 \,. \tag{2.4}$$

To deal with other integrals involving δf, one makes a factorization ansatz

$$\int d^3p \, Q \, \delta f_u \to u \int d^3p \, Q \frac{E}{p_z} \, f_v \tag{2.5}$$

for any quantity Q. This procedure was shown in ref. [77] to lead to nonsingular diffusion in front of supersonic walls, so long as one carefully evaluates the full v-dependence of A_v, rather than linearizing it in v, and weighting the Boltzmann equation by the moments 1, p_z/E.

However ref. [77] only considered the case of CP-odd perturbations, where $\delta\tau$ plays no significant role and hence was omitted. Our purpose in this work is to extend those results to include $\delta\tau$, whose value is needed for the full solutions to the field equations determining the shape and speed of the bubble walls. To determine this additional perturbation, a third moment is needed. We find that by choosing the weighting factor E, in addition to 1 and p_z/E (all defined in the wall frame), the resulting A_v matrix becomes

$$A_v = \begin{pmatrix} C_v^{1,1} & \gamma v C_0^{-1,0} & D_v^{0,0} \\ C_v^{0,1} & \gamma(C_v^{-1,1} - v C_v^{0,2}) & D_v^{-1,0} \\ C_v^{2,2} & \gamma(C_v^{1,2} - v C_v^{2,3}) & D_v^{1,1} \end{pmatrix} \tag{2.6}$$

where the dimensionless functions $C_v^{m,n}$ and $D_v^{m,n}$ are defined as

$$C_v^{m,n} = T^{m-n-3} \int \frac{d^3p}{(2\pi)^3} \frac{p_z^n}{E^m} (-f_v') \,,$$
$$D_v^{m,n} = T^{m-n-3} \int \frac{d^3p}{(2\pi)^3} \frac{p_z^n}{E^m} f_v \,.$$

With this choice, $\det A_v$ has no singularity for wall speeds between $v = 0$ and 1, and it gives the desired behavior in which diffusion ahead of the wall only gets suppressed in the limit $v \to 1$. The source term becomes

$$S = \gamma v \frac{(m^2)'}{2T^2} \begin{pmatrix} C_v^{1,0} \\ C_v^{0,0} \\ C_v^{2,1} \end{pmatrix} . \tag{2.7}$$

In previous literature, the coefficients corresponding to $C_v^{m,n}$ and $D_v^{m,n}$ were usually calculated in the limit of vanishing mass (as well as only leading order in v), but we find that the variation of $m^2(z)$ for the relevant particles within the wall can have a significant impact on the shape of the solutions. We thus retain the full mass- and v-dependence of those functions. Moreover, it is possible to analytically determine the v-dependence by boosting to the plasma frame (see Appendix 2.A).

We have also updated the components of the collision matrix Γ to account for the new choice of moments. The calculation of ref. [2] is improved by correcting some errors pointed out in ref. [80] and by using a Monte Carlo algorithm to compute more accurately the collision integrals. The new values of the collision terms are given in Appendix 2.B.

2.4 Solutions for a Standard Model-like plasma

Next we apply the improved fluid equations to a SM-like plasma in the context of a first order electroweak phase transition. The species that couple most strongly to the Higgs boson are the top quark t and the electroweak gauge bosons. The W and Z bosons are approximated as having the same distribution functions, and we will refer to them collectively as W bosons. The remaining particles form a background fluid which is assumed to be in thermal equilibrium ($\mu_{\rm bg} = 0$) at a z-dependent temperature $T + \delta\tau_{\rm bg}(z)$ [2]. Even if they are not driven out of chemical equilibrium by the phase transition, these lighter fields still play an important role in the dynamics of the bubble wall. One might also expect the Higgs

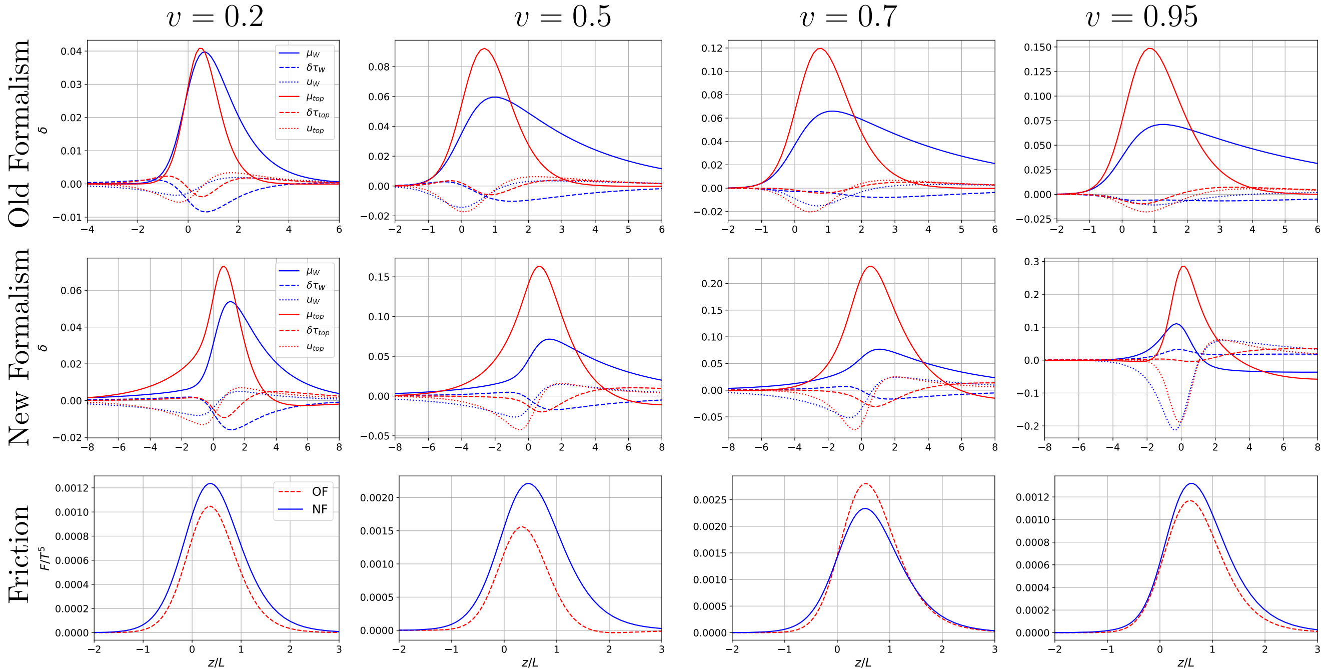

Figure 2.1: First row: solutions for the perturbations of the W and t fluids within the old formalism, for $T = 100\,\mathrm{GeV}$, $L = 5\gamma/T$, $h_0 = 150\,\mathrm{GeV}$ and wall velocities $v = 0.2,\ 0.5,\ 0.7,\ 0.95$, as a function of z/L. Second row: corresponding results for the improved fluid equations. Third row: comparison of the friction term (2.15) obtained with both formalisms, with solid curves for NF and dashed for OF. The symmetric phase in front of the bubble wall is to the left.

boson distribution to be perturbed, but its small number of degrees of freedom makes its contribution negligible compared to that of t or W. It is therefore included in the background fluid (and similar reasoning could also be applied to additional fields not present in the SM, *e.g.,* a singlet scalar).

The complete set of matrix equations for the t, W and background components is

$$A_t(q_t' + q_{\rm bg}') + \Gamma_t q_t = S_t$$

$$A_W(q_W' + q_{\rm bg}') + \Gamma_W q_W = S_W$$

$$A_{\rm bg} q_{\rm bg}' + \Gamma_{{\rm bg},t} q_t + \Gamma_{{\rm bg},W} q_W = 0$$

where A_t, A_W, S_t and S_W are given in eqs. (2.6) and (2.7), using the appropriate equilibrium distribution functions. The A matrix for the background fluid is

$$A_{\rm bg} = N_f A_t|_{m=0} + N_b A_W|_{m=0}, \tag{2.8}$$

with N_f and N_b respectively the fermionic and bosonic number of degrees of freedom included in the background fluid ($N_f = 78$ and $N_b = 19$ in the SM). We evaluate A_t and A_W at $m = 0$ because all the particles in the background fluid are approximately massless. Energy and momentum conservation fixes $\Gamma_{{\rm bg},t} = -12\Gamma_t$ and $\Gamma_{{\rm bg},W} = -9\Gamma_W$ [65], and Γ_t and Γ_W are evaluated in Appendix B.

To solve the system (2.8), one can eliminate $q'_{\rm bg}$ using the third equation; however the fact that $\mu_{\rm bg} = 0$ makes one of the three "bg" equations redundant. We have chosen to keep the first and third "bg" component equations (corresponding to the weighting factors 1 and p_z/E), since this leaves $A_{\rm bg}$ nonsingular for $v \in (0,1)$. The result is

$$q'_{\rm bg} = -\tilde{A}^{-1}_{\rm bg}(\Gamma_{{\rm bg},t} q_t + \Gamma_{{\rm bg},W} q_W) \tag{2.9}$$

where $\tilde{A}^{-1}_{\rm bg}$ is the inverse of the 2×2 $A_{\rm bg}$ matrix, projected onto the 1,3 columns and 2,3 rows of a 3×3 matrix. It can be written in terms of the 3 matrices

$$P_1 = \begin{pmatrix} 0 & 0 & 0 \\ 0 & 1 & 0 \\ 0 & 0 & 1 \end{pmatrix}, \; P_2 = \begin{pmatrix} 1 & 0 & 0 \\ 0 & 0 & 0 \\ 0 & 0 & 1 \end{pmatrix}, \; P_3 = \begin{pmatrix} 0 & 0 & 0 \\ 1 & 0 & 0 \\ 0 & 0 & 0 \end{pmatrix}$$

and the 3×3 $A_{\rm bg}$ matrix defined in (2.8):

$$\tilde{A}^{-1}_{\rm bg} = (P_2 A_{\rm bg} P_1 + P_3)^{-1} - P_3^{\intercal} \tag{2.10}$$

The six remaining equations take the form

$$A\,q' + \Gamma\,q = S \tag{2.11}$$

with

$$\begin{aligned} A &= \begin{pmatrix} A_W & 0 \\ 0 & A_t \end{pmatrix}, \; S = \begin{pmatrix} S_W \\ S_t \end{pmatrix}, \; q = \begin{pmatrix} q_W \\ q_t \end{pmatrix}, \\ \Gamma &= \begin{pmatrix} \Gamma_W - A_W \tilde{A}_{\rm bg}^{-1} \Gamma_{{\rm bg},W} & -A_W \tilde{A}_{\rm bg}^{-1} \Gamma_{{\rm bg},t} \\ -A_t \tilde{A}_{\rm bg}^{-1} \Gamma_{{\rm bg},W} & \Gamma_t - A_t \tilde{A}_{\rm bg}^{-1} \Gamma_{{\rm bg},t} \end{pmatrix} \end{aligned} \tag{2.12}$$

To compare the new and old formalisms (denoted by NF and OF in the following) for a generic first order phase transition, we model the bubble wall using a tanh ansatz for the background Higgs field,

$$h(z) = \frac{h_0}{2}\big[1 + \tanh(z/L)\big] \tag{2.13}$$

where h_0 is the VEV of the Higgs in the broken phase and L is the wall thickness. As an example we solve eqs. (2.11) within the OF and NF for $T = 100\,\text{GeV}$, $h_0 = 150\,\text{GeV}$, $L/\gamma = 5/T$ [4] and several wall velocities, using the collision rates given in [2] for the OF and the ones evaluated in Appendix B for the NF. We include a factor γ in L in order for the wall to have a constant thickness in the plasma frame. The solutions are shown in Figure 2.1, for a series of increasing wall velocities.

One can notice that within the NF, the perturbations in front of the wall ($z < 0$) vanish only in the limit $v \to 1$, as required by causality. This is not the case in the OF, whose solutions always vanish in front of the wall for $v > 1/\sqrt{3}$. As argued in ref. [3], this behavior is unphysical, since there is no reason for particles not to be able to diffuse in front as long as their v_z velocity component is higher than v.

As a consistency check, we observe that the linearization of the Boltzmann equation in

[4] L/γ is the wall thickness as measured in the plasma frame. Fixing LT/γ rather than LT makes it easier to see that the diffusion tails in front of the wall disappear as $v \to 1$.

δX and u is justified, since all the perturbations are generally well below unity in magnitude. We have tested that this condition holds for most wall parameters; the linearization starts to break down only in the extreme cases of very fast ($v \gtrsim 0.95$) and thin walls ($L \lesssim 1/T$).

2.5 Consequences for wall friction

An important application is the calculation of the friction term F in the Higgs equation of motion multiplied by $h' = dh/dz$ [65],

$$E_h \equiv h''h' - \left.\frac{\partial V_{\text{eff}}}{\partial z}\right|_T - F = 0, \tag{2.14}$$

where $V_{\text{eff}}|_T$ is the finite-temperature potential evaluated at the unperturbed background temperature, and

$$\begin{aligned} F(z) &= \sum_i \frac{dm_i^2}{dz} N_i \int \frac{d^3p}{(2\pi)^3 2E} (\delta f_{u,i} - f'_{v,i}\delta\bar{X}_i) \\ &= \sum_i \frac{dm_i^2}{dz} \frac{N_i T^2}{2} \left[C_0^{1,0}\mu_i + C_0^{0,0}(\delta\tau_i + \delta\tau_{bg}) + D_v^{0,-1}(u_i + u_{bg}) \right]. \end{aligned}$$

Here the sum is over the species t and W, and N_i is the corresponding number of degrees of freedom. An exact solution to eq. (2.14) exists only for a specific wall velocity and shape, and so the accurate estimation of F is important for determining the wall properties. An ansatz such as (2.13) can give a rough approximate solution, where v and L are determined by demanding that two moments of eq. (2.14) vanish [2, 65, 68], for example

$$\begin{aligned} M_1 &\equiv \int dz\, E_h = 0, \\ M_2 &\equiv \int dz\, E_h(2h - h_0) = 0 \end{aligned}$$

We plot $F(z)$ constructed from the OF and NF solutions in the bottom row of Figure 2.1. At small v, the friction predicted by NF is $\sim 20\%$ larger, leading us to expect the NF

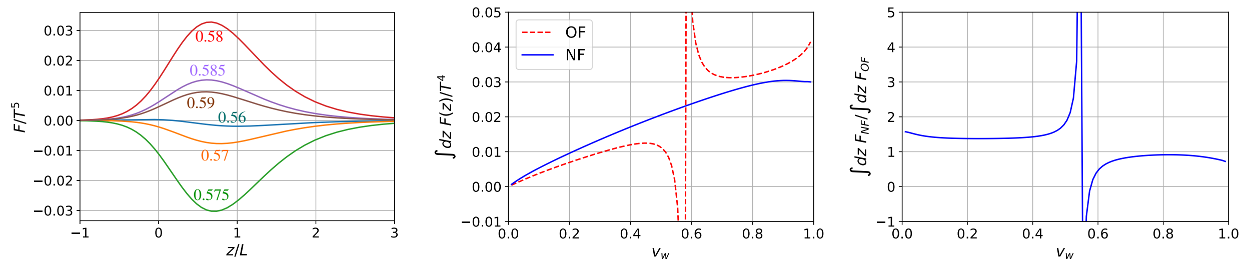

(a) (b) (c)

Figure 2.2: (a): Evolution of the friction with v in the old formalism (OF), showing discontinuous behavior across the sound barrier. Each $F(z)$ curve is labeled by its value of v. (b): The spatial integral of the friction in the OF (blue) and NF (orange) as a function of v, further illustrating the discontinuous behavior of the OF around the sound speed, and the smooth behavior of the NF. (c): The ratio of the two curves in (b). All the curves were obtained with $T = 100\,\mathrm{GeV}$, $L = 5/T$ and $h_0 = 150\,\mathrm{GeV}$.

to predict a smaller wall velocity than the OF for subsonic walls. This difference is mainly due to our improved calculation of the collision integrals and the fact that we keep the full mass dependence of the $C_v^{m,n}$ and $D_v^{m,n}$ functions. In this very coarse grid on velocity space, $v = 0.2,\ 0.5,\ 0.7,\ 0.95$, the friction appears to be qualitatively similar in shape at each velocity, involving primarily a modest rescaling factor to relate the results of the two approaches.

Despite the appearance in Fig. 2.1 of no dramatic difference between the two formalisms, more careful investigation in the vicinity of the sound speed reveals the crucial pathology of the OF. In Fig. 2.2(a) we plot $F(z)$ for a series of wall speeds from 0.56 to 0.59 within the OF, revealing that it briefly becomes *negative* before suddenly becoming positive again. This is even more clear in terms of the integral of the friction $\int dz\, F(z)$, which we plot as a function of v for the OF and NF in Fig. 2.2(b). The integral undergoes a discontinuity near $v = c_s$ in the OF, while remaining smooth and continuous in the NF. The ratio of the integrals between the NF and OF is plotted in fig. (2.2)(c), underscoring the relatively good two agreement of the two, except close to c_s.

In addition to giving incorrect results close to $v = c_s$, this discontinuous behavior of the OF makes it difficult to automate searches for wall properties, since the jump in $\int F\, dz$ leads to a similar discontinuity in the moment M_1 whose zero is being searched for. As expected, the second moment M_2 is also discontinuous in the OF. This was the practical difficulty that prompted our investigation. In contrast the NF gives smooth results, which we have argued is the expected behavior on physical grounds, since diffusion should not be greatly sensitive to whether the speed is slightly above or below c_s.

2.6 Conclusion

In this work we have pointed out a shortcoming at high wall speeds ($v \gtrsim c_s$) with the fluid equations that have been used, since their introduction in ref. [2], to calculate the friction F on electroweak bubble walls. We have also proposed a modification to these equations that solves the problem. It is reassuring that the two approaches give results that are not too different from each other at low wall speeds—and there the difference arises mainly because we have improved estimates of the collision rates, rather than the changes in formalism that become important at high v. Near the sound barrier and above, the differences are more significant, with our new results evolving continuously as a function of v, whereas the old ones exhibit a discontinuity in F at $v = c_s$. The new system predicts lower friction at high $v > c_s$ compared to the old one, which is likely to lead to faster walls. At low v the opposite is true. Application of these methods to a realistic model is underway [4].

The new elements in our treatment are a different choice of weighting factors for taking moments of the Boltzmann equation, and a different treatment of the velocity perturbation. The latter has long been recognized and recently highlighted in the high-v context in ref. [3]. While there are strong theoretical motivations for the velocity perturbation, the choice of weighting factors is more arbitrary, and cannot be justified *a priori*.

Instead we have made a phenomenological determination, by finding a set of moments that give the expected behavior for the fluid perturbations as a function of v. One could characterize it as an educated guess, that should be validated by finding a more exact solution of the full Boltzmann equations. There are several ways one could imagine doing this. Instead of three moments and three perturbations, one could increase this number to N and look for convergence of a physical quantity like the friction with increasing N. Alternatively, one could approximate the distribution function f by taking N bins in momentum space and seeking convergence with growing N. This is an investigation we hope to undertake in future work.

Acknowledgment. We thank A. Friedlander, K. Kainulainen and D. Tucker-Smith for useful discussions. This work was supported by NSERC (Natural Sciences and Engineering Research Council, Canada) and FRQNT (Fonds de recherche Nature et technologies, Québec).

2.A v-dependence of the $C_v^{m,n}$ and $D_v^{m,n}$ functions

The coefficients appearing in the A matrix generally depend on the local particle masses $m(z)/T$ and the wall velocity v. They can be evaluated numerically directly from their definition (2.7), but it is also possible to analytically calculate their v-dependence, by making the substitution $E \to \gamma(E + vp_z)$ and $p_z \to \gamma(p_z + vE)$ to boost the integration variables to the plasma frame. This transforms f_v to f_0, the equilibrium distribution function evaluated at $v = 0$, and leaves the combination d^3p/E invariant.

In this way, the $C_v^{m,n}$ and $D_v^{m,n}$ functions can be expressed as a sum (finite or infinite) of $C_0^{m,n}$ and $D_0^{m,n}$, the corresponding functions evaluated at $v = 0$. One can show that (henceforth omitting the subscript 0)

$$\begin{aligned}
C_v^{-1,1} &= \gamma^3 v \left[C^{-2,0} + (2 + v^2)C^{0,2}\right] \\
C_v^{0,0} &= \gamma\, C^{0,0} \\
C_v^{0,1} &= \gamma^2 v \left(C^{-1,0} + C^{1,2}\right) \\
C_v^{0,2} &= \gamma^3 \left[v^2 C^{-2,0} + (1 + 2v^2)C^{0,2}\right]
\end{aligned}$$

$$
\begin{aligned}
C_v^{1,0} &= C^{1,0} \\
C_v^{1,1} &= \gamma v\, C^{0,0} \\
C_v^{1,2} &= \gamma^2 (C^{1,2} + v^2 C^{-1,0}) \\
C_v^{2,1} &= v\, C^{1,0} - \frac{1}{\gamma^2} \sum_{n=1}^{\infty} v^{2n-1} C^{2n+1,2n} \\
C_v^{2,2} &= \gamma v^2 C^{0,0} + \frac{1}{\gamma^3} \sum_{n=1}^{\infty} v^{2n-2} C^{2n,2n} \\
C_v^{2,3} &= \gamma^2 v^3 C^{-1,0} + \gamma^2 v (v^4 - 3v^2 + 3)\, C^{1,2} - \frac{1}{\gamma^4} \sum_{n=2}^{\infty} v^{2n-3} C^{2n-1,2n} \\
D_v^{-1,0} &= \gamma^2 (D^{-1,0} + v^2 D^{1,2}) \\
D_v^{0,0} &= \gamma D^{0,0} \\
D_v^{1,1} &= \gamma v D^{0,0}
\end{aligned}
$$

With these, it is sufficient to compute the required $C^{m,n}$ and $D^{m,n}$ at only a few values of m/T and use interpolation to quickly compute them for any m/T. The infinite series are all well-behaved: they are exact at $v = 0$ and $v = 1$ using only the first term of the series, and an accuracy of less than 1% for all $v \in [0, 1]$ is achieved using a small number of terms.

2.B Evaluation of the collision rates

We discuss here the calculation of the collision integrals by a corrected and improved version of the method used in ref. [2]. The collision term for a given particle species is

$$
\begin{aligned}
\mathcal{C}[f_v(p)] &= \sum_i \frac{1}{2N_p E_p} \int \frac{d^3k\, d^3p'\, d^3k'}{(2\pi)^5 2E_k 2E_{p'} 2E_{k'}} \, |\mathcal{M}_i|^2 \delta^4(p + k - p' - k')\, \mathcal{P}[f_v(p)]\, ; \\
\mathcal{P}[f(p)] &= f(p) f(k) \big(1 \pm f(p')\big) \big(1 \pm f(k')\big) - f(p') f(k') \big(1 \pm f(p)\big) \big(1 \pm f(k)\big)\, ,
\end{aligned}
$$

where the sum is over all the relevant processes listed in Table 2.1, p is the momentum of the incoming particle whose distribution is being computed, N_p is its number of degrees of freedom, k is the momentum of the other incoming particle, and p', k' are the momenta of the outgoing particles. $|\mathcal{M}_i|^2$ is the squared scattering amplitude, summed over the helicities and colors of all the external particles. The distribution functions appearing in $\mathcal{P}$ are Fermi-Dirac or Bose-Einstein depending the respective external particles, and the $\pm$ is $+$ for bosons and $-$ for fermions.

$\mathcal{P}$ can be simplified by expanding it to linear order in the perturbations. Using the definition (2.1) of the distribution function with $\delta X(p) = \mu + \beta\gamma\delta\tau(E_p - vp_z) - \delta f/f'_v$, one can show that $\mathcal{P}$ becomes

$$\mathcal{P}[f] = f(p)f(k)(1 \pm f(p'))(1 \pm f(k')) \sum (\pm \delta X) \tag{2.15}$$

where the sum is over the external particles not in equilibrium and the $\pm$ in front of δX is $+$ for incoming particles and $-$ for outgoing particles.

The quantities needed for the fluid equations are the moments of $\mathcal{C}[f]$. These have the general form

$$\begin{aligned}
&\sum_i \frac{1}{2N_p E_p} \int \frac{d^3k\, d^3p'\, d^3k'}{(2\pi)^5 2E_k 2E_{p'} 2E_{k'}} |\mathcal{M}_i|^2 \delta^4(p + k - p' - k')\, \mathcal{P}[f_v]\, \frac{p_z^n}{E_p^m} \\
=&\sum_i \frac{1}{2N_p E_p} \int \frac{d^3k\, d^3p'\, d^3k'}{(2\pi)^5 2E_k 2E_{p'} 2E_{k'}} |\mathcal{M}_i|^2 \delta^4(p + k - p' - k')\, \mathcal{P}[f_v]\, \gamma^{n-m} \frac{(p_z + vE_p)^n}{(E_p + vp_z)^m}
\end{aligned}$$

where we boosted to the plasma frame to get the second line. Using the substitution (2.5), the perturbations become in that frame

$$\delta X(p) = \mu + \beta E_p \delta\tau - \left(\frac{E_p + vp_z}{p_z + vE_p}\right)\left(\frac{f_0}{f'_0}\right) u \tag{2.16}$$

Following the treatment of ref. [2], the calculation of the collision rates has been done to leading log accuracy, where it is justified to neglect the masses of all the external particles, which implies $E_p = p$. One can also neglect s-channel contributions and the interference

Process	$\lvert\mathcal{M}\rvert^2$
Top quark:	
$\bar{t}t \to gg$	$-\frac{128}{3} g_s^4 \frac{st}{(t-m_q^2)^2}$
$tg \to tg$	$-\frac{128}{3} g_s^4 \frac{su}{(u-m_q^2)^2} + 96 g_s^4 \frac{s^2+u^2}{(t-m_g^2)^2}$
$tq \to tq$	$160 g_s^4 \frac{s^2+u^2}{(t-m_g^2)^2}$
W bosons:	
$Wq \to qg$	$-72 g_s^2 g_w^2 \frac{st}{(t-m_q^2)^2}$
$Wg \to \bar{q}q$	$-72 g_s^2 g_w^2 \frac{st}{(t-m_q^2)^2}$
$WW \to \bar{f}f$	$-\frac{27}{2} g_w^4 st \left[\frac{3}{(t-m_q^2)^2} + \frac{1}{(t-m_l^2)^2}\right]$
$Wf \to Wf$	$360 g_w^4 \frac{u^2}{(t-m_W^2)^2} - \frac{27}{2} g_w^4 su \left[\frac{3}{(u-m_q^2)^2} + \frac{1}{(u-m_l^2)^2}\right]$

Table 2.1: Relevant processes for the top quark and W bosons and their corresponding scattering amplitude in the leading log approximation.

between diagrams because they are not logarithmic. To account for thermal effects, we use propagators of the form $1/(t-m^2)$ or $1/(u-m^2)$, where m is the exchanged particle's thermal mass. It is given by $m_g^2 = 2g_s^2T^2$ for gluons, $m_q^2 = g_s^2T^2/6$ for quarks, $m_W^2 = 5g_w^2T^2/3$ for W bosons and $m_l^2 = 3g_w^2T^2/32$ for leptons [81].

The top quark collisions are dominated by their strong interactions; we include only contributions to $|\mathcal{M}|^2$ of order g_s^4 for t interactions. For the W bosons, we include terms of order $g_s^2g_w^2$ and g_w^4. The relevant processes are shown with their corresponding $|\mathcal{M}|^2$ in Table 2.1 [5].

To evaluate the integrals in (2.16), one can first use the delta function and the symmetry of the integrand to analytically perform five of the twelve integrals. This can be done efficiently using the parametrization detailed in refs. [80, 82, 83]. The remaining seven integrals can be evaluated analytically using several approximations, justified to leading log accuracy. However, we have found that it is more precise to numerically compute these integrals, which can be done with a Monte Carlo algorithm. One can use a stratified sampling algorithm or VEGAS to reduce the variance, but this is generally not necessary since it only

[5] As pointed out in ref. [80], there were some errors in the expressions of the scattering amplitudes in [2]. They failed to include a 1/2 symmetry factor in the amplitude for $\bar{t}t \to gg$ and made some algebraic errors in $tq \to tq$ and $Wf \to Wf$.

takes a few seconds to get an accuracy of $\sim 1\%$ in most cases.

With the linearization of $\mathcal{P}[f]$ made in (2.15), the moments of the collision term can be written as linear combinations of the three perturbations: $T\left(\Gamma^{(i)}_\mu \mu + \Gamma^{(i)}_\tau \delta\tau + \Gamma^{(i)}_u u\right)$. Then the Γ matrix appearing in eq. (2.2) takes the form

$$\Gamma = T\begin{pmatrix} \Gamma^{(1)}_\mu & \Gamma^{(1)}_\tau & \Gamma^{(1)}_u \\ \Gamma^{(2)}_\mu & \Gamma^{(2)}_\tau & \Gamma^{(2)}_u \\ \Gamma^{(3)}_\mu & \Gamma^{(3)}_\tau & \Gamma^{(3)}_u \end{pmatrix} \tag{2.17}$$

where the $\Gamma^{(j)}_i$ coefficients are dimensionless. The v-dependence of the upper-left 2×2 block can be expressed analytically, giving

$$\begin{aligned} \Gamma^{(1)}_{\mu,t} &= \quad 0.00196, \quad \Gamma^{(1)}_{\mu,W} = 0.00239 \\ \Gamma^{(1)}_{\tau,t} &= \quad 0.00445, \quad \Gamma^{(1)}_{\tau,W} = 0.00512 \\ \Gamma^{(2)}_{\mu,t} &= \quad 0.00445\,\gamma, \quad \Gamma^{(2)}_{\mu,W} = 0.00512\,\gamma \\ \Gamma^{(2)}_{\tau,t} &= \quad 0.0177\,\gamma, \quad \Gamma^{(2)}_{\tau,W} = 0.0174\,\gamma \end{aligned}$$

The remaining components have been fitted to quartic polynomials:

$$
\begin{aligned}
\Gamma^{(1)}_{u,t} &= (5.36v - 4.49v^2 + 7.44v^3 - 5.90v^4) \times 10^{-3} \\
\Gamma^{(1)}_{u,W} &= (4.10v - 3.28v^2 + 5.51v^3 - 4.47v^4) \times 10^{-3} \\
\Gamma^{(2)}_{u,t} &= \gamma(1.67v + 1.38v^2 - 5.46v^3 + 2.85v^4) \times 10^{-2} \\
\Gamma^{(2)}_{u,W} &= \gamma(1.36v + 0.610v^2 - 2.90v^3 + 1.36v^4) \times 10^{-2} \\
\Gamma^{(3)}_{u,t} &= (4.07 - 2.14v^2 + 4.76v^3 - 4.37v^4) \times 10^{-3} \\
\Gamma^{(3)}_{u,W} &= (2.42 - 1.33v^2 + 3.14v^3 - 2.43v^4) \times 10^{-3} \\
\Gamma^{(3)}_{\mu,t} &= (0.948v + 2.38v^2 - 4.51v^3 + 3.07v^4) \times 10^{-3} \\
\Gamma^{(3)}_{\mu,W} &= (1.18v + 2.79v^2 - 5.31v^3 + 3.66v^4) \times 10^{-3} \\
\Gamma^{(3)}_{\tau,t} &= (2.26v + 4.82v^2 - 9.32v^3 + 6.54v^4) \times 10^{-3} \\
\Gamma^{(3)}_{\tau,W} &= (2.48v + 6.27v^2 - 11.9v^3 + 8.12v^4) \times 10^{-3}
\end{aligned}
$$

Our results and differ from those of [2] by factors of $\mathcal{O}(1)$. Even taking account of the errors previously mentioned, our results are still roughly 2 times smaller. As discussed in ref. [68], this discrepancy is due to the various leading log approximations made in [2] in order to analytically evaluate the collision integrals. Either procedure is valid to leading accuracy, which gives an estimate of the theoretical uncertainty associated with this approximation. It may be worthwhile (though quite laborious) to include subleading contributions for future studies relying upon these fluid equations.

References

[2] Guy D. Moore and Tomislav Prokopec. "How fast can the wall move? A Study of the electroweak phase transition dynamics". In: *Phys. Rev. D* 52 (1995), pp. 7182–7204. DOI: 10.1103/PhysRevD.52.7182. arXiv: hep-ph/9506475.

[3] James M. Cline and Kimmo Kainulainen. "Electroweak baryogenesis at high bubble wall velocities". In: *Phys. Rev. D* 101.6 (2020), p. 063525. DOI: 10.1103/PhysRevD.101.063525. arXiv: 2001.00568 [hep-ph].

[4] James M. Cline et al. "Baryogenesis and gravity waves from a UV-completed electroweak phase transition". In: (Feb. 2021). arXiv: 2102.12490 [hep-ph].

[25] K. Kajantie et al. "Is there a hot electroweak phase transition at $m_H \geq m_W$?" In: *Phys. Rev. Lett.* 77 (1996), pp. 2887–2890. DOI: 10.1103/PhysRevLett.77.2887. arXiv: hep-ph/9605288.

[40] James M. Cline. "Baryogenesis". In: *Les Houches Summer School - Session 86: Particle Physics and Cosmology: The Fabric of Spacetime*. Sept. 2006. arXiv: hep-ph/0609145.

[59] David E. Morrissey and Michael J. Ramsey-Musolf. "Electroweak baryogenesis". In: *New J. Phys.* 14 (2012), p. 125003. DOI: 10.1088/1367-2630/14/12/125003. arXiv: 1206.2942 [hep-ph].

[60] K. Kajantie et al. "The Electroweak phase transition: A Nonperturbative analysis". In: *Nucl. Phys. B* 466 (1996), pp. 189–258. DOI: 10.1016/0550-3213(96)00052-1. arXiv: hep-lat/9510020.

[61] Mark Trodden. "Electroweak baryogenesis". In: *Rev. Mod. Phys.* 71 (1999), pp. 1463–1500. DOI: 10.1103/RevModPhys.71.1463. arXiv: hep-ph/9803479.

[62] Chiara Caprini et al. "Science with the space-based interferometer eLISA. II: Gravitational waves from cosmological phase transitions". In: *JCAP* 04 (2016), p. 001. DOI: 10.1088/1475-7516/2016/04/001. arXiv: 1512.06239 [astro-ph.CO].

[63] Chiara Caprini et al. "Detecting gravitational waves from cosmological phase transitions with LISA: an update". In: *JCAP* 03 (2020), p. 024. DOI: 10.1088/1475-7516/2020/03/024. arXiv: 1910.13125 [astro-ph.CO].

[64] Jose R. Espinosa et al. "Energy Budget of Cosmological First-order Phase Transitions". In: *JCAP* 06 (2010), p. 028. DOI: 10.1088/1475-7516/2010/06/028. arXiv: 1004.4187 [hep-ph].

[65] Thomas Konstandin, Germano Nardini, and Ingo Rues. "From Boltzmann equations to steady wall velocities". In: *JCAP* 09 (2014), p. 028. DOI: 10.1088/1475-7516/2014/09/028. arXiv: 1407.3132 [hep-ph].

[66] Stephan J. Huber and Miguel Sopena. "An efficient approach to electroweak bubble velocities". In: (2013). arXiv: 1302.1044 [hep-ph].

[67] Ariel Mégevand and Alejandro D. Sánchez. "Velocity of electroweak bubble walls". In: *Nuclear Physics B* 825 (2010), p. 151. ISSN: 0550-3213. DOI: 10.1016/j.nuclphysb.2009.09.019. arXiv: 0908.3663 [hep-ph].

[68] Jonathan Kozaczuk. "Bubble Expansion and the Viability of Singlet-Driven Electroweak Baryogenesis". In: *JHEP* 10 (2015), p. 135. DOI: 10.1007/JHEP10(2015)135. arXiv: 1506.04741 [hep-ph].

[69] Dietrich Bodeker and Guy D. Moore. "Can electroweak bubble walls run away?" In: *JCAP* 05 (2009), p. 009. DOI: 10.1088/1475-7516/2009/05/009. arXiv: 0903.4099 [hep-ph].

[70] Dietrich Bodeker and Guy D. Moore. "Electroweak Bubble Wall Speed Limit". In: *JCAP* 05 (2017), p. 025. DOI: 10.1088/1475-7516/2017/05/025. arXiv: 1703.08215 [hep-ph].

[71] Ariel Mégevand. "Friction forces on phase transition fronts". In: *JCAP* 07 (2013), p. 045. DOI: 10.1088/1475-7516/2013/07/045. arXiv: 1303.4233 [astro-ph.CO].

[72] Guy D. Moore and Tomislav Prokopec. "Bubble wall velocity in a first order electroweak phase transition". In: *Phys. Rev. Lett.* 75 (1995), pp. 777–780. DOI: 10.1103/PhysRevLett.75.777. arXiv: hep-ph/9503296.

[73] P. John and M.G. Schmidt. "Do stops slow down electroweak bubble walls?" In: *Nucl. Phys. B* 598 (2001). [Erratum: Nucl.Phys.B 648, 449–452 (2003)], pp. 291–305. DOI: 10.1016/S0550-3213(00)00768-9. arXiv: hep-ph/0002050.

[74] Stephan J. Huber and Miguel Sopena. "The bubble wall velocity in the minimal supersymmetric light stop scenario". In: *Phys. Rev. D* 85 (2012), p. 103507. DOI: 10.1103/PhysRevD.85.103507. arXiv: 1112.1888 [hep-ph].

[75] Glauber C. Dorsch, Stephan J. Huber, and Thomas Konstandin. "Bubble wall velocities in the Standard Model and beyond". In: *JCAP* 12 (2018), p. 034. DOI: 10.1088/1475-7516/2018/12/034. arXiv: 1809.04907 [hep-ph].

[76] Michael Joyce, Tomislav Prokopec, and Neil Turok. "Nonlocal electroweak baryogenesis. Part 2: The Classical regime". In: *Phys. Rev. D* 53 (1996), pp. 2958–2980. DOI: 10.1103/PhysRevD.53.2958. arXiv: hep-ph/9410282.

[77] James M. Cline, Michael Joyce, and Kimmo Kainulainen. "Supersymmetric electroweak baryogenesis". In: *JHEP* 07 (2000), p. 018. DOI: 10.1088/1126-6708/2000/07/018. arXiv: hep-ph/0006119.

[78] Lars Fromme, Stephan J. Huber, and Michael Seniuch. "Baryogenesis in the two-Higgs doublet model". In: *JHEP* 11 (2006), p. 038. DOI: 10.1088/1126-6708/2006/11/038. arXiv: hep-ph/0605242.

[79] Lars Fromme and Stephan J. Huber. "Top transport in electroweak baryogenesis". In: *JHEP* 03 (2007), p. 049. DOI: 10.1088/1126-6708/2007/03/049. arXiv: hep-ph/0604159.

[80] Peter Arnold, Guy David Moore, and Laurence G Yaffe. "Transport coefficients in high temperature gauge theories (I): leading-log results". In: *JHEP* 0011 (2000), p. 001. DOI: 10.1088/1126-6708/2000/11/001. arXiv: hep-ph/0010177 [hep-ph].

[81] H. Arthur Weldon. "Effective Fermion Masses of Order gT in High Temperature Gauge Theories with Exact Chiral Invariance". In: *Phys. Rev. D* 26 (1982), p. 2789. DOI: 10.1103/PhysRevD.26.2789.

[82] Peter Arnold, Guy D Moore, and Laurence G Yaffe. "Transport coefficients in high temperature gauge theories: (II) Beyond leading log". In: *Journal of High Energy Physics* 0305 (2003), p. 051. DOI: 10.1088/1126-6708/2003/05/051. arXiv: hep-ph/0302165 [hep-ph].

[83] Guy D Moore. "Transport coefficients in large Nf gauge theory: testing hard thermal loops". In: *Journal of High Energy Physics* 0105 (2001), p. 039. ISSN: 1029-8479. DOI: 10.1088/1126-6708/2001/05/039. arXiv: hep-ph/0104121 [hep-ph].

Bridge

Now that we have derived an improved set of fluid equations reliable for all wall velocities, all the properties of the first-order EWPT within a given model can, in principle, be completely determined. More specifically, the BAU and GW spectrum produced during the PT, which are quite sensitive to the wall's velocity and shape, can be predicted. In the next chapter, we apply the new formalism previously developed to the Z_2-symmetric singlet scalar extension of the SM. We propose a UV-completed model with a vectorlike top partner, which yields a dimension-5 CP-violating operator. We then perform a scan of the parameter space to determine the likelihood of obtaining the observed BAU and a detectable GW signal.

Chapter 3

Baryogenesis and gravity waves from a UV-completed electroweak phase transition

Work published with James M. Cline, Avi Friedlander, Dong-Ming He, Kimmo Kainulainen and David Tucker-Smith as Ref. [4].

Abstract

We study gravity wave production and baryogenesis at the electroweak phase transition, in a real singlet scalar extension of the Standard Model, including vector-like top partners to generate the CP violation needed for electroweak baryogenesis (EWBG). The singlet makes the phase transition strongly first-order through its coupling to the Higgs boson, and it spontaneously breaks CP invariance through a dimension-5 contribution to the top quark mass term, generated by integrating out the heavy top quark partners. We improve on previous studies by incorporating updated transport equations, compatible with large bubble wall velocities. The wall speed and thickness are computed directly from the microphysical parameters rather than treating them as free parameters, allowing for a first-principles computation of the baryon asymmetry. The size of the CP-violating dimension-5 operator needed for EWBG is constrained

by collider, electroweak precision, and renormalization group running constraints. We identify regions of parameter space that can produce the observed baryon asymmetry or observable gravitational (GW) wave signals. Contrary to standard lore, we find that for strong deflagrations, the efficiencies of large baryon asymmetry production and strong GW signals can be *positively* correlated. However we find the overall likelihood of observably large GW signals to be smaller than estimated in previous studies. In particular, only detonation-type transitions are predicted to produce observably large gravitational waves.

3.1 Introduction

Phase transitions in the early universe provide an opportunity for probing physics at high scales through cosmological observables, in particular, if the transition is first order. In that case, it may be possible to explain the origin of baryonic matter through electroweak baryogenesis (EWBG) [6–9] or variants thereof [84]. Such transitions can also produce relic gravitational waves (GWs) that may be detectable by future experiments like LISA [63, 85], BBO [86], DECIGO [87, 88] and AEDGE [89].

It is remarkable that even though the electroweak phase transition (EWPT) is a smooth crossover in the standard model (SM) [25, 26], it can become first order with the addition of modest new physics input, in particular a singlet scalar coupling to the Higgs [28–37], that can also be probed in collider experiments [20, 90–100]. There have been many studies of such new physics models with respect to their potential to produce observable cosmological signals [10, 11, 15, 17, 19, 101–109]. However, it is challenging to make a first-principles connection between microphysical models and the baryon asymmetry or GW production, since these can be sensitive to the velocity v_w and thickness L_w of the bubble walls in the phase transition, which are numerically demanding to compute [2, 65, 68–70, 72, 73, 110–114]. Most previous studies that encompass EWBG and GW studies of the EWPT therefore leave v_w and L_w as free parameters. This limitation was addressed recently in Ref. [115], which undertook a comprehensive investigation of the EWPT enhanced by coupling the Higgs boson to a scalar singlet with Z_2 symmetry. The simplicity of this model facilitates doing an exhaustive search of its parameter space.

In the present work we continue the investigation started in Ref. [115], which determined v_w and L_w over much of the model parameter space, but did not try to predict the baryon asymmetry or GW production. Moreover, that study was limited to subsonic wall speeds, due to a breakdown of the fluid equations that determine the friction on the wall. Recently a set of improved fluid equations was postulated in Refs. [1, 3], that do not suffer from the subsonic limitation. We use these in the present work in order to fully explore the parameter space, where high v_w can be favorable to observable GWs, and also compatible with EWBG. It will be shown that for strong deflagrations, the fluid velocity in front of the wall saturates and even decreases with increasing wall velocity v_w. Since the walls become thinner at the same time, the baryon asymmetry is enhanced at larger wall velocities for these transitions, becoming *positively* correlated with a strong GW signal. Despite this positive correlation, we find that producing the observed baryon asymmetry together with a GW signal detectable in next generation observations is not possible, in contrast to previous estimates [15, 20]. The difference comes from several factors working in the same direction. For example, we find larger wall velocities and thicknesses than Ref. [15], which suppress the baryon asymmetry. Moreover, our GW fits include a recently derived suppression factor due to shock reheating [116, 117], which leads to a much weaker GW signal for strong deflagrations.

A further improvement in this work is to present an ultraviolet completion of the effective coupling that gives rise to the CP-violation needed for EWBG. We introduce heavy vectorlike top partners which when integrated out induce a CP-violating coupling of the singlet scalar s to top quarks, giving the source term for EWBG.[6] Although the effective operator description of this term is quite adequate for quantitatively understanding EWBG

[6] Hints of the presence of such a particle in LHC data were recently presented in Ref. [118].

[119, 120], its resolution in terms of underlying physics is necessary for quantifying how large its coefficient can be, consistent with laboratory constraints. We present the details in section 3.2, including comprehensive collider limits on the top partners and the subsequent constraints on the effective theory. The finite-temperature effective potential of the theory is also outlined there, along with a discussion of cosmological constraints on the small explicit breaking of the Z_2 symmetry, that is necessary for EWBG.

The paper continues in Sect. 3.3 with a brief description of our methodology for finding the high-temperature first-order phase transitions, and characterizing their strength. This is followed in Sect. 3.4 by a detailed account of how the bubble wall speed and shape are determined. The techniques for computing the baryon asymmetry and GW production are described in Sect. 3.5. We present the results of a Monte Carlo exploration of the model parameter space with respect to these observables in Sect. 3.6, with emphasis on the interplay between successful EWBG and potentially observable GWs. Conclusions are given in Sect. 3.7, followed by several appendices containing details about construction of the finite-temperature effective potential, solving junction conditions for the phase transition boundaries, and predicting GW production.

3.2 Z_2-symmetric singlet model

We study the Z_2-symmetric singlet scalar extension of the SM with a real singlet s coupled to the Higgs doublet H. The scalar potential is

$$V(H,s) = \mu_h^2 H^\dagger H + \lambda_h \left(H^\dagger H\right)^2 + \frac{\lambda_{hs}}{2}\left(H^\dagger H\right) s^2 + \frac{\mu_s^2}{2} s^2 + \frac{\lambda_s}{4} s^4. \tag{3.1}$$

We work in unitary gauge, which consists of taking $H = h/\sqrt{2}$; the Goldstone bosons still contribute to the one-loop and thermal corrections, but they are set to zero in the tree-level potential. We assume $\mu_h^2 < 0$ and $\mu_s^2 < 0$, which implies that the potential has non-trivial minimums at $v \equiv h = \pm|\mu_h|/\sqrt{\lambda_h} \approx 246$ GeV, $s = 0$ and $h = 0$, $s = \pm|\mu_s|/\sqrt{\lambda_s}$. The scalar fields' mass in the vacuum can then be written in terms of the parameters of the potential as $m_h^2 = -2\mu_h^2 \approx (125 \text{ GeV})^2$ and $m_s^2 = -\lambda_{hs}\mu_h^2/(2\lambda_h) + \mu_s^2$.

The other relevant interaction of s is a dimension-5 operator yielding an imaginary contribution to the top quark mass [121]:

$$\mathcal{L}_{BG} = -\frac{y_t}{\sqrt{2}} h\bar{t}_L \left(1 + i\frac{s}{\Lambda}\right) t_R + \text{H.c.} \tag{3.2}$$

This term will be ignored during the discussion on the phase transition; however it is essential for generating the baryon asymmetry, since it gives the CP-violating source term when s temporarily gets a VEV in the bubble walls of the electroweak phase transition. In Eq. (3.2) we have adopted a special limit of a more general model, in which the dimension-5 contribution is purely imaginary. This can be understood as a consequence of imposing CP in the effective Lagrangian, with s coupling like a pseudoscalar, $s \to -s$. Hence it is consistent to omit terms odd in s in the scalar potential (3.1), even though Eq. (3.2) is odd in s. The CP symmetry prevents a VEV from being generated for s by loops.

The effective operator is generated by integrating out a heavy singlet vectorlike top quark partner T, whose mass term and couplings to the third generation quarks $q_L = (t_L, b_L)$, Higgs and singlet fields are

$$y_t \bar{q}_L H t_R + \eta_1 \bar{q}_L H T_R + i\eta_2 \bar{T}_L s t_R + M\bar{T}_L T_R + \text{H.c.} \tag{3.3}$$

including also the SM q_L-Higgs coupling. This is invariant under CP if $s \to -s$.[7] Integrating out T leads to the effective operator in (3.2) with scale

$$\Lambda = \frac{y_t M}{\eta_1 \eta_2}\,. \tag{3.4}$$

We consider experimental constraints on the scale Λ below.

[7] The interaction term $i\eta_3 \overline{T}_L s T_R$ also respects CP for real η_3. We neglect it to simplify our analysis.

In previous literature, thermal corrections were frequently approximated by including just the first term of the high-temperature expansion of the thermal functions presented in the Appendix B. However, this approximation fails at temperatures below the mass of particles strongly coupled to the Higgs, as can happen in models with a high degree of supercooling. Therefore, we employ the full one-loop thermal functions. This will be shown to have a large impact on the values of the tunneling action, and thus of the nucleation temperature. In addition to the tree-level potential and the thermal corrections, we also include the one-loop correction and the thermal mass Parwani resummation [122]. The complete effective potential then becomes

$$V_{\text{eff}} = V_{\text{tree}} + V_{\text{CW}} + V_T + \delta V. \tag{3.5}$$

The details are presented in Appendix 3.A.

3.2.1 Laboratory constraints

It is important to determine how low the scale Λ of the dimension-5 operator in Eq. (3.4) can be, since it has a strong impact on the baryon asymmetry η_b; in the limit of large Λ, η_b scales as $1/\Lambda$. The relevant masses and couplings are constrained by direct searches for the top partner and precision electroweak studies. Moreover the properties of the singlet s are constrained by collider searches.

After electroweak symmetry breaking, a Dirac mass term $(\bar{t}_L, \bar{T}_L)\left(\begin{smallmatrix} m_t & \mu \\ 0 & M \end{smallmatrix}\right)\left(\begin{smallmatrix} t_R \\ T_R \end{smallmatrix}\right)$ is generated for t, T, with $m_t = y_t v/\sqrt{2}$ and $\mu = \eta_1 v/\sqrt{2}$ that is diagonalized by separate rotations on (t_R, T_R) and (t_L, T_L), with mixing angles

$$\tan 2\theta_L = 2\frac{M\mu}{M^2 - m_t^2 - \mu^2}, \quad \tan 2\theta_R = 2\frac{m_t\mu}{M^2 + \mu^2 - m_t^2}\,. \tag{3.6}$$

For example, we consider a benchmark point with $\eta_1 = 0.55$ and a physical T mass $M_T = 800$ GeV, which correspond to $M = 794\,\text{GeV}$ and mixing angles $\theta_L = 0.126$ and $\theta_R = 0.027$. The relations between y_t and the physical top mass differ from the SM ones by less than 1%, which is allowed by current LHC constraints [123, 124]. For sufficiently large η_2, decays of T to $ht/Zt/Wb$ induced by mixing are highly subdominant to $T \to st$, and searches for vector-like top partners that focus on the former channels are evaded. Near the Goldstone-equivalent limit (which should apply reasonably well for $M_T = 800$ GeV and relatively small s masses, $m_s \sim 100$ GeV), the branching ratio for $T \to st$ is

$$B(T \to st) \simeq \frac{\eta_2^2}{\eta_2^2 + 2\eta_1^2} \,. \tag{3.7}$$

We roughly estimate from Refs. [125, 126] that for $M_T = 800$ GeV, vector-like quark searches that target SM final states are evaded provided $B(T \to st) \gtrsim 90\%$, corresponding to $\eta \gtrsim 2.4$ for our benchmark point. Ref. [127] (see Fig. 1 of contribution 5; also [128]) has reinterpreted collider bounds to constrain the parameter space (m_s, M_T) for models in which $T \to st$ dominates, finding that top partner masses above ~ 750 GeV are allowed in the case where s decays 100% into two gluons. This is true in our model, where the dominant s decays are induced by the loop diagrams shown in Fig. 3.1. One can estimate that the gluon final state dominates over that of b quarks by a factor of $(g_s^2 m_s / g_w^2 m_b)^2 \gtrsim 10^3$, and over decays into photons by $(g_s/e)^4 \sim 300$. Precision electroweak data constrain the additional contributions to the oblique parameters, especially T, which is corrected by [129]

$$\Delta T = T_{\rm sm} s_L^2 \left(-(1 + c_L^2) + s_L^2\, r + 2 c_L^2\, \frac{r}{r-1} \ln r \right) \lesssim 0.1 \,, \tag{3.8}$$

where $T_{\rm sm} = 1.19$ is the SM value, $c_L = \cos\theta_L$, $s_L = \sin\theta_L$, and $r = (M_T/m_t)^2$; the upper limit is from section 10 of [130]. The benchmark point chosen above almost saturates this constraint, giving $\Delta T \simeq 0.09$.

There are also direct searches for resonant production of the singlet, by gluon-gluon fusion. The coupling of s to t in the mass eigenstate basis is $y_{st} = \eta_2 \cos\theta_R \sin\theta_L \sim \eta_2\theta_L$, while that to T is $y_{sT} = -\eta_2 \cos\theta_L \sin\theta_R \sim -\eta_2\theta_R$. The squared matrix element for the

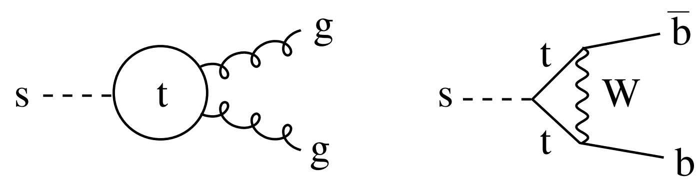

Figure 3.1: Feynman diagrams for decay of the singlet s. The decay into gluons is by far the dominant channel.

decays $s \to gg$ is [131]

$$|\mathcal{M}|^2 = \left(\frac{\alpha_s}{\pi}\right)^2 m_s^4 \left| \sum_{i=t,T} \frac{y_{si}}{m_i} \tau_i \left[\sin^{-1}\left(\tau_i^{-1/2}\right)\right]^2 \right|^2, \tag{3.9}$$

where $\tau_i = 4m_i^2/m_s^2$. The parton-level production cross section for $gg \to s$ is $\hat{\sigma} = \pi|\mathcal{M}|^2\delta(\hat{s} - m_s^2)/(256\,\hat{s})$ where the 256 comes from averaging over gluon colors and spins. Integrating this over the gluon PDFs gives the hadron-level cross section

$$\sigma(pp \to s) = \frac{\pi}{256\,m_s^4}|\mathcal{M}|^2\mathcal{L}_g \equiv \frac{\pi}{256\,m_s^4}|\mathcal{M}|^2 \int_{m_s^2/s}^1 \frac{dx}{x}[xf_g](x)[xf_g](m_s^2/sx) \tag{3.10}$$

in which dependence on m_s drops out except in the parton luminosity factor $\mathcal{L}_g$. This production is probed via decays $s \to \gamma\gamma$, whose branching ratio is approximately $B(s \to \gamma\gamma) = (8/9)\alpha^2/\alpha_s^2$ [131]. For the dominant $s \to gg$ decay into gluons, in principle LHC dijet resonance searches could be constraining, but these exist only for $m_s \gtrsim 500\,\mathrm{GeV}$ which is beyond the range of interest for the present study. To a good approximation, $\sigma(pp \to s)$ is determined by m_s and Λ. In Fig. 3.2(a) we show limits from ATLAS [132, 133] and CMS [134] on $\sigma B(s \to \gamma\gamma)$ as a function of m_s, along with the predictions for various Λ, and in Fig. 3.2(b) we show the associated lower bounds on Λ. In the low-mass region (65 GeV $< m_s <$ 110 GeV), lower bounds on Λ range roughly from 400 GeV to 650 GeV; in the intermediate-mass region (110 GeV $< m_s <$ 160 GeV), Λ is not yet constrained by diphoton resonance searches, and for much of the high-mass region ($m_s >$ 160 GeV), Λ is bounded to be above 1 TeV. For our subsequent scans of parameter space, we adopt a fixed reference

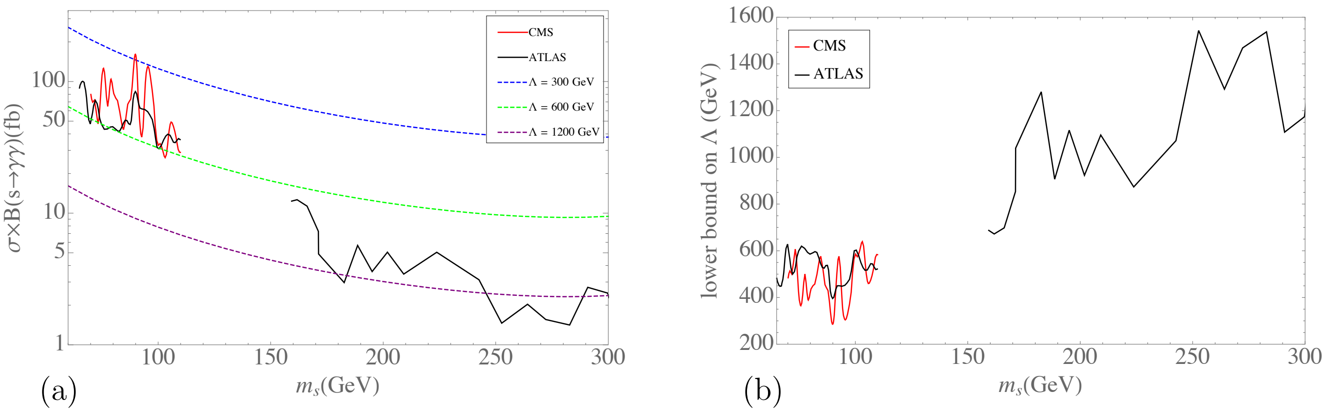

Figure 3.2: Left (a): experimental limits from ATLAS [132, 133] and CMS [134] for resonant production of s by gg fusion followed by decays into photons (solid lines), versus predictions at different values of of Λ. Right (b): corresponding lower bounds on Λ.

value for Λ,

$$\Lambda_{\text{ref}} = 540 \text{ GeV}, \tag{3.11}$$

which is large enough to be consistent with much of the low-m_s region. Because Λ_{ref} is well below the lower-bounds on Λ in the high-mass region, we confine our scans to $m_s < 160$ GeV for consistency.[8]

The constraints from precision electroweak data, diphoton resonance searches, and vector-like quark searches are shown in the η_1-η_2 plane in Fig. 3.3, for $M_T = 800$ GeV, where we approximate the T search constraints by the requirement $B(T \to st) > 0.9$, and for $M_T = 1300$ GeV, heavy enough to evade T searches for any $B(T \to st)$. For the chosen m_s, it is apparent that the reference value $\Lambda = 540$ GeV is attainable for $\eta_2 \gtrsim 2.5$ for $M_T = 800$ GeV and $\eta_2 \gtrsim 3$ for $M_T = 1300$ GeV. For slightly heavier s in the window 110 GeV $< m_s <$ 160 GeV, diphoton resonance searches are evaded and the red contours disappear. In this case even lower values of Λ are allowed provided one is willing to consider larger values of η_2. Since the baryon asymmetry η_b scales roughly as $1/\Lambda$, it is straightforward to reinterpret our final results for larger (or smaller) Λ. From the results of Section 3.6 one

[8]Although we do not pursue this point here, lower values of Λ are consistent with $m_s > 160$ GeV if $B(s \to \gamma\gamma)$ is suppressed, for example by a dominant invisible decay channel; LHC constraints on $t\bar{t}$ plus missing energy [135, 136] are in that case evaded for $M_T \gtrsim 1350$ GeV.

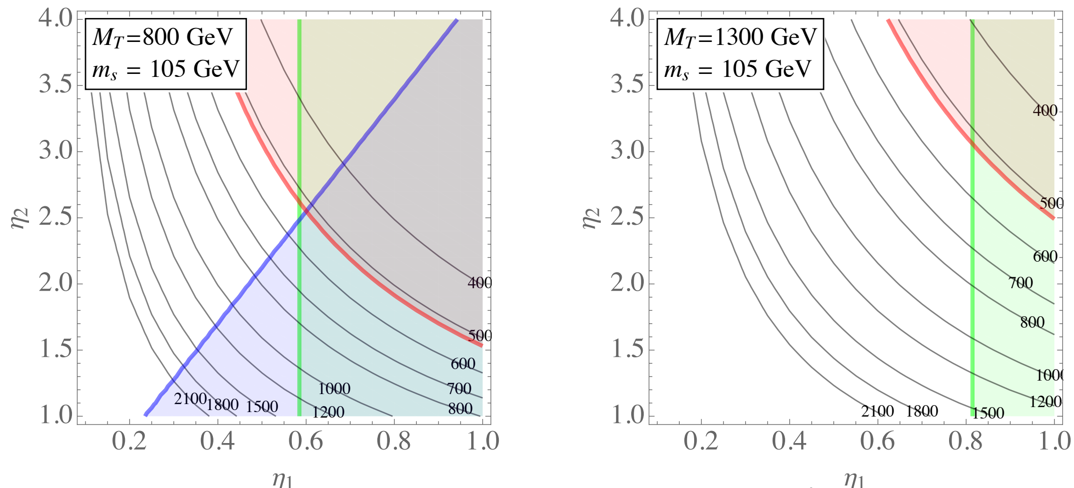

Figure 3.3: For selected T and s masses, constraints on η_1 and η_2 from precision electroweak data (green), diphoton resonance searches [133, 134](red), and searches for vector-like quarks [125] (blue), along with contours of Λ in GeV. The allowed region is unshaded.

can infer that a significant fraction of models remain viable for baryogenesis for $\Lambda = 2\Lambda_{\rm ref}$ (or for even larger Λ), a scale consistent with more modest couplings, $\eta_2 \sim 1.5$.

Allowing for very large values of η_2 could invalidate the effective theory above the heavy top partner threshold M at scales only slightly larger than M, which would require us to specify additional new physics in order to have a complete description. There are two principal challenges arising from the running of the couplings,

$$\frac{d\eta_2}{d\ln\mu} \cong \frac{\eta_2^3}{4\pi^2} \tag{3.12}$$

$$\frac{d\lambda_s}{d\ln\mu} \cong \frac{9\,\lambda_s^2}{8\pi^2} - \frac{3\,\eta_2^4}{2\pi^2} + \frac{\lambda_s\eta_2^2}{2\pi^2} \tag{3.13}$$

where μ denotes the renormalization scale. The most serious problem is that for large values of η_2, the self-coupling λ_s is quickly driven to zero, and the scalar potential becomes unstable. The second is that η_2 reaches a Landau pole at somewhat higher scales. The first problem could be ameliorated by coupling additional scalars to s, without impacting our results for EWBG or GWs. For this reason, we do not limit the scope of our investigation based on the running of λ_s. Regarding the second problem, we note that even for $\eta_2 = 3$, the Landau pole is nearly an order of magnitude above M, which we consider to be an acceptably large range of validity for the effective theory.

3.2.2 Explicit breaking of Z_2 symmetry

Since we are considering a scenario where the Z_2 symmetry $s \to -s$ is spontaneously broken during the early universe and restored at the EWPT, domain walls form before the EWPT, and the universe will consist of domains with random signs of the s condensate. The source term for EWBG that arises from Eq. (3.2) is linear in s, resulting in baryon asymmetries of opposite signs, that could average to zero after completion of the EWPT. To avoid this outcome, the Z_2 symmetry should be explicitly broken, by potential terms

$$V_b = \mu_b s(h^2 - v^2) + \mu_b' s^3 \tag{3.14}$$

with small coefficients μ_b, μ_b'. We have used the freedom of shifting s by a constant to remove a possible tadpole of s at the true vacuum $(h, s) = (v, 0)$.

The presence of the biasing potential V_b can prevent the baryon washout in several ways. First, if the transition to the broken-s phase is of second order, even a small tilt can suffice to make the lower-energy vacuum dominate. Second, in a first order transition, symmetry breaking terms can bias the bubble nucleation rates to prefer the lower-energy vacuum. Indeed, the number of bubbles nucleated during the transition is $n \sim \int_{t_c}^{t_*} \mathrm{d}t\, \Gamma(t)$, where t_* is the time when transition completes, and $\Gamma(t) \sim \exp(-S_3/T)$. Writing the action as $S_{3\pm} = \bar{S}_3 \mp \delta S$ in the two respective vacua, the relative number density of bubbles in each phase at the end of the transition becomes $n_+/n_- \approx \exp(2\,\delta S_*/T_*)$. In general [137] $S_3 \propto E$, where E is the coefficient of the cubic term in the potential. Using this scaling we may write $\delta S_* = (\delta E/E_0)\bar{S}_3^*$, where typically $S_3^*/T_* \approx 100$. In our model $E_0 \approx (3\lambda_s)^{3/2} T/12\pi$, so taking $V_b = \mu_{b'} s^3$, corresponding to $\delta E = \mu_{b'}$, and $T_* \approx 100\,\mathrm{GeV}$, the condition for single-phase vacuum dominance becomes $\mu_{b'} \gtrsim 0.1\,\lambda_s^{3/2}\,\mathrm{GeV}$. Barring very large λ_s, this condition is easily met with no limitations on our analysis.

Even if a domain wall network forms, the higher-energy domains will collapse due to pressure gradients, and we should ensure that this process completes before the EWPT. The collapse starts with the acceleration of a wall at relative position R according to $\ddot{R} = -\Delta V/\tau$, where $\tau \sim \sqrt{\lambda_s} w^3$ is the surface tension (distinct from the tension σ used above in the nucleation estimate), $\Delta V \sim V_b(0, w) \sim \mu_b' w^3$ is the difference in the vacuum energies, and $w \sim \mu_s/\sqrt{\lambda_s}$ is the singlet VEV. Using $H = 1/2t$ and $T \approx 100\,\mathrm{GeV}$, one finds that walls reach light speed in time

$$\frac{\delta t}{t} = \frac{\tau H}{\delta V} \sim 10^{-5}\sqrt{\lambda_s}\left(\frac{\mathrm{eV}}{\mu_{b'}}\right) , \tag{3.15}$$

which is practically instantaneous on the timescales of interest, for reasonable values of $\mu_{b'}$. We note that global symmetries like Z_2 are expected to be broken by quantum gravity effects, so that it could be reasonable to anticipate $\mu_b' \sim v^2/M_p \sim 0.1\,\mathrm{eV}$, which is large enough from the perspective of Eq. (3.15).

The higher energy domains subsequently collapse at the speed of light, since there is no appreciable friction. The time required for this process to complete is determined by $R_* = 2a(t_1)\int_{t_1}^{t_2} dt/a(t)$, where R_* is the comoving size of the domain wall separation. By the Kibble mechanism one expects that $R_* = AH_*^{-1}$ with $A \lesssim 1$, leading to the ratio of domain wall collapse to formation times $t_2/t_1 = (1+A/2)^2$. The temperature interval corresponding to this time interval is $\Delta T/T \approx A$, assuming that the growth phase also proceeded at the speed of light.

The temperature of the first phase transition, T_1 can be estimated as that when $\partial^2 V/\partial s^2$ becomes negative. In the approximation of neglecting V_b, and keeping only leading terms in the high-T expansion, one finds $T_1^2 - T_c^2 \sim \lambda_h w_c^2/c_s$ where T_c is the critical temperature of the EWPT, and $c_s = (3\lambda_s + 2\lambda_{hs})/12$. Thus the temperature difference between transitions is of order $\Delta T_{1c} \sim \lambda_h w^2/(c_s T_c)$. Requiring that $\Delta T_{1c}/T_c > A$ then gives

$$A < \frac{12\lambda_h}{3\lambda_s + 2\lambda_{hs}}\,\frac{w_c^2}{T_c^2} \sim O(1)\,. \tag{3.16}$$

Given that $A \sim (T_*/S_3^*)(\Delta T/T)_* \sim 10^{-2}$-$10^{-4}$ [2], this is a very weak constraint. We conclude that it is easy to avoid cosmological problems associated with the domain walls by small symmetry breaking terms, that do not affect the rest of our analysis.

3.3 Phase Transition and Bubble Nucleation

In the examples of interest for this work, the phase transition in the Z_2-symmetric singlet model proceeds in two steps: starting from the high-temperature global minimum $h = s = 0$, a transition first occurs to nonzero s, while the Higgs field remains at $h = 0$. This is followed by the EWPT, in which s returns to zero and h develops its VEV. The h^2s^2 interaction provides the potential barrier to make this a first order transition.

As usual, the first order transition occurs at the bubble nucleation temperature T_n, which is below the critical temperature T_c, where the two potential minima become degenerate,

$$V_{\text{eff}}(h, s, T_c)\big|_{\substack{h=0,\\ s=w_c}} = V_{\text{eff}}(h, s, T_c)\big|_{\substack{h=v_c,\\ s=0}} \tag{3.17}$$

Bubble nucleation occurs when the vacuum decay rate per unit volume Γ_d becomes comparable to H^4, the Hubble rate per Hubble volume. The decay rate is [23]

$$\Gamma_d \cong T^4 \left(\frac{S_3}{2\pi T}\right)^{3/2} \exp\left(-\frac{S_3}{T}\right) , \tag{3.18}$$

where S_3 is the O(3) symmetric action,

$$S_3 = 4\pi \int r^2 dr \left(\frac{1}{2}\left(\frac{dh}{dr}\right)^2 + \frac{1}{2}\left(\frac{ds}{dr}\right)^2 + V_{\text{eff}}\right) . \tag{3.19}$$

The precise criterion that we use for nucleation is

$$\exp\left(-S_3/T_n\right) = \frac{3}{4\pi}\left(\frac{H\left(T_n\right)}{T_n}\right)^4 \left(\frac{2\pi T_n}{S_3}\right)^{3/2} , \tag{3.20}$$

which is satisfied when $S_3/T_n \cong 140$ [138]. We used the package CosmoTransitions [24] to calculate S_3. The action obtained with the full potential can differ significantly from the commonly used thin wall approximation [139, 140] or the approximation of evaluating it along the minimal integration path for the potential [15]. We compare the predictions for nucleation of these approximations to the full one-loop result, for several exemplary models, in Table 3.1. The approximate methods tend to underestimate the action, giving a higher nucleation temperature; hence we use the values derived from the full one-loop action in the following.

λ_{hs}	m_s (GeV)	$S_3/T\vert_{T=100\text{ GeV}}$			T_n (GeV)		
		Thin wall	MPP	1-loop	Thin wall	MPP	1-loop
1	120	234	277	427	93.5	92.6	89.8
1.7	200	68.7	101	151	115.6	109.8	100.1
3.2	300	37.9	36.8	54.3	134.3	133.8	121.6

Table 3.1: Examples of the dimensionless tunneling action S_3/T, evaluated at $T = 100\,\text{GeV}$, and ensuing nucleation temperatures, computed within the thin wall and minimal potential path (MPP) approximations, compared with the value obtained using the resummed one-loop potential. In there example, $\lambda_s = 1$ and $\Lambda = 540$ GeV.

There are two complementary parameters for characterizing the strength of the first order transition. One is the ratio of the Higgs VEV to the temperature at the time of nucleation, v_n/T_n, which is especially relevant for EWBG, as we will discuss in Sect. 3.5.2. The other, which is more important for GW production, is the ratio of released vacuum energy density to the radiation energy density [141, 142]:

$$\alpha = \frac{1}{\rho_\gamma}\left(\Delta V - \frac{T_n}{4}\Delta\frac{dV}{dT}\right), \tag{3.21}$$

where $\rho_\gamma = g_*\pi^2 T_n^4/30$, g_* is the effective number of degrees of freedom in the plasma (we use $g_* = 106.75$) and Δ denotes the difference between the unbroken and broken phase. α quantifies the amount of supercooling that occurs prior to nucleation, which determines how much free energy is available for the production of GWs.

3.4 Wall velocity and shape

The derivation of the wall velocity and field profiles is a technically demanding problem [2], that was first addressed in the context of Higgs plus singlet models in Refs. [65, 68, 143], in various approximations. One must solve the equations of motion (EOM) for the scalar sector coupled to a perfect fluid,

$$\begin{aligned} E_h(z) &\equiv -h''(z) + \frac{dV_{\text{eff}}(h,s;T_+)}{dh} + \sum_i N_i \frac{dm_i^2}{dh} \int \frac{d^3p}{(2\pi)^3 2E}\, \delta f_i(\vec{p},z) = 0, \\ E_s(z) &\equiv -s''(z) + \frac{dV_{\text{eff}}(h,s;T_+)}{ds} + \sum_i N_i \frac{dm_i^2}{ds} \int \frac{d^3p}{(2\pi)^3 2E}\, \delta f_i(\vec{p},z) = 0, \end{aligned} \tag{3.22}$$

where z is the direction normal to the wall, that is to a good approximation planar by the time it has reached its terminal velocity. We use a sign convention where the wall is moving to the left, so that $z > 0$ corresponds to the broken phase. The sum is over all the relevant species coupled to h or s in the plasma, with N_i and m_i respectively denoting the number of degrees of freedom and the field-dependent mass of the corresponding species, and δf_i the deviation from equilibrium of its distribution function. All the temperature-dependent quantities appearing in these equations are evaluated at T_+, which is the plasma's temperature just in front of the wall. We calculate T_+ in Appendix 3.B using the method described in Ref. [142], and δf_i will be computed in Sect. 3.4.1.

The terms in Eqs. (3.22) with δf_i represent the friction[9] of the plasma on the wall, that leads to a terminal wall speed $v_w < 1$, unless the friction is too small and the wall runs away to speeds close to that of light. Following previous work, we take the dominant sources of friction to be from the top quark ($i = t$) and electroweak gauge bosons ($i = W$), neglecting the contributions to friction from the Higgs itself and from the singlet. This approximation is bolstered by the smaller number of degrees of freedom $N_h = N_s = 1$ compared to $N_t = 12$ and $N_W = 9$, as well as the smallness of the Higgs self-coupling λ_h and the not-too-large values

[9] The term "friction" is strictly speaking not correct, but we adopt this commonly used terminology. More accurately, the last terms in (3.22) represent the additional pressure created by the out-of-equilibrium perturbations, which modify the effective action in the same way as the usual thermal excitations.

of the cross-coupling λ_{hs} that will be favored in the subsequent analysis. Then the friction term for the s equation of motion vanishes, since s couples only to itself and to the Higgs, apart from its suppressed dimension-5 coupling to t. This allows for some simplification in the following procedure.

In Ref. [115], a similar study of the present model was done, where no *a priori* restriction of the wall shape was assumed, but it was found that the actual shapes conform to a very good approximation to the tanh profiles

$$\begin{aligned} h(z) &= \frac{h_0}{2}[1+\tanh(z/L_h)], \\ s(z) &= \frac{s_0}{2}[1-\tanh(z/L_s+\delta)], \end{aligned} \tag{3.23}$$

where h_0 and s_0 are respectively the vacuum expectation values (VEV) of the h and s fields in the broken and unbroken phases. Hence we adopt the ansatz (3.23), which allows the singlet and Higgs wall profiles to have different widths, and to be offset from each other by a distance $L_s\delta$. The s field's VEV is taken to be the usual one evaluated at T_+, which solves the equation $dV_{\text{eff}}(0,s;T_+)/ds\big|_{s=s_0}=0$. The situation is more complicated for the h field, for which the Higgs VEV should be evaluated at T_-, the plasma's temperature behind the wall. Since we are fixing a constant temperature T_+ in the potential, the change in the effective action due to the shift in the background temperature must be accounted for by the perturbation in the broken phase. As a consequence we are choosing h_0 so that it solves the equation

$$\left(\frac{dV_{\text{eff}}(h,0;T_+)}{dh}+\sum_i N_i\frac{dm_i^2}{dh}\int\frac{d^3p}{(2\pi)^3 2E}\,\delta f_i(\vec{p},z)\right)\Bigg|_{h=h_0,z\to\infty}=0\,. \tag{3.24}$$

This choice guarantees that the Higgs EOM is satisfied far behind the wall. We will estimate the uncertainty of our results due to this approximation in Sect. 3.6.4.

To approximately solve the Higgs EOM, one can define two independent moments $M_{1,2}$ of $E_h(z)$, and assume that they both vanish at the optimal values of v_w and L_h. A convenient

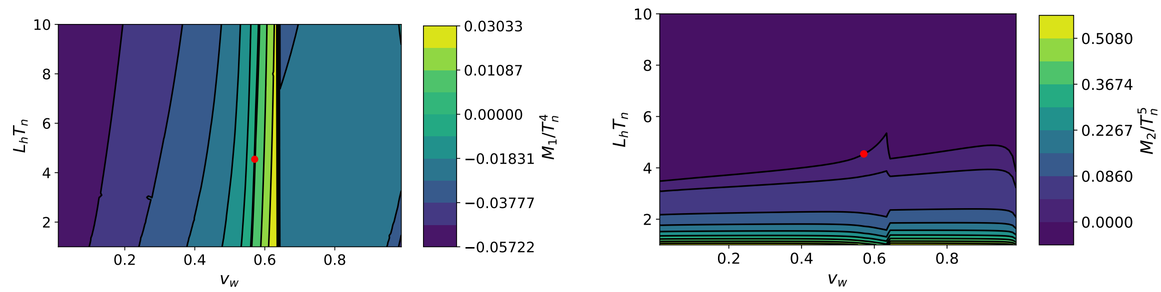

(a) (b)

Figure 3.4: Moments of the Higgs EOM (a) M_1 and (b) M_2 as a function of the wall velocity v_w and the Higgs wall width L_h for a model with parameters $\lambda_{hs} = 1$, $\lambda_s = 1$ and $m_s = 130$ GeV. The red dot is the solution of Eqs. (3.25,3.26). As expected, M_1 is roughly independent of L_h while M_2 depend mainly on L_h. The moments are discontinuous at $v_w \approx 0.63$ because this corresponds (for this specific model) to the boundary between hybrid and detonation walls, where v_+ and T_+ are discontinuous.

choice is [65]

$$M_1 \equiv \int dz\, E_h(z)\, h'(z) = 0, \tag{3.25}$$

$$M_2 \equiv \int dz\, E_h(z)[2h(z) - h_0]\, h'(z) = 0. \tag{3.26}$$

These also have intuitive physical interpretations that naturally distinguish them as good predictors of the wall speed and thickness, respectively. M_1 is a measure of the net pressure on the wall, so that Eq. (3.25) can be interpreted as the requirement that a stationary wall should have a vanishing total pressure; nonvanishing M_1 would cause it to accelerate. Therefore one expects that Eq. (3.25) principally determines the wall speed v_w, while depending only weakly on the thickness L_h. With our sign convention, M_1 can be interpreted as the pressure in front of the wall minus the pressure behind it, so that $M_1 > 0$ corresponds to a net force slowing down the wall. On the other hand, M_2 is a measure of the pressure gradient in the wall. If nonvanishing, it would lead to compression or stretching of the wall, causing L_h to change. Hence Eq. (3.26) mainly determines L_h, and depends only weakly on v_w. The two equations are approximately decoupled, facilitating their numerical solution. This is illustrated in Fig. 3.4, which shows the dependence of M_1 and M_2 on v_w and L_h.

We chose a different approach to determine the singlet wall parameters L_s and δ. Instead of solving moment equations analogous to (3.25,3.26), one can determine their values by minimizing the s field action

$$\begin{aligned} S(L_s,\delta) &= \int dz \left\{ \frac{1}{2}(s')^2 + [V_{\text{eff}}(h,s,T_+) - V_{\text{eff}}(h,s^*,T_+)] \right\} \\ &= \frac{s_0^2}{6L_s} + \int dz \; [V_{\text{eff}}(h,s,T_+) - V_{\text{eff}}(h,s^*,T_+)] \,, \end{aligned} \tag{3.27}$$

with respect to L_s and δ. Here s^* is a field configuration with arbitrary fixed parameters L_s^* and δ^*, that we choose to be $L_s^* = L_h$ and $\delta^* = 0$. The second term is just a constant, but it allows for the convergence of the integral by canceling the contributions of V_{eff} at $z \to \pm\infty$. This method has the advantage that it does not depend on any arbitrary choice of moments, and it is more efficient to numerically minimize the function of two variables than to solve the system of equations for the moments of the EOMs.

3.4.1 Transport equations for fluid perturbations

The final step toward the complete determination of the velocity and the shape of the wall is to compute the distribution functions' deviations from equilibrium δf_i, by solving the Boltzmann equation for each relevant species in the plasma. The method of approximating the full Boltzmann equation by a truncated set of coupled fluid equations was originally carried out in Ref. [2], for the regime of slowly-moving walls (see also Ref. [65]). This approach was recently improved in Ref. [1] in order to be able to treat wall speeds close to or exceeding the speed of sound consistently. We briefly summarize the formalism, which we use in the present study.

The out-of-equilibrium distribution function can be parametrized in the wall frame as

$$f = \frac{1}{\exp[\beta\gamma(E - v_+ p_z)(1-\delta\tau) - \mu] \pm 1} + \delta f_u, \tag{3.28}$$

where $\beta = 1/T_+$ and the $\pm$ is $+$ for fermions and $-$ for bosons. $\delta\tau$ and μ are the dimensionless temperature and chemical potential perturbations from equilibrium, and δf_u is a velocity perturbation whose form is unspecified, but is constrained by $\int d^3p\, \delta f_u = 0$. By assuming that the perturbations are small, one can expand f to linear order in μ, $\delta\tau$ and the velocity perturbation δf_u to obtain

$$\delta f \approx \delta f_u - f'[\mu + \beta\gamma\, \delta\tau(E - v_+ p_z)], \tag{3.29}$$

with

$$f' = \frac{d}{dX}\frac{1}{e^X \pm 1}\bigg|_{X=\beta\gamma(E-v_+p_z)}. \tag{3.30}$$

To simplify the problem, one models the plasma as being made of three different species: the top quark, the W bosons (shorthand for $W^\pm$ and Z) and a background fluid, which includes all the remaining degrees of freedom. It is convenient to write the velocity perturbation as $u \propto \int d^3p\,(p_z/E)\,\delta f_u$ when constructing the moments of the linearized Boltzmann equation. By taking three such moments, using the weighting factors 1, E and p_z/E, the perturbations are determined by transport equations

$$\begin{aligned} Aq' + \Gamma q &= S, & (3.31)\\ q'_{\rm bg} &= -\tilde{A}^{-1}_{\rm bg}(\Gamma_{{\rm bg},t}q_t + \Gamma_{{\rm bg},W}q_W), & (3.32) \end{aligned}$$

where prime denotes d/dz, $q_i = (\mu_i, \delta\tau_i, u_i)^\intercal$, $q = (q_W^\intercal, q_t^\intercal)^\intercal$, the Γ matrices are collision terms, and S is the source term, whose definitions, as well as those of the the matrices A, Γ, $\tilde{A}^{-1}_{\rm bg}$, $\Gamma_{{\rm bg},t}$, $\Gamma_{{\rm bg},W}$, can be found in Ref. [1]. If A and Γ were independent of z, one could use the Green's function method to solve Eq. (3.31); however, A is a function of $m_i(z)/T$. To deal with this dependence on z, we discretize space, $z \to z_0 + n\Delta z$ with $n = 0, \cdots, N-1$, and Fourier transform Eq. (3.31),

$$\frac{2\pi i}{\Delta z}\left(\frac{k}{N} - \left\lfloor\frac{2k}{N}\right\rfloor\right)\tilde{q}_k + \frac{1}{N}\sum_{l=0}^{N-1}\widetilde{(A^{-1}\Gamma)}_{(k-l)\,{\rm mod}\,N}\,\tilde{q}_l = \widetilde{(A^{-1}S)}_k, \quad k = 0, \cdots, N-1, \tag{3.33}$$

where the tilde denotes the discrete Fourier transform. This is a linear system that is straightforward to numerically solve for $\tilde{q}_k$. Once $\tilde{q}_k$ is known, it can be transformed back and interpolated to obtain $q(z)$. Eq. (3.32) can then be integrated using a Runge-Kutta algorithm.

Finally, one can substitute Eq. (3.29) into the Higgs EOM (3.22) to express the friction in terms of the fluid perturbations μ_i, $\delta\tau_i$ and u_i. This leads to the result

$$\int \frac{d^3p}{(2\pi)^3 2E}\,\delta f_i = \frac{T_+^2}{2}\left[C_0^{1,0}\mu_i + C_0^{0,0}(\delta\tau_i + \delta\tau_{\rm bg}) + D_v^{0,-1}(u_i + u_{\rm bg})\right], \tag{3.34}$$

where the functions $C_v^{m,n}$ and $D_v^{m,n}$ can be found in Ref. [1].

3.5 Cosmological signatures

We have now established the machinery needed to compute all the relevant properties of the first order phase transition bubbles, starting from the fundamental parameters of the microscopic Lagrangian. In this section we describe how to apply these results for the estimation of GW spectra and the baryon asymmetry.

3.5.1 Gravitational Waves

We follow the methodology of Refs. [63, 116, 117, 142, 144] to estimate future gravitational wave detectors' sensitivity to the GW signals that can be produced by a first-order electroweak phase transition in the models under consideration. The GW spectrum $\Omega_{\rm gw}(f)$ is the contribution per frequency octave to the energy density in gravitational waves, *i.e.*, $\int \Omega_{\rm gw}\, d\ln f$ is the fraction of energy density compared to the critical density of the universe. The spectrum gets separate contributions from the scalar fields, sound waves in the plasma and magnetohydrodynamical turbulence created by the phase transition:

$$\Omega_{\rm gw}(f) = \Omega_\phi(f) + \Omega_{\rm sw}(f) + \Omega_{\rm m}(f)\,, \tag{3.35}$$

Each of these contributions depends on the wall velocity v_w, the supercooling parameter α (Eq. (3.21)), and the inverse duration of the phase transition, defined as

$$\beta = H(T_n)T_n \, \frac{d}{dT}\frac{S_3}{T}\bigg|_{T=T_n} . \tag{3.36}$$

Another useful quantity is the mean bubble separation, which can be written in terms of v_w and β as [63]

$$R = \frac{(8\pi)^{1/3}}{\beta}\,\max[c_s, v_w]. \tag{3.37}$$

It has been shown in Ref. [70] that interactions with gauge bosons prevent the wall from running away indefinitely towards $\gamma \to \infty$. In that case, the contribution from the scalar fields has been shown to be negligible. Furthermore, the estimates for the magnetohydrodynamical turbulence are very uncertain and sensitive to the details of the phase transition dynamics [145], and are expected to be much smaller than the contribution from sound waves. Hence, we consider only the effects from the latter, and set $\Omega_{\rm m}(f) = \Omega_\phi(f) = 0$. For convenience, we reproduce the numerical fits of the GW spectra derived in Refs. [63, 116, 117, 142, 144] in appendix 3.C.

We will use these predictions with respect to four proposed space-based GW detectors: LISA [5], AEDGE [89], BBO [146] and DECIGO [87]. A successful GW detection depends upon having a large enough signal-to-noise ratio [147],

$$\mathrm{SNR} = \sqrt{\mathcal{T}\int_{f_{\rm min}}^{f_{\rm max}} df \left[\frac{\Omega_{\rm gw}(f)}{\Omega_{\rm sens}(f)}\right]^2} \tag{3.38}$$

where $\Omega_{\rm sens}(f)$ denotes the sensitivity of the detector[10] and $\mathcal{T}$ is the duration of the mission. The sensitivity curves for the detector LISA, BBO and DECIGO were obtained from Ref. [148]. Whenever SNR is greater than a given threshold $\mathrm{SNR}_{\rm thr}$, we conclude that the signal

[10]For AEDGE, we use the envelope of minimal strain that can be achieved by each resonance, with its width scaled to approximate $\Omega_{\rm sens}(f)$. This curve is expected to reproduce the correct SNR up to about 10%.

can be detected. In general, this threshold can depend upon the configuration of the detector. For all the experiments, we take $\mathrm{SNR}_{\mathrm{thr}} = 10$ and $\mathcal{T} = 1.26 \times 10^8$ s. In the following, $\mathrm{SNR}_{\mathrm{max}}$ will designate the maximum signal-to-noise ratio detected by one of the detectors:

$$\mathrm{SNR}_{\mathrm{max}} \equiv \max[\mathrm{SNR}_{\mathrm{LISA}}, \mathrm{SNR}_{\mathrm{AEDGE}}, \mathrm{SNR}_{\mathrm{BBO}}, \mathrm{SNR}_{\mathrm{DECIGO}}]. \tag{3.39}$$

While $\Omega_{\mathrm{sens}}(f)$ can be obtained from the noise spectrum of a detector, it is not practical to compare it to the GW spectrum directly; one needs to compute the SNR to determine if a signal is detectable. A useful tool for visualizing the sensitivity of a detector is the peak-integrated sensivity curve (PISC) defined in Refs. [149–151], which is a generalization of the power-law sensitivity curve [152]. The main advantage of the former is that it does not assume a power-law spectrum, hence it conserves all the information about the SNR. In the simple case where one considers the contribution from only one GW source, the PISC can be obtained by factorizing the GW spectrum as

$$\Omega_{\mathrm{gw}}(f) = \Omega_{\mathrm{p}}\, S(f, f_{\mathrm{p}}), \tag{3.40}$$

where f_{p} and $\Omega_{\mathrm{p}} = \max[\Omega_{\mathrm{gw}}(f)]$ are the peak frequency and GW amplitude and S is a function that parametrizes the spectrum's shape, with a maximum at $f = f_{\mathrm{p}}$ and $S(f_{\mathrm{p}}, f_{\mathrm{p}}) = 1$. One can then write the SNR as

$$\mathrm{SNR} = \mathrm{SNR}_{\mathrm{thr}}\, \frac{\Omega_{\mathrm{p}}}{\Omega_{\mathrm{PISC}}(f_{\mathrm{p}})}, \tag{3.41}$$

with the PISC

$$\Omega_{\mathrm{PISC}}(f_{\mathrm{p}}) = \mathrm{SNR}_{\mathrm{thr}} \left[\mathcal{T} \int_{f_{\mathrm{min}}}^{f_{\mathrm{max}}} df \left(\frac{S(f, f_{\mathrm{p}})}{\Omega_{\mathrm{sens}}(f)}\right)^2\right]^{-1/2}. \tag{3.42}$$

By construction, any GW signal that peaks above the PISC has $\mathrm{SNR} > \mathrm{SNR}_{\mathrm{thr}}$ and can therefore be detected.

3.5.2 Baryogenesis

The mechanism of electroweak baryogenesis is sensitive to the speed and shape of the bubble wall during the phase transition. In most previous studies, these quantities were treated as free parameters to be varied, but in this work we have already derived them, as was discussed in Section 3.4. An important requirement for EWBG is to avoid the washout, by baryon-violating sphaleron interactions, of the generated asymmetry inside the bubbles of broken phase, once they have formed. This leads to the well-known constraint [51]

$$\frac{v_n}{T_n} > 1.1\,, \tag{3.43}$$

which was derived within the SM for low Higgs masses where a first order EWPT was possible. The bound can be slightly higher (up to 1.2) in singlet-extended models [52], depending upon the parameters, due to the sphaleron energy being modified. Here we adopt the SM constraint (3.43); we checked that taking the more stringent bound 1.2 removes $\sim 5\%$ of viable models in the scan over parameter space to be described below.

Near the bubble wall, CP-violating processes associated with the effective interaction in Eq. (3.2) give rise to perturbations of the plasma, that result in a local chemical potential μ_{B_L} for left-handed baryons, which by imposing the chemical equilibrium of strong-sphaleron interactions, is related to those of the t_L, t_R^c and b_L quarks by

$$\mu_{B_L} = \frac{1}{2}\left(1+4K_1^t\right)\mu_t + \frac{1}{2}\left(1+4K_1^b\right)\mu_b - 2K_1^t\mu_{t^c}\,, \tag{3.44}$$

where the K_1^a functions were defined in [79] ($K_1^a = D_0^a$ in the notation of [3]). The μ_{B_L} potential biases sphalerons, leading to baryon number violation, whose associated Boltzmann equation can be integrated to obtain the baryon to photon ratio[11]

$$\eta_b = \frac{405\,\Gamma_{\rm sph}}{4\pi^2 v_w \gamma_w g_* T}\int dz\,\mu_{B_L} f_{\rm sph} e^{-45\Gamma_{\rm sph}|z|/4v_w}\,, \tag{3.45}$$

[11]The extra factor of $\gamma_w = 1/\sqrt{1-v_w^2}$ in the denominator was pointed out by Ref. [3].

where $f_{\rm sph}$ quantifies the diminution of the sphaleron rate in the broken phase [153, 154]. The most challenging step for the computation of EWBG is in the determination of the chemical potentials μ_{t_L}, $\mu_{t_R^c}$ and μ_{b_L} appearing in Eq. (3.44). They satisfy fluid equations resembling the network (3.31,3.32), except that the potentials relevant for EWBG are CP-odd, whereas those determining the wall profiles are CP-even.

The CP-odd transport equations have been discussed extensively in the literature, leading to two schools of thought as to how best to compute the source term for the CP asymmetries. These are commonly known as the VEV-insertion [155, 156] or WKB (semiclassical) [76, 77, 157–160] methods, respectively. A detailed discussion and comparison of the two approaches was recently given in Ref. [3], which quantified the well-known fact that the VEV-insertion source tends to predict a larger baryon asymmetry than the WKB source, by a factor of ~ 10. In the present work we adopt the WKB approach, which was updated in Ref. [3] to allow for consistently treating walls moving near or above the sound speed. In addition, that reference computed the source term arising from the same effective interaction (3.2) as in the present model, so we can directly adopt the CP-odd fluid equations studied there.

3.6 Monte Carlo results

To study the properties of the phase transition, we performed a scan over the parameter space of the models, imposing several constraints. We found that variations in λ_s do not qualitatively change the results, prompting us to initially fix its value at $\lambda_s = 1$, leaving λ_{hs} and m_s as the free scalar potential parameters. We will first discuss this slice of parameter space, and later consider the quantitative dependence on λ_s. We also chose $\Lambda = 540$ GeV, which is conservative since there are no collider constraints on its value for singlet masses in the region $m_s = [110, 160]$ GeV. Recall that Λ is important for the determination of the baryon asymmetry η_b, which is expected to scale roughly as $1/\Lambda$. Finally, in order to prevent Higgs invisible decays, we imposed $m_s > m_h/2$.

We used a Markov Chain Monte Carlo algorithm to efficiently explore the regions of parameter space having desired phase transition properties. Starting with an initial model satisfying the sphaleron bound (3.43), one generates a new trial model by randomly varying the parameters λ_i by small increments δ_i. The trial model is added to the chain using a conditional probability

$$P = \min\left[\frac{v_n/T_n}{1.1}, 1\right] \tag{3.46}$$

that favors models having strong first order phase transitions, and for which a solution to the nucleation condition (3.20) can be found. We adjust the δ_i so that roughly half of the models are kept in successive trials, with larger values of δ_i being more likely to result in a rejection.

This procedure yielded 842 models with strong phase transitions, of which 712 were amenable to finding solutions for the moment equations (3.25-3.26). Our analysis typically works for $\gamma \lesssim 10$; for faster walls, the algorithm for determining the wall properties becomes numerically unstable and does not yield reliable results. This is due to the large (500×500) matrix $(\widetilde{A^{-1}\Gamma})$ of eq. (3.33) becoming singular as $v_w \to 1$. It is therefore difficult to determine the type of solution of the 130 remaining models using our methodology alone: they could either stabilize at ultrarelativistic speeds, or (from a naive perspective—see below) run away indefinitely towards $\gamma \to \infty$. The value of the baryon asymmetry should not be affected by this ambiguity since it is negligible for $v_w \approx 1$. The GW spectrum produced during the phase transition is sensitive to this distinction since runaway walls have a nonnegligible fraction of their energy stored in the wall, while for non-runaway walls, the energy gets dissipated into the plasma, so the fraction of energy in the wall becomes negligible. This ambiguity can be lifted using the result of Ref. [70], which found that in the limit $\gamma \to \infty$, interactions between gauge bosons and the wall create a pressure proportional to γ, preventing it from running away.[12] We therefore assume that the 130 models without a solution to the moment

[12]More recently, the authors of Ref. [111] have carried out an all-orders resummation at leading-log acuracy, finding that the pressure is in fact proportional to γ^2 for fast-moving walls.

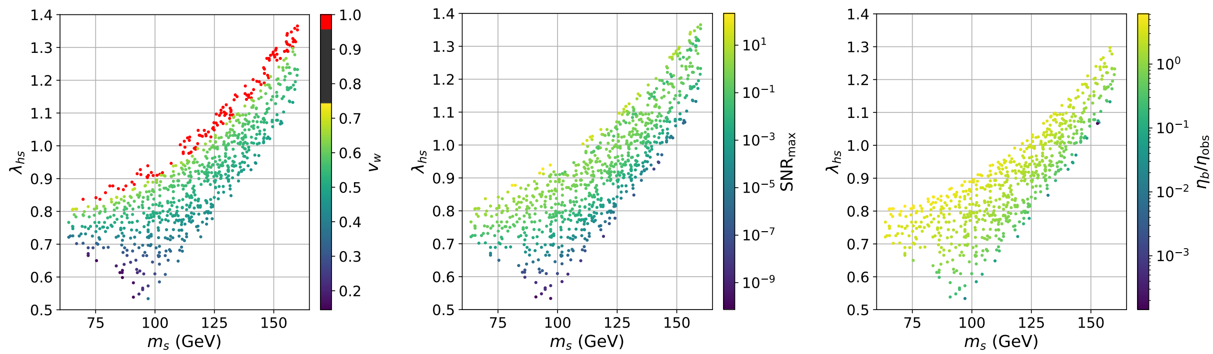

(a) (b) (c)

Figure 3.5: Scan of the parameter space with $\lambda_s = 1$ and $\Lambda = 540$ GeV. The colors represent (a) the terminal wall velocity v_w, (b) the maximum signal-to-noise ratio of gravitational waves that could be detected by either LISA, AEDGE, BBO or DECIGO and (c) the baryon asymmetry (in units of the observed value) produced by the phase transition. The red dots in (a) correspond to detonation solutions with $v_w \approx 1$, and the latter are not included in (c) since they are expected to produce a negligible baryon asymmetry (see text).

equations (3.25-3.26) correspond to non-runaway walls with $v_w \approx 1$. The results of this scan, showing the calculated wall velocity, signal-to-noise ratio of gravity waves observable by at least one of the proposed experiments (LISA, AEDGE, BBO or DECIGO), and the predicted baryon asymmetry (in units of the observed value) are presented in Fig. 3.5, in the plane of of λ_{hs} versus m_s.

3.6.1 Deflagration versus detonation solutions

A striking feature of these results is that all the detonation solutions have $v_w \approx 1$.[13] We have tested that this is not specific to the choice of fixed parameter values, but also holds for all models having $0.01 < \lambda_s < 8$ and $\Lambda > 110$ GeV; hence it seems to be a general property of phase transitions in the Z_2-symmetric singlet framework. One can understand this behavior by considering the net pressure opposing the wall's expansion, M_1 (recall Eq. (3.25-3.26)), as a function of the wall velocity, as illustrated in Fig. 3.6. It shows how M_1 differs when evaluated with the appropriate quantities v_+, T_+ rather than the incorrect ones v_w, T_n. Using

[13]Strictly speaking there are models with $v_w < 1$ detonation solutions but these always have another solution at a lower velocity corresponding to a deflagration or hybrid wall. Then only the latter solution is physically relevant, since the bubble is created at $v_w = 0$ and accelerates until it reaches the solution with the lowest velocity.

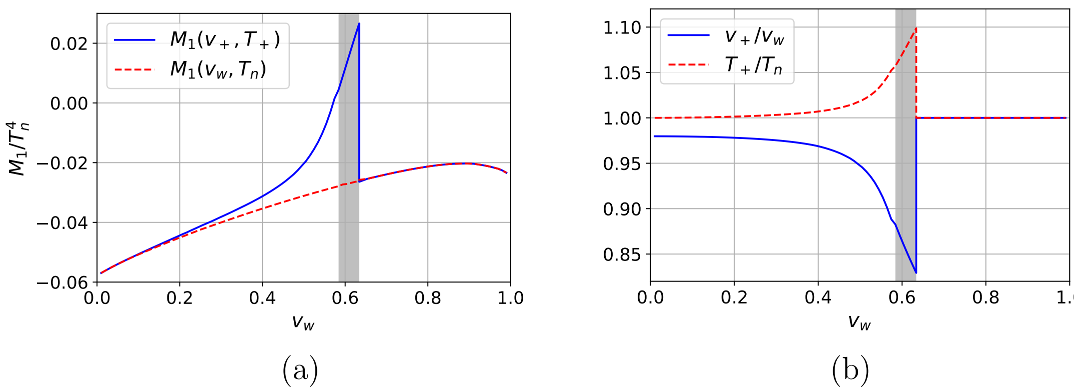

Figure 3.6: Left (a): Pressure on the wall M_1 as a function of the wall velocity v_w. The solid (dashed) line corresponds to the pressure evaluated at the velocity v_+ (v_w) and the temperature T_+ (T_n). Right (b): Relation between the naive variables v_w, T_n and the ones relevant for evaluating M_1, namely v_+ and T_+. Both plots were obtained using the parameters $m_s = 130$ GeV, $\lambda_{hs} = \lambda_s = 1$ and $L_h = 5/T_n$. The shaded region corresponds to hybrid wall solutions characterized by $c_s < v_w < \xi_J$.

the latter, we would find no solution to the equation $M_1 = 0$ for the exemplary model used in Fig. 3.6, and would then incorrectly conclude that it satisfies $v_w \approx 1$. The relevant quantities are those measured right in front of the wall, v_+ and T_+. The speed v_+ is smaller than v_w for $v_w < \xi_J$, which would lower the pressure against the wall (ξ_J is the Jouguet velocity, defined as the smallest velocity a detonation solution can have). However, in the same region, the temperature T_+ is larger than T_n, which causes the pressure to increase. The latter effect turns out to dominate over the former. Indeed, the actual pressure, represented by the solid blue line in Fig. 3.6, increases much more rapidly than $M_1(v_w, T_n)$ close to the speed of sound. This qualitative difference allows for a solution to $M_1 = 0$, which would have been missed if we had used the naive quantities v_w and T_n.

We find that the previous statements apply quite generally: for all models, $T_+ > T_n$ when $v_w < \xi_J$, and this always leads to a much higher pressure on the wall, even if the difference between T_+ and T_n is quite small; the pressure barrier at $v_w = \xi_J$ is always greater than the maximum possible value for a detonation solution. Therefore, if the phase transition is strong enough to overcome the pressure barrier at ξ_J, the solution becomes a detonation, but the pressure in the region $v_w > \xi_J$ is never enough to prevent it from accelerating towards

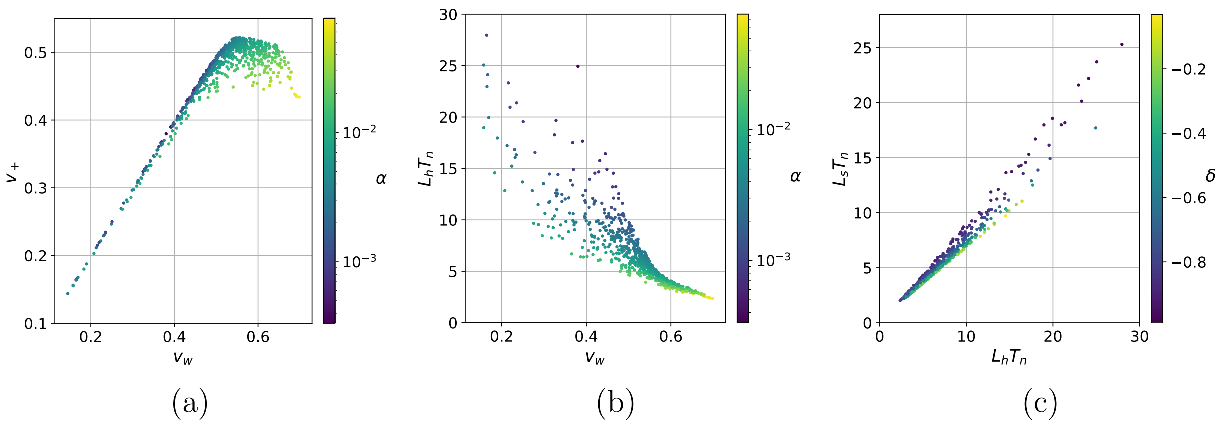

Figure 3.7: Shape and velocity of the deflagration solutions. (a) Correlation between the wall velocity v_w and the fluid velocity in front of the wall, v_+; (b) dimensionless wall width $L_h \times T_n$ versus v_w; and (c) correlation of the s and h wall widths. Colors indicate the supercooling parameter α (Eq. (3.21)) in (a,b), or the wall offset δ (Eq. (3.23)) in (c).

$v_w \approx 1$. If the phase transition is weaker, the pressure barrier is high enough to impede the detonation, and it becomes a deflagration or hybrid solution.

The wall thickness and speed for the models with deflagration[14] solutions are shown in Fig. 3.7, which demonstrates that the behaviors for subsonic (deflagration) and supersonic (hybrid) walls are qualitatively different. Subsonic walls generally have $v_+ \approx v_w$, which is expected since the fluid should not be strongly perturbed by a slowly moving wall. The wall width is not uniquely determined by v_w, but there exists a clear correlation, with slower walls being thicker. For supersonic cases, the correlation between v_+ and v_w gets inverted: higher wall velocity leads to lower v_+. The wall width becomes uniquely determined by v_w and the relation between these two variables is to a good approximation linear. One observes that stronger phase transitions, quantified by higher values of α, generally produce faster and thinner walls. Even for the strongest transitions our solutions still have wall thickness $LT \gtrsim 3$. Since the semiclassical force mostly affects particles with momenta $\langle k_z \rangle \sim T$, we find $L\langle k_z \rangle \gtrsim 3$, so that the semiclassical approximation is still valid. In fact the semiclassical picture has been shown to remain valid for surprisingly narrow walls [161], working very well for $L\langle k_z \rangle \approx 4$ and still reasonably for $L\langle k_z \rangle \approx 2$. There is a linear correlation between the h

[14]Henceforth we take "deflagration" to also include hybrid solutions

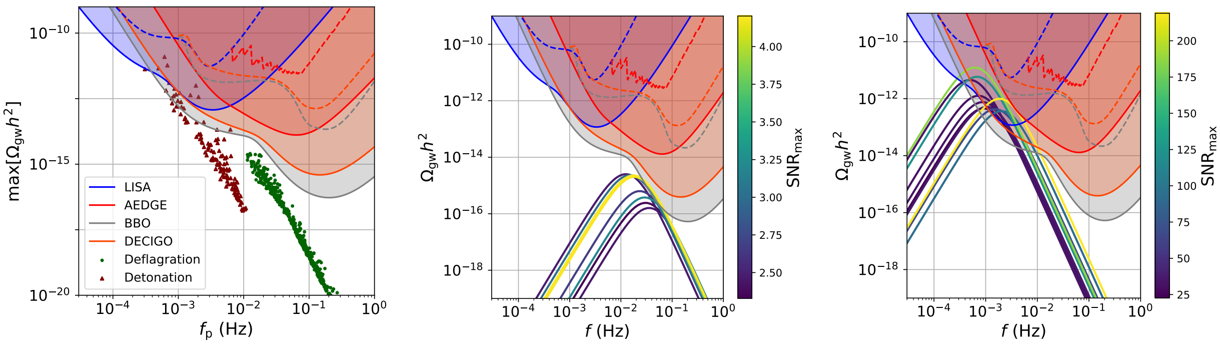

(a) (b) (c)

Figure 3.8: (a): Maximum amplitude of GW as a function of the peak frequency $f_{\rm p}$ with the peak-integrated sensitivity curve $\Omega_{\rm PISC}h^2$ (solid line) and the sensitivity $\Omega_{\rm sens}h^2$ (dashed line) of the four considered detectors. (b) and (c): Spectrum of GWs produced by the 10 models with the highest $\text{SNR}_{\rm max}$ for (b) deflagration and (c) detonation solutions.

and s wall widths, but the slope is not 1; in all cases, we find that $L_h > L_s$. The distribution of wall offset values δ is also indicated in Fig. 3.7(c).

3.6.2 Baryogenesis and gravity wave production

Of the 842 sampled models, 517 are able to generate the baryon asymmetry at a level large enough to agree with observations, and 20 detonation walls can produce observable gravitational waves. We found no detectable deflagration solutions. More detailed results are presented in Table 3.2. The complementarity of the experiments considered here, with respect to the present model, can be appreciated by considering the relation between the maximum GW amplitude[15] $\max[\Omega_{\rm gw}h^2]$ and the frequency of this peak amplitude $f_{\rm max}$, as shown in Fig. 3.8 (a). The peak frequency of the strongest detonation walls are positioned exactly in LISA's region of maximal sensitivity, while the peak frequency of the deflgration solutions are closer to the peak sensitivity of AEDGE, DECIGO and BBO. The complete spectrum's shape are also shown in Fig. 3.8 (b,c) for deflagration and detonation solutions respectively. We conclude that detonation walls could be probed by LISA, DECIGO and BBO, but not by AEDGE.

[15] $h = 0.678$ is the reduced Hubble constant defined by $H_0 = 100h\,\text{km}\,\text{s}^{-1}\,\text{Mpc}^{-1}$ [38].

In previous studies, where the wall velocity was considered as a free parameter, there was an expectation that baryogenesis would be less efficient with increasing v_w, whereas gravity waves would become more so. In the present study, where v_w is not adjustable but is a derived parameter, we surprisingly find that rather than EWBG and stronger GWs being anticorrelated, instead they are positively correlated, as is illustrated in Fig. 3.9 (a). This can be understood from the fact (see Fig. 3.7 (b)) that L_h is a decreasing function of v_w, which enhances EWBG. Moreover, the relevant velocity for EWBG is v_+, which is a decreasing function of v_w for supersonic walls, and is bounded by $v_+ < c_s$; this effect also enhances EWBG for fast-moving walls. The actual relation between η_b and v_w is shown in Fig. 3.9 (b) and, at least for supersonic walls, there is a positive correlation between these two variables. Fig. 3.9 also indicates that the supercooling parameter α is positively correlated with both η_b and $\mathrm{SNR}_{\mathrm{max}}$: stronger phase transitions generally lead to both higher GW and baryon production.

Detailed predictions for EWBG in the Z_2 symmetric model were previously made in Refs. [15] and [20], as opposed to merely requiring the sphaleron bound (3.43) to be satisfied. Comparisons with the present work are hindered by the fact that different source terms for the CP asymmetry were assumed. In Ref. [15], the dimension-6 coupling $i(y_t/\sqrt{2})(s/\Lambda)^2\bar{h}t_L t_R$ was used, rather than the dimension-5 coupling in Eq. (3.2). Moreover, a value $v_w = 0.2$ was taken for the wall velocity, and an estimate $L_h = v_n/\sqrt{8V_b}$ was made for the wall width, where v_n is the Higgs VEV at the nucleation temperature, and V_b is the potential barrier between the two minima. For the same potential parameters ($\lambda_s = 0.1$) as in [15], we find no values of v_w below 0.43, and our determination of L_h is two to three times larger than the estimate in [15]. Both of these discrepancies would lead to overestimating the efficiency of EWBG, helping to explain why Ref. [15] obtains a high frequency of successful models, despite the extra suppression that should result from using a dimension-6 source term.

In Ref. [20], the dimension-5 coupling to leptons rather than the top quark was studied, and a different formalism (the VEV insertion approximation) for computing the CP

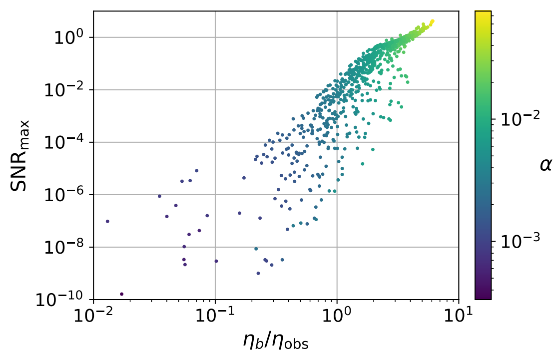

(a)

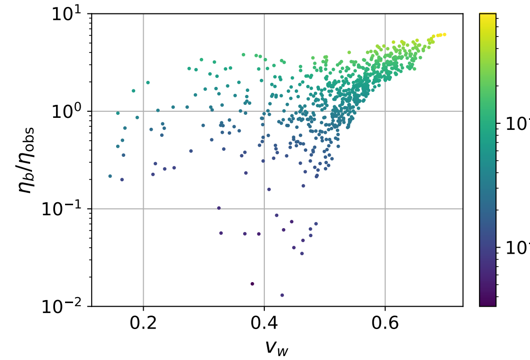

(b)

Figure 3.9: (a): Relation between the $\mathrm{SNR}_{\max}$ and the baryon asymmetry produced by the phase transition. (b): Baryon asymmetry as a function of the wall velocity. Both plots only show the deflagration models.

asymmetry was employed, which tends to give significantly larger estimates for the baryon asymmetry than the WKB method that we adopt [3]. For the parameters of the benchmark models taken in that paper, we find significantly higher wall velocities, $v_w \sim 0.6$-0.7 than the values $v_w \lesssim 0.1$ that were needed to match the observed baryon asymmetry there. This can be compensated by increasing the CP-violating phase $\phi = 0.02$ assumed there by a factor of ~ 10. We are reanalyzing this alternative source term within the EWBG formalism used in the present paper (work in progress).

3.6.3 Dependence on λ_s and Λ

To study the quantitative dependence on the singlet self-coupling λ_s, we performed 3 other scans similar to the one previously described, taking $\lambda_s = 0.01,\ 0.1$ and 8 (the largest value being near the limit of perturbative unitarity) and $\Lambda = 540$ GeV. The results of these scans are summarized in Table 3.2. We find that EWBG remains efficient for $\lambda_s \gtrsim 0.1$. Again, we found no deflagration walls producing detectable GW, and no models detectable by AEDGE. These results confirm that only detonation solutions, which are not good candidates for EWBG, could be probed by GW detectors. Increasing λ_s generally leads to stronger phase transitions, resulting in more models with successful EWBG and detectable GWs.

The value of Λ (recall Eq. (3.4)) can in principle also have an effect on the strength of the phase transition, through the effective potential's dependence on the top quark mass. The leading thermal term added to the potential varies like $h^2s^2T^2/\Lambda^2$, which becomes negligible at high Λ, but could significantly modify the behavior of the phase transition for $\Lambda \sim T_n$, resulting in a larger baryon asymmetry and GW production. We have verified that this term is already subdominant when $\Lambda = 540$ GeV. However, for $m_s > 110$ GeV, the weaker constraints allow for values of Λ as low as 300 GeV, which could have an important effect on the phase transition.

To test the sensitivity to lower values of Λ, we repeated the previous scans using $\Lambda = \Lambda_{\text{min}}(m_s)$, where Λ_{min} is given by

$$\Lambda_{\text{min}}(m_s) = \begin{cases} 540\text{ GeV}, & m_s < 110\text{ GeV} \\ 300\text{ GeV}, & 110\text{ GeV} < m_s < 160\text{ GeV} \end{cases} \tag{3.47}$$

The results are shown in Table 3.2[16]. As one could anticipate from the relation $\eta_b \sim 1/\Lambda$, EWBG is more efficient at lower values of Λ. One can also see that the number of detonation walls or walls generating detectable GW does not change substantially, which indicates that the lower values of Λ do not change the character of the phase transition.

3.6.4 Theoretical uncertainties

In Ref. [1], the integrals that determine the collision rates Γ appearing in the Boltzmann equation network (3.31-3.32) were reevaluated, and it was noticed that the leading log approximation that was used in their derivation leads to theoretical uncertainties of $\mathcal{O}(1)$ in the fractional error. To study the impact of these uncertainties on our results, we recomputed the wall velocity with uniformly rescaled collision rates, $\Gamma \to 2\Gamma$ and $\Gamma \to \Gamma/2$. The ensuing variations of velocity Δv and wall width ΔL are shown in Figs. 3.10 (a) and (b) respectively.

[16] The $\lambda_s = 0.01$ scan is omitted since all accepted models satisfy $m_s < 110$ GeV, making the results identical to those of the previous scan.

Λ	λ_s	$\eta_b/\eta_{\text{obs}} > 1$	Detonation				
			Total	$\text{SNR}_{\text{max}} > 10$	$\text{SNR}_{\text{LISA}} > 10$	$\text{SNR}_{\text{BBO}} > 10$	$\text{SNR}_{\text{DECIGO}} > 10$
540 GeV	0.01	0	80.5	2.68	0.8	2.5	0.27
	0.1	10.1	53	0.89	0.2	0.89	0.2
	1	$61.4^{-5.6}_{+4.6}$	$15.4^{+2.4}_{-1.4}$	2.38^{+0}_{-0}	0.83^{+0}_{-0}	2.38^{+0}_{-0}	0.71^{+0}_{-0}
	8	73.3	26.4	6.2	2.81	6.2	3.16
Λ_{min}	0.1	21.6	49.3	1.39	0.69	1.19	0.4
	1	69.6	18.1	2.21	0.97	2.07	0.97
	8	85.7	13.8	3.55	1.01	3.55	1.52

Table 3.2: Statistics from the scans performed with $\lambda_s = 0.01, 0.1, 1, 8$ and $\Lambda = 540$ GeV and Λ_{min}. Each entry corresponds to the percentage of models satisfying the indicated constraint. In the row for $\lambda_s = 1$ and $\Lambda = 540$ GeV, the exponents (indices) correspond to the error obtained by substituting the collision matrix Γ for 2Γ ($\Gamma/2$). Λ_{min} is the minimum value of Λ allowed by laboratory constraints.

The effect on v_w can be significant for slow walls, leading to a $\pm 40\,\%$ change when $v_w \sim 0.2$. On the other hand for nearly supersonic walls, $v_w \gtrsim c_s$, the wall speed is quite insensitive to Γ. The variation of L_h is generally below 5%, much smaller than the corresponding variation in Γ.

This behavior is not surprising since, near the speed of sound, the pressure on the wall is mainly determined by the variation of T_+, which does not depend on Γ. Likewise, the results for the baryon asymmetry and GW production turn out to be relatively robust against variations in Γ. This is demonstrated by the error intervals in the $\lambda_s = 1$ row of Table 3.2. The error on the ratio of models satisfying $\eta_b/\eta_{\text{obs}} > 1$ or $\text{SNR}_i > 10$ is of order 10%, which is much smaller than the range of variation in Γ.

Another source of uncertainty is the discrepancy between the temperatures computed with the Boltzmann equation (see Section 3.4.1) and the conservation of the energy-momentum tensor (see Appendix 3.B). Ideally one should obtain $T_+ = T_{\text{BE}}(z \to -\infty)$ and $T_- = T_{\text{BE}}(z \to \infty)$, where $T_{\text{BE}}(z) = T_+(1 + \delta\tau_{\text{bg}}(z))$ is the local temperature calculated with the Boltzmann equation. The first condition is always satisfied since we impose the boundary condition $\delta\tau_{\text{bg}}(-\infty) = 0$, but we fail to recover the second one due to the different approximations made in the two methods. The discrepancy becomes larger as v_w approaches the Jouguet velocity ξ_J, where T_+ increases compared to $T_- \approx T_n$ (see Fig. 3.6 (b)). On the other hand,

$\delta\tau_{\rm bg}$ does not change significantly in the same region. Hence, we observe an error in the temperature of order $\Delta T = T_- - T_{\rm BE}(\infty) \approx T_- - T_+$. Since the temperature is not accurate in the broken phase, the Higgs EOM is not automatically satisfied asymptotically. To solve that problem, we shift the actual Higgs VEV h_- evaluated in the broken phase by an amount $-\Delta h$, so that the adjusted VEV $h_0 = h_- - \Delta h$ asymptotically solves the EOM (see Eq. (3.24)). This gives an additional source of uncertainty for v_w and L_h.

We estimate the errors induced on v_w and L_h by ΔT and Δh, assuming they are small enough to justify keeping just the first order terms. Assuming that v_w is completely determined by the solution of $M_1 = 0$ and L_h by $M_2 = 0$, the error on these solutions can be obtained by expanding around the estimated values. For example, for the error in the wall velocity is estimated by

$$0 = M_1(v_w+\Delta v, h_0+\Delta h, T(z)+\Delta T(z)) \approx M_1(v_w, h_0, T(z)) + \frac{\partial M_1}{\partial v_w}\Delta v + \int dz \frac{\delta M_1}{\delta T(z)}\Delta T(z) + \Delta_h M_1, \tag{3.48}$$

where $\Delta_h M_1 = M_1(v_w, h_0 + \Delta h, T) - M_1(v_w, h_0, T)$, and we integrate over the temperature variation because M_1 is a functional of $T(z)$. Since v_w is the solution of $M_1(v_w, h_0, T(z)) = 0$, the absolute errors on v_w and L_h are estimated as

$$\begin{aligned} |\Delta v| &\approx (|\Delta_T M_1| + |\Delta_h M_1|)\left|\frac{\partial M_1}{\partial v_w}\right|^{-1}, \\ |\Delta L| &\approx (|\Delta_T M_2| + |\Delta_h M_2|)\left|\frac{\partial M_2}{\partial L}\right|^{-1}, \end{aligned} \tag{3.49}$$

where $\Delta_T M_i = \int dz (\delta M_i/\delta T(z))\Delta T(z)$. Notice that Eq. (3.49) overestimates the errors since $\Delta_T M_i$ and $\Delta_h M_i$ have opposite signs. From Eqs. (3.22,3.25,3.26), one can see that the functional derivative $\delta M_i/\delta T(z)$ can be approximated by $\frac{d}{dT}(\partial V_{\rm eff}/\partial h)$, so that

$$\Delta_T M_i \approx \int dz \frac{d}{dT}\left(\frac{\partial V_{\rm eff}}{\partial h}\right) F_i(z)\Delta T(z)\,, \tag{3.50}$$

where $F_1 = h'$ and $F_2 = h'(2h - h_0)$. We can simplify this integral with the approximation

$\Delta T(z) \approx (T_- - T_+)[1 + \tanh(z/L_h)]/2$. Furthermore, we approximate $\frac{d}{dT}\left(\frac{\partial V}{\partial h}\right)$ as being constant and half of its maximal value, occurring near $z = 0$. Then

$$\Delta_T M_i \approx \frac{1}{2}(T_- - T_+)C_i \, \frac{d}{dT}\left(\frac{\partial V_{\text{eff}}}{\partial h}\right)\bigg|_{z=0}, \tag{3.51}$$

where $C_1 = \int dz F_1(z)[1+\tanh(z/L_h)]/2 = h_0/2$ and $C_2 = h_0^2/6$. Substituting this expression in Eq. (3.49), we finally obtain that the errors on v_w and L_h are given by

$$\begin{aligned} |\Delta v| &\approx \left\{\left|\frac{1}{4}(T_- - T_+)h_0 \frac{d}{dT}\left(\frac{\partial V_{\text{eff}}}{\partial h}\right)\bigg|_{z=0}\right| + |\Delta_h M_1|\right\}\left|\frac{\partial M_1}{\partial v_w}\right|^{-1}, \\ |\Delta L| &\approx \left\{\left|\frac{1}{12}(T_- - T_+)h_0^2 \frac{d}{dT}\left(\frac{\partial V_{\text{eff}}}{\partial h}\right)\bigg|_{z=0}\right| + |\Delta_h M_2|\right\}\left|\frac{\partial M_2}{\partial L_h}\right|^{-1}. \end{aligned} \tag{3.52}$$

The relative errors are presented in Fig. 3.10 (c) for the scan with $\lambda_s = 1$ and $\Lambda = 540$ GeV. The error on v_w is below 7% for 97% of the models, and exhibits no strong correlation with v_w. This happens because $\Delta T = T_- - T_+$ and dM_1/dv_w are roughly proportional (see Fig. 3.6), and therefore cancel each others' contributions. The relative error on L_h is small at low velocity (or large L_h), but becomes more significant near the speed of sound, however without ever exceeding 10%.

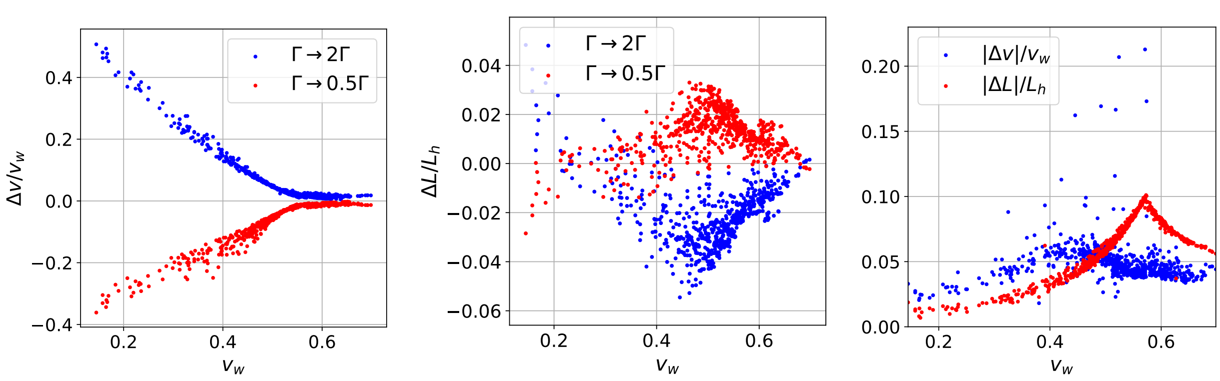

(a) (b) (c)

Figure 3.10: (a) and (b): Relative changes $\Delta v/v_w$ and $\Delta L/L_h$ in the wall velocities and widths obtained by substituting $\Gamma \to 2\Gamma$ or $\Gamma/2$ respectively. (c): Absolute error on v_w and L_h due to the discrepancy between the temperatures computed with the Boltzmann equation and the conservation of the energy-momentum tensor (see Eq. (3.52)).

3.6.5 Comparison of the GW signal with previous studies

We end this section with a brief comparison with recent studies of the GW produced during a first-order electroweak phase transition. With the prospect of the upcoming LISA experiment, numerous forecasts of the GW spectrum have been made for various extensions of the Standard Model [10–14]. Most of these find regions of model parameter space that would produce detectable GWs. Here we focus on studies of the singlet scalar extensions [15–20].

Our results agree qualitatively with the conclusions of previous work, in the prediction of GWs detectable by LISA, DECIGO and BBO. However there are distinctions stemming from differences in methodology. To compute the GW contribution from the sound waves, previous authors used the numerical fit presented in Ref. [85], while we used the updated formulas of Refs. [116, 117]. This leads to a smaller peak frequency, decreasing the number of detectable models. Ref. [85] also does not include the factor $1-(1+2HR/\sqrt{K_{\rm sw}})^{-1/2}$ in the GW amplitude (see Appendix 3.C). We find that this factor is generally quite small (of order 10^{-3}-10^{-2} for deflagrations and 10^{-2}-10^{-1} for detonations); hence the predicted GW signals are considerably reduced.

Another significant difference arises from our determination of the wall velocity, which was treated as a free parameter in previous work, whereas we have computed it from the microphysics. The GW spectrum and hence signal-to-noise ratio and ultimately the detectability are strongly dependent on the wall speed. For example, Ref. [16] assumed $v_w = 0.95$ for all models, which considerably enhanced GW production and led to more optimistic predictions. Moreover, using a fixed value for v_w hides the discontinuous transition between the deflagration and detonation solutions shown in Fig. 3.8.

3.7 Conclusion

In this work we have taken a first step toward making complete predictions for baryogenesis and gravity waves from a first order electroweak phase transition, starting from a renormalizable Lagrangian that gives rise to the effective operator needed for CP-violation. This is in contrast to previous studies in which quantities like the bubble wall velocity or thickness were treated as free parameters, instead of being derived from the microphysical input parameters as we have done here. This is a necessary step for properly assessing the chances of having successful EWBG and potentially observable GWs, since the two observables are correlated in a nontrivial way, when they are both computed from first principles.

We have incorporated improved fluid equations, both for the CP-even perturbations that determine the friction acting on the bubble wall [1], and for the CP-odd ones that are necessary for baryogenesis [3], that can properly account for wall speeds close to the sound barrier. Earlier versions of these equations were singular at the sound speed, making reliable predictions impossible for fast-moving walls. Contrary to previous lore, we find that EWBG can be more efficient for faster walls, due in part to the tendency for fast walls to be thinner.

The Z_2-symmetric singlet model with vector-like top partners, analyzed in this work, was chosen for its simplicity, but the methods we used can be applied to other particle physics models that could enhance the EWPT. For example, singlets with no Z_2 symmetry have additional parameters, and would thus be likely to have more freedom to simultaneously yield large GW production and sufficient baryogenesis. It would be interesting to identify other UV-completed models with these properties. A limitation we identified with the Z_2-symmetric model is that for the large values of the η_2 coupling that are desired for EWBG, the singlet self-coupling is rapidly driven toward zero by renormalization group running, above the top partner threshold.

For future work, some improvements could be made to the analysis presented here. The wall velocity might be more accurately determined at low v_w by using collision rates for the fluid perturbation equations beyond leading-log accuracy, and by including the singlet and Higgs out-of-equilibrium (friction) contributions. Another limitation is that the current state-of-the-art for predicting the GW spectrum is subject to large systematic uncertainties for wall velocities close to the speed of sound. Since a large fraction of deflagration transitions have $0.5 \lesssim v_w \lesssim \xi_J$, our analysis of the GW production could greatly benefit from more accurate fits in that range of wall speeds.

Acknowledgments. We thank T. Flacke, H. Guo, M. Lewicki, K. Schmitz, G. Servant and K.-P. Xie for helpful correspondence. The work of JC and BL was supported by the Natural Sciences and Engineering Research Council (Canada). The work of BL was also supported by the Fonds de recherche Nature et technologies (Québec). The work of KK was supported by the Academy of Finland grant 31831.

3.A Effective Potential

We describe here the full effective potential used to describe the phase transition in the Z_2-symmetric singlet model. It takes the general form

$$V_{\text{eff}}(h,s,T) = V_{\text{tree}}(h,s) + V_{\text{CW}}(h,s,T) + V_T(h,s,T) + \delta V(h,s). \tag{3.53}$$

V_{tree} is the scalar degrees of freedom's tree-level potential obtained in the unitary gauge by setting in Eq. (3.1) $H \to h/\sqrt{2}$ and by omitting the V_{BG} term:

$$V_{\text{tree}}(h,s) = \frac{\mu_h^2}{2}h^2 + \frac{\lambda_h}{4}h^4 + \frac{\lambda_{hs}}{4}h^2 s^2 + \frac{\mu_s^2}{2}s^2 + \frac{\lambda_s}{4}s^4. \tag{3.54}$$

V_{CW} is the Coleman-Weinberg potential in the $\overline{\text{MS}}$ renormalization scheme that incorporates the vacuum one-loop corrections and V_T is the thermal potential:

$$\begin{aligned} V_{\text{CW}}(h,s,T) &= \frac{1}{64\pi^2} \sum_{i=W,Z,\gamma_L,1,2,\chi,t} n_i \tilde{\mathscr{M}}_i^4(h,s,T) \left[\log \frac{\tilde{\mathscr{M}}_i^2(h,s,T)}{\mu^2} - C_i\right], \\ V_T(h,s,T) &= \sum_{i=W,Z,\gamma_L,1,2,\chi,t} \frac{n_i T^4}{2\pi^2} \int_0^\infty dy\, y^2 \log\left[1 \pm e^{-\sqrt{y^2+\mathscr{M}_i^2(h,s,T)/T^2}}\right] - \frac{\tilde{g}\pi^2 T^4}{90}, \end{aligned} \tag{3.55}$$

where the sums go over all the massive particles, including the thermal mass. Here, we include the contribution from the W and Z gauge bosons, the photon's longitudinal polarization γ_L, the Goldstone bosons χ, the top quark and the eigenvalues of the mass matrix of the Higgs boson and singlet scalar m_1 and m_2. We impose the renormalization energy scale as $\mu = v$, where $v = 246$ GeV is the Higgs vacuum expectation value. The $\pm$ in the thermal integral is $+$ for fermion and $-$ for bosons and $\tilde{g} = \sum\limits_B N_B + \frac{7}{8}\sum\limits_F N_F = 85.25$ with the sums running over all the lighter degrees of freedom not included in the first term of V_T. The C_i's are constants given by

$$C_{1,2,\chi,t} = 3/2 \quad \text{and} \quad C_{W,Z,\gamma_L} = 5/6, \tag{3.56}$$

and the n_i's are the particle's number of degrees of freedom:

$$n_{W_T} = 4, n_{W_L} = n_{Z_T} = 2, n_{Z_L} = n_{\gamma_L} = 1, n_{1,2} = 1, n_\chi = 3, n_t = -12. \tag{3.57}$$

We adopt the method developed by Parwani [122] to resum the Matsubara zero-modes for the bosonic degrees of freedom. It consists of replacing the bosons' vacuum mass $m_i^2(h,s)$ by the thermal-corrected one $\mathscr{M}_i^2(h,s,T) = m_i^2(h,s) + \Pi_i(T)$, with the self-energy given by

$$\begin{aligned}
\Pi_s(T) &= \left(\frac{1}{4}\lambda_s + \frac{1}{6}\lambda_{sh}\right)T^2, \\
\Pi_h(T) = \Pi_\chi(T) &= \left[\frac{1}{16}\left(3g_1^2 + g_2^2\right) + \frac{1}{2}\lambda_h + \frac{1}{4}y_t^2 + \frac{1}{24}\lambda_{hs}\right]T^2, \\
\Pi_{W_L}(T) &= \frac{11}{6}g_1^2 T^2, \\
\Pi_{W_T}(T) &= \Pi_{Z_T}(T) = \Pi_{\gamma_T}(T) = 0.
\end{aligned} \tag{3.58}$$

The thermal masses for the longitudinal mode of the photon and Z boson are

$$\begin{aligned}
\mathscr{M}_{Z_L}^2(s,h,T) &= \frac{1}{2}\left[m_Z^2(s,h) + \frac{11}{6}\frac{g_1^2}{\cos^2\theta_w}T^2 + \Delta(s,h,T)\right] \text{ and} \\
\mathscr{M}_{\gamma_L}^2(s,h,T) &= \frac{1}{2}\left[m_Z^2(s,h) + \frac{11}{6}\frac{g_1^2}{\cos^2\theta_w}T^2 - \Delta(s,h,T)\right],
\end{aligned} \tag{3.59}$$

with

$$\Delta(s,h,T) = \left[m_Z^4(s,h) + \frac{11}{3}\frac{g_1^2 \cos^2 2\theta_w}{\cos^2\theta_w}\left(m_Z^2(s,h) + \frac{11}{12}\frac{g_1^2}{\cos^2\theta_w}T^2 \right) T^2 \right]^{1/2}. \qquad (3.60)$$

At low temperature ($m_i^2/T^2 \gg 1$), one would expect all the thermal effects to be Boltzmann suppressed, since the species i becomes essentially absent from the plasma. This is manifestly the case for V_T, since the thermal integrals decay exponentially in the limit $\mathscr{M}_i^2/T^2 \approx m_i^2/T^2 \gg 1$. However, in the same limit, $V_{\rm CW}$ would depend quadratically on T if we used the thermal masses defined above. This would spoil the potential's low-T behaviour. Therefore, we define a regulated thermal mass[17] $\tilde{\mathscr{M}}_i^2 = m_i^2 + R(m_i^2/T^2)\Pi_i$, that should only be used in $V_{\rm CW}$. $R(x)$ is a regulator chosen to recover the right behaviour in the low and high-T limit. In order to do so, it should be a smooth function satisfying $R(x=0)=1$ and $R(x) \sim e^{-\sqrt{|x|}}$ when $|x| \gg 1$. We choose here the integrated Boltzmann number density function given by

$$R(x) = \frac{1}{2}[x]K_2\left(\sqrt{[x]}\right), \qquad (3.61)$$

where K_2 is the modified Bessel function of the second kind and $[x] = x\tanh(x)$ is a smoothed absolute value.

The last term of Eq. (3.53) contains the following counterterms:

$$\delta V(h,s) = Ah^2 + Bh^4 + Cs^2 + D, \qquad (3.62)$$

[17]For the photon and Z boson's longitudinal mode, we define $\Pi_i = \mathscr{M}_i^2 - m_i^2$, which should reproduce the desired behaviour.

which are fixed by requiring the renormalization conditions

$$\begin{aligned}
0 &= \left.\frac{\partial V_{\rm eff}}{\partial h}\right|_{h=v,s=0,T=0} \\
m_h^2 &= \left.\frac{\partial^2 V_{\rm eff}}{\partial h^2}\right|_{h=v,s=0,T=0} \\
m_s^2 &= \left.\frac{\partial^2 V_{\rm eff}}{\partial s^2}\right|_{h=v,s=0,T=0} \\
0 &= V_{\rm eff}\big|_{h=v,s=0,T=0} \,.
\end{aligned} \tag{3.63}$$

While the use of the resummed one-loop potential is a clear improvement over the leading thermal-mass-corrected approximation, one should keep in mind that higher loop corrections and even nonperturbative physics may be relevant, in particular for very strong transitions [162–164].

3.B Relativistic fluid equation

We here calculate the hydrodynamical properties of the plasma close to the wall using the method described in Ref. [142]. The quantities of interest are the temperatures $T_\pm$ and the velocities of the plasma measured in the wall frame $v_\pm$. The subscript $+$ and $-$ indicate that the quantity is measured in front or behind the wall respectively.

By integrating the conservation of the energy-momentum tensor equation across the wall, one can show that the quantities $T_\pm$ and $v_\pm$ are related by the equations

$$\begin{aligned}
v_+ v_- &= \frac{1-(1-3\alpha_+)r}{3-3(1+\alpha_+)r}, \\
\frac{v_+}{v_-} &= \frac{3+(1-3\alpha_+)r}{1+3(1+\alpha_+)r},
\end{aligned} \tag{3.64}$$

where α_+ and r are defined as

$$\begin{aligned}
\alpha_+ &\equiv \frac{\epsilon_+ - \epsilon_-}{a_+ T_+^4}, \\
r &\equiv \frac{a_+ T_+^4}{a_- T_-^4}, \\
a_\pm &\equiv -\frac{3}{4T_\pm^3} \left.\frac{\partial V_{\text{eff}}}{\partial T}\right|_\pm, \\
\epsilon_\pm &\equiv \left.\left(-\frac{T_\pm}{4}\frac{\partial V_{\text{eff}}}{\partial T} + V_{\text{eff}}\right)\right|_\pm .
\end{aligned} \tag{3.65}$$

These quantities are often approximated by the so-called bag equation of state, which is given in Ref. [142]. This approximation is expected to hold when the masses of the plasma's degrees of freedom are very different from T, which is not necessarily true in the broken phase. Therefore, we keep the full relations (3.65) in our calculations.

Subsonic walls always come with a shock wave in front of the phase transition front. The Eqs. 3.64 can be used to relate $T_\pm$ and $v_\pm$ at the wall and the shock wave, but we need to understand how the temperature and fluid velocity evolve between these two regions. Assuming a spherical bubble and a thin wall, one can derive from the conservation of the energy-momentum tensor the following differential equations

$$\begin{aligned}
2\frac{v}{\xi} &= \gamma^2 (1 - v\xi) \left(\frac{\mu^2}{c_s^2} - 1\right) \partial_\xi v, \\
\partial_\xi T &= T\gamma^2 \mu \partial_\xi v,
\end{aligned} \tag{3.66}$$

where v is the fluid velocity in the frame of the bubble's center and $\xi = r/t$ is the independent variable, with r the distance from the bubble center t the time since the bubble nucleation. With that choice of coordinates, the wall is positioned at $\xi = v_w$. μ is the Lorentz-transformed fluid velocity

$$\mu(\xi, v) = \frac{\xi - v}{1 - \xi v}, \tag{3.67}$$

and c_s is the speed of sound in the plasma

$$c_s^2 = \frac{\partial V_{\text{eff}}/\partial T}{T\partial^2 V_{\text{eff}}/\partial T^2} \approx \frac{1}{3}. \tag{3.68}$$

The last approximation is valid for relativistic fluids, which models well the unbroken phase. In the broken phase, the particles get a mass that can be of the same order as the temperature, and it causes the speed of sound to become slightly smaller.

One can find three different types of solutions for the fluid's velocity profile: deflagration walls ($v_w < c_s^-$) have a shock wave propagating in front of the wall, detonation walls ($v_w > \xi_J$) have a rarefaction wave behind it and hybrid walls ($c_s^- < v_w < \xi_J$) have both shock and rarefaction waves. ξ_J is the model-dependent Jouguet velocity, which is defined as the smallest velocity a detonation solution can have. Each type of wall have different boundary conditions that determine the characteristics of the solution. Detonation walls are supersonic solutions where the fluid in front of the wall is unperturbed. Therefore, it satisfies the boundary conditions $v_+ = v_w$ and $T_+ = T_n$. For that type of solution, Eqs. (3.64) can be solved directly for v_- and T_-.

Subsonic walls always have a deflagration solution with a shock wave at a position ξ_{sh} that solves the equation $v_{sh}^- \xi_{sh} = (c_s^+)^2$, where v_{sh}^- is the fluid's velocity just behind the shock wave measured in the shock wave's frame. It satisfies the boundary conditions $v_- = v_w$ and $T_{sh}^+ = T_n$. Because these boundary conditions are given at two different points, the solution of this system can be somewhat more involved than for the detonation case. Indeed, one has to use a shooting method which consists of choosing an arbitrary value for T_-, solving Eqs. (3.64) for T_+ and v_+, integrating Eqs. (3.66) with the initial values $T(v_w) = T_+$ and $v(v_w) = \mu(v_w, v_+)$ until the equation $\mu(\xi, v(\xi))\xi = (c_s^+)^2$ gets satisfied. One can then restart this procedure with a different value of T_- until the Eqs. (3.64) are satisfied at the shock wave. Hybrid walls satisfy $v_+ < c_s^- < v_w$ and they have the boundary conditions $v_- = c_s^-$ and $T_{sh}^+ = T_n$, which make them very similar to the deflagration walls.

3.C Gravitational Wave Production

For the convenience of the reader, we here reproduce the formulae from Refs. [63, 116, 117, 142, 144] that determine the GW spectrum from sound waves and turbulence in a first order phase transition. The spectrum is [116, 117]

$$\Omega_{\rm sw}(f) = 8.83\times 10^{-7} K_{\rm sw}^2 \left(\frac{HR}{c_s}\right)\left(1-\left(1+\frac{2HR}{\sqrt{K_{\rm sw}}}\right)^{-1/2}\right)\left(\frac{100}{g_*}\right)^{1/3} S_{\rm sw}\,(f), \tag{3.69}$$

where $K_{\rm sw} = \kappa_{\rm sw}\alpha/(1+\alpha)$, with $\kappa_{\rm sw}$ the efficiency coefficient of the sound wave. As previously stated, we assume that all the walls have non-runaway solutions and that the contribution from turbulence is negligible; hence we set $\Omega_{\rm sw} = \Omega_\phi(f) = 0$. The function parametrizing the shape of the GW spectrum is

$$S_{\rm sw}(f) = \left(\frac{f}{f_{\rm sw}}\right)^3 \left(\frac{7}{4+3\left(f/f_{\rm sw}\right)^2}\right)^{\frac{7}{2}}, \tag{3.70}$$

and the peak frequency $f_{\rm sw}$ is

$$f_{\rm sw} = 2.6\times 10^{-5}\,{\rm Hz}\left(\frac{1}{HR}\right)\left(\frac{T_n}{100~{\rm GeV}}\right)\left(\frac{g_*}{100}\right)^{\frac{1}{6}}. \tag{3.71}$$

Numerical fits for the efficiency coefficient $\kappa_{\rm sw}$ (the fractions of the available vacuum energy that go into kinetic energy) were presented in [142]. For non-runaway walls, these fits depend on the wall velocity and are given by

$$\kappa_{\rm sw} = \begin{cases} \frac{c_s^{11/5}\kappa_a\kappa_b}{(c_s^{11/5}-v_w^{11/5})\kappa_b + v_w c_s^{6/5}\kappa_a}, & v_w \lesssim c_s \\ \kappa_b + (v_w - c_s)\delta\kappa + \frac{(v_w-c_s)^3}{(\xi_J-c_s)^3}\left[\kappa_c - \kappa_b - (\xi_J - c_s)\delta\kappa\right], & c_s < v_w < \xi_J \\ \frac{(\xi_J-1)^3\xi_J^{5/2}v_w^{-5/2}\kappa_c\kappa_d}{[(\xi_J-1)^3-(v_w-1)^3]\xi_J^{5/2}\kappa_c + (v_w-1)^3\kappa_d}, & v_w \gtrsim \xi_J \end{cases} \tag{3.72}$$

where $c_s = 1/\sqrt{3}$ is the sound velocity and the different parameters are given by

$$\begin{aligned}
\xi_J &= \frac{\sqrt{2\alpha/3+\alpha^2}+c_s}{1+\alpha} & \delta\kappa &= -0.9\log\frac{\sqrt{\alpha}}{1+\sqrt{\alpha}} \\
\kappa_a &= \frac{6.9 v_w^{6/5}\alpha}{1.36-0.037\sqrt{\alpha}+\alpha} & \kappa_b &= \frac{\alpha^{2/5}}{0.017+(0.997+\alpha)^{2/5}} \\
\kappa_c &= \frac{\sqrt{\alpha}}{0.135+\sqrt{0.98+\alpha}} & \kappa_d &= \frac{\alpha}{0.73+0.083\sqrt{\alpha}+\alpha}
\end{aligned} \tag{3.73}$$

We caution that while these fits, when used as input for a signal-to-noise estimate, are useful to get an overall estimate for the GW signal in a given model, their precise predictions should be interpreted with care. The fit for the sound wave production is reliable for relatively weak transitions $\alpha < 0.1$, which is the range where most of our models fall. For stronger transitions the fit can overestimate the GW-signal by as much as a factor of thousand (strong deflagrations) [165]. In addition to the strength of the transition, fit parameters have also been shown to be sensitive to the shape of the effective potential [166] and the wall velocity [63, 117]. As explained in Ref. [63] Eqs. (3.69-3.71) are not expected to be accurate for $0.5 \lesssim v_w \lesssim \xi_J$, which includes a large fraction of the deflagration models found in this work. Thus, pending improvements in the theoretical predictions for GW spectra in this range of wall speeds, the results should not be regarded as conclusive.

References

[1] Benoit Laurent and James M. Cline. "Fluid equations for fast-moving electroweak bubble walls". In: *Phys. Rev. D* 102.6 (2020), p. 063516. DOI: 10.1103/PhysRevD.102.063516. arXiv: 2007.10935 [hep-ph].

[2] Guy D. Moore and Tomislav Prokopec. "How fast can the wall move? A Study of the electroweak phase transition dynamics". In: *Phys. Rev. D* 52 (1995), pp. 7182–7204. DOI: 10.1103/PhysRevD.52.7182. arXiv: hep-ph/9506475.

[3] James M. Cline and Kimmo Kainulainen. "Electroweak baryogenesis at high bubble wall velocities". In: *Phys. Rev. D* 101.6 (2020), p. 063525. DOI: 10.1103/PhysRevD.101.063525. arXiv: 2001.00568 [hep-ph].

[5] Pau Amaro-Seoane et al. "Laser Interferometer Space Antenna". In: (Feb. 2017). arXiv: 1702.00786 [astro-ph.IM].

[6] A. I. Bochkarev, S. V. Kuzmin, and M. E. Shaposhnikov. "Electroweak baryogenesis and the Higgs boson mass problem". In: *Phys. Lett.* B244 (1990), pp. 275–278. DOI: 10.1016/0370-2693(90)90069-I.

[7] Andrew G. Cohen, David B. Kaplan, and Ann E. Nelson. "Weak scale baryogenesis". In: *Phys. Lett.* B245 (1990), pp. 561–564. DOI: 10.1016/0370-2693(90)90690-8.

[8] Andrew G. Cohen, David B. Kaplan, and Ann E. Nelson. "Baryogenesis at the weak phase transition". In: *Nucl. Phys.* B349 (1991), pp. 727–742. DOI: 10.1016/0550-3213(91)90395-E.

[9] Neil Turok and John Zadrozny. "Electroweak baryogenesis in the two doublet model". In: *Nucl. Phys.* B358 (1991), pp. 471–493. DOI: 10.1016/0550-3213(91)90356-3.

[10] Ankit Beniwal et al. "Gravitational waves and electroweak baryogenesis in a global study of the extended scalar singlet model". In: *JHEP* 02 (2019), p. 183. DOI: 10.1007/JHEP02(2019)183. arXiv: 1810.02380 [hep-ph].

[11] John Ellis, Marek Lewicki, and Ville Vaskonen. "Updated predictions for gravitational waves produced in a strongly supercooled phase transition". In: (July 2020). arXiv: 2007.15586 [astro-ph.CO].

[12] Tomislav Prokopec, Jonas Rezacek, and Bogumiła Świeżewska. "Gravitational waves from conformal symmetry breaking". In: *JCAP* 02 (2019), p. 009. DOI: 10.1088/1475-7516/2019/02/009. arXiv: 1809.11129 [hep-ph].

[13] Carlo Marzo, Luca Marzola, and Ville Vaskonen. "Phase transition and vacuum stability in the classically conformal B–L model". In: *Eur. Phys. J. C* 79.7 (2019), p. 601. DOI: 10.1140/epjc/s10052-019-7076-x. arXiv: 1811.11169 [hep-ph].

[14] P. S. Bhupal Dev et al. "Gravitational Waves from First-Order Phase Transition in a Simple Axion-Like Particle Model". In: *JCAP* 11 (2019), p. 006. DOI: 10.1088/1475-7516/2019/11/006. arXiv: 1905.00891 [hep-ph].

[15] Ville Vaskonen. "Electroweak baryogenesis and gravitational waves from a real scalar singlet". In: *Phys. Rev. D* 95.12 (2017), p. 123515. DOI: 10.1103/PhysRevD.95.123515. arXiv: 1611.02073 [hep-ph].

[16] Zhaofeng Kang, P. Ko, and Toshinori Matsui. "Strong first order EWPT \& strong gravitational waves in Z_3-symmetric singlet scalar extension". In: *JHEP* 02 (2018), p. 115. DOI: 10.1007/JHEP02(2018)115. arXiv: 1706.09721 [hep-ph].

[17] Ankit Beniwal et al. "Gravitational wave, collider and dark matter signals from a scalar singlet electroweak baryogenesis". In: *JHEP* 08 (2017), p. 108. DOI: 10.1007/JHEP08(2017)108. arXiv: 1702.06124 [hep-ph].

[18] Alexandre Alves et al. "Collider and Gravitational Wave Complementarity in Exploring the Singlet Extension of the Standard Model". In: *JHEP* 04 (2019), p. 052. DOI: 10.1007/JHEP04(2019)052. arXiv: 1812.09333 [hep-ph].

[19] Marcela Carena, Zhen Liu, and Yikun Wang. “Electroweak phase transition with spontaneous Z_2-breaking”. In: *JHEP* 08 (2020), p. 107. DOI: 10.1007/JHEP08(2020)107. arXiv: 1911.10206 [hep-ph].

[20] Ke-Pan Xie. “Lepton-mediated electroweak baryogenesis, gravitational waves and the 4τ final state at the collider”. In: *JHEP* 02 (2021), p. 090. DOI: 10.1007/JHEP02(2021)090. arXiv: 2011.04821 [hep-ph].

[23] Andrei D. Linde. “Fate of the False Vacuum at Finite Temperature: Theory and Applications”. In: *Phys. Lett.* 100B (1981), pp. 37–40. DOI: 10.1016/0370-2693(81)90281-1.

[24] Carroll L. Wainwright. “CosmoTransitions: Computing Cosmological Phase Transition Temperatures and Bubble Profiles with Multiple Fields”. In: *Comput. Phys. Commun.* 183 (2012), pp. 2006–2013. DOI: 10.1016/j.cpc.2012.04.004. arXiv: 1109.4189 [hep-ph].

[26] K. Kajantie et al. “A Nonperturbative analysis of the finite T phase transition in SU(2) x U(1) electroweak theory”. In: *Nucl. Phys.* B493 (1997), pp. 413–438. DOI: 10.1016/S0550-3213(97)00164-8. arXiv: hep-lat/9612006 [hep-lat].

[28] Greg W. Anderson and Lawrence J. Hall. “The Electroweak phase transition and baryogenesis”. In: *Phys. Rev. D* 45 (1992), pp. 2685–2698. DOI: 10.1103/PhysRevD.45.2685.

[29] John McDonald. “Electroweak baryogenesis and dark matter via a gauge singlet scalar”. In: *Phys. Lett. B* 323 (1994), pp. 339–346. DOI: 10.1016/0370-2693(94)91229-7.

[30] Jarny Choi and R. R. Volkas. “Real Higgs singlet and the electroweak phase transition in the Standard Model”. In: *Phys. Lett. B* 317 (1993), pp. 385–391. DOI: 10.1016/0370-2693(93)91013-D. arXiv: hep-ph/9308234.

[31] Jose Ramon Espinosa and Mariano Quiros. “Novel Effects in Electroweak Breaking from a Hidden Sector”. In: *Phys. Rev. D* 76 (2007), p. 076004. DOI: 10.1103/PhysRevD.76.076004. arXiv: hep-ph/0701145.

[32] Stefano Profumo, Michael J. Ramsey-Musolf, and Gabe Shaughnessy. “Singlet Higgs phenomenology and the electroweak phase transition”. In: *JHEP* 08 (2007), p. 010. DOI: 10.1088/1126-6708/2007/08/010. arXiv: 0705.2425 [hep-ph].

[33] Jose R. Espinosa, Thomas Konstandin, and Francesco Riva. “Strong Electroweak Phase Transitions in the Standard Model with a Singlet”. In: *Nucl. Phys.* B854 (2012), pp. 592–630. DOI: 10.1016/j.nuclphysb.2011.09.010. arXiv: 1107.5441 [hep-ph].

[34] James M. Cline et al. “Update on scalar singlet dark matter”. In: *Phys. Rev. D* 88 (2013). [Erratum: Phys.Rev.D 92, 039906 (2015)], p. 055025. DOI: 10.1103/PhysRevD.88.055025. arXiv: 1306.4710 [hep-ph].

[35] P. H. Damgaard et al. “Effective Field Theory and Electroweak Baryogenesis in the Singlet-Extended Standard Model”. In: *JHEP* 02 (2016), p. 107. DOI: 10.1007/JHEP02(2016)107. arXiv: 1512.01963 [hep-ph].

[36] Gowri Kurup and Maxim Perelstein. “Dynamics of Electroweak Phase Transition In Singlet-Scalar Extension of the Standard Model”. In: *Phys. Rev. D* 96.1 (2017), p. 015036. DOI: 10.1103/PhysRevD.96.015036. arXiv: 1704.03381 [hep-ph].

[37] Cheng-Wei Chiang, Yen-Ting Li, and Eibun Senaha. “Revisiting electroweak phase transition in the standard model with a real singlet scalar”. In: *Phys. Lett. B* 789 (2019), pp. 154–159. DOI: 10.1016/j.physletb.2018.12.017. arXiv: 1808.01098 [hep-ph].

[38] N. Aghanim et al. “Planck 2018 results. VI. Cosmological parameters”. In: *Astron. Astrophys.* 641 (2020), A6. DOI: 10.1051/0004-6361/201833910. arXiv: 1807.06209 [astro-ph.CO].

[39] Richard H. Cyburt. “Primordial nucleosynthesis for the new cosmology: Determining uncertainties and examining concordance”. In: *Phys. Rev. D* 70 (2004), p. 023505. DOI: 10.1103/PhysRevD.70.023505. arXiv: astro-ph/0401091.

[40] James M. Cline. “Baryogenesis”. In: *Les Houches Summer School - Session 86: Particle Physics and Cosmology: The Fabric of Spacetime*. Sept. 2006. arXiv: hep-ph/0609145.

[41] W. Buchmuller, P. Di Bari, and M. Plumacher. “Leptogenesis for pedestrians”. In: *Annals Phys.* 315 (2005), pp. 305–351. DOI: 10.1016/j.aop.2004.02.003. arXiv: hep-ph/0401240.

[42] W. Buchmuller, P. Di Bari, and M. Plumacher. “Some aspects of thermal leptogenesis”. In: *New J. Phys.* 6 (2004), p. 105. DOI: 10.1088/1367-2630/6/1/105. arXiv: hep-ph/0406014.

[43] W. Buchmuller, R. D. Peccei, and T. Yanagida. “Leptogenesis as the origin of matter”. In: *Ann. Rev. Nucl. Part. Sci.* 55 (2005), pp. 311–355. DOI: 10.1146/annurev.nucl.55.090704.151558. arXiv: hep-ph/0502169.

[44] Mu-Chun Chen. "TASI 2006 Lectures on Leptogenesis". In: *Theoretical Advanced Study Institute in Elementary Particle Physics: Exploring New Frontiers Using Colliders and Neutrinos*. Mar. 2007, pp. 123–176. arXiv: `hep-ph/0703087`.

[45] Ian Affleck and Michael Dine. "A New Mechanism for Baryogenesis". In: *Nucl. Phys. B* 249 (1985), pp. 361–380. DOI: `10.1016/0550-3213(85)90021-5`.

[51] Guy D. Moore. "Measuring the broken phase sphaleron rate nonperturbatively". In: *Phys. Rev. D* 59 (1999), p. 014503. DOI: `10.1103/PhysRevD.59.014503`. arXiv: `hep-ph/9805264`.

[52] Kaori Fuyuto and Eibun Senaha. "Improved sphaleron decoupling condition and the Higgs coupling constants in the real singlet-extended standard model". In: *Phys. Rev. D* 90.1 (2014), p. 015015. DOI: `10.1103/PhysRevD.90.015015`. arXiv: `1406.0433 [hep-ph]`.

[54] J. H. Christenson et al. "Evidence for the 2π Decay of the K_2^0 Meson". In: *Phys. Rev. Lett.* 13 (1964), pp. 138–140. DOI: `10.1103/PhysRevLett.13.138`.

[55] Bernard Aubert et al. "Observation of CP violation in the B^0 meson system". In: *Phys. Rev. Lett.* 87 (2001), p. 091801. DOI: `10.1103/PhysRevLett.87.091801`. arXiv: `hep-ex/0107013`.

[62] Chiara Caprini et al. "Science with the space-based interferometer eLISA. II: Gravitational waves from cosmological phase transitions". In: *JCAP* 04 (2016), p. 001. DOI: `10.1088/1475-7516/2016/04/001`. arXiv: `1512.06239 [astro-ph.CO]`.

[63] Chiara Caprini et al. "Detecting gravitational waves from cosmological phase transitions with LISA: an update". In: *JCAP* 03 (2020), p. 024. DOI: `10.1088/1475-7516/2020/03/024`. arXiv: `1910.13125 [astro-ph.CO]`.

[64] Jose R. Espinosa et al. "Energy Budget of Cosmological First-order Phase Transitions". In: *JCAP* 06 (2010), p. 028. DOI: `10.1088/1475-7516/2010/06/028`. arXiv: `1004.4187 [hep-ph]`.

[65] Thomas Konstandin, Germano Nardini, and Ingo Rues. "From Boltzmann equations to steady wall velocities". In: *JCAP* 09 (2014), p. 028. DOI: `10.1088/1475-7516/2014/09/028`. arXiv: `1407.3132 [hep-ph]`.

[68] Jonathan Kozaczuk. "Bubble Expansion and the Viability of Singlet-Driven Electroweak Baryogenesis". In: *JHEP* 10 (2015), p. 135. DOI: `10.1007/JHEP10(2015)135`. arXiv: `1506.04741 [hep-ph]`.

[70] Dietrich Bodeker and Guy D. Moore. "Electroweak Bubble Wall Speed Limit". In: *JCAP* 05 (2017), p. 025. DOI: `10.1088/1475-7516/2017/05/025`. arXiv: `1703.08215 [hep-ph]`.

[77] James M. Cline, Michael Joyce, and Kimmo Kainulainen. "Supersymmetric electroweak baryogenesis". In: *JHEP* 07 (2000), p. 018. DOI: `10.1088/1126-6708/2000/07/018`. arXiv: `hep-ph/0006119`.

[78] Lars Fromme, Stephan J. Huber, and Michael Seniuch. "Baryogenesis in the two-Higgs doublet model". In: *JHEP* 11 (2006), p. 038. DOI: `10.1088/1126-6708/2006/11/038`. arXiv: `hep-ph/0605242`.

[79] Lars Fromme and Stephan J. Huber. "Top transport in electroweak baryogenesis". In: *JHEP* 03 (2007), p. 049. DOI: `10.1088/1126-6708/2007/03/049`. arXiv: `hep-ph/0604159`.

[80] Peter Arnold, Guy David Moore, and Laurence G Yaffe. "Transport coefficients in high temperature gauge theories (I): leading-log results". In: *JHEP* 0011 (2000), p. 001. DOI: `10.1088/1126-6708/2000/11/001`. arXiv: `hep-ph/0010177 [hep-ph]`.

[81] H. Arthur Weldon. "Effective Fermion Masses of Order gT in High Temperature Gauge Theories with Exact Chiral Invariance". In: *Phys. Rev. D* 26 (1982), p. 2789. DOI: `10.1103/PhysRevD.26.2789`.

[82] Peter Arnold, Guy D Moore, and Laurence G Yaffe. "Transport coefficients in high temperature gauge theories: (II) Beyond leading log". In: *Journal of High Energy Physics* 0305 (2003), p. 051. DOI: `10.1088/1126-6708/2003/05/051`. arXiv: `hep-ph/0302165 [hep-ph]`.

[83] Guy D Moore. "Transport coefficients in large Nf gauge theory: testing hard thermal loops". In: *Journal of High Energy Physics* 0105 (2001), p. 039. ISSN: 1029-8479. DOI: `10.1088/1126-6708/2001/05/039`. arXiv: `hep-ph/0104121 [hep-ph]`.

[84] Andrew J. Long, Andrea Tesi, and Lian-Tao Wang. "Baryogenesis at a Lepton-Number-Breaking Phase Transition". In: *JHEP* 10 (2017), p. 095. DOI: `10.1007/JHEP10(2017)095`. arXiv: `1703.04902 [hep-ph]`.

[85] Chiara Caprini et al. "Science with the space-based interferometer eLISA. II: Gravitational waves from cosmological phase transitions". In: *JCAP* 04 (2016), p. 001. DOI: `10.1088/1475-7516/2016/04/001`. arXiv: `1512.06239 [astro-ph.CO]`.

[86] Jeff Crowder and Neil J. Cornish. “Beyond LISA: Exploring future gravitational wave missions”. In: *Phys. Rev. D* 72 (2005), p. 083005. DOI: 10.1103/PhysRevD.72.083005. arXiv: gr-qc/0506015.

[87] Naoki Seto, Seiji Kawamura, and Takashi Nakamura. “Possibility of direct measurement of the acceleration of the universe using 0.1-Hz band laser interferometer gravitational wave antenna in space”. In: *Phys. Rev. Lett.* 87 (2001), p. 221103. DOI: 10.1103/PhysRevLett.87.221103. arXiv: astro-ph/0108011.

[88] Shuichi Sato et al. “The status of DECIGO”. In: *J. Phys. Conf. Ser.* 840.1 (2017). Ed. by Domencio Giardini and Philippe Jetzer, p. 012010. DOI: 10.1088/1742-6596/840/1/012010.

[89] Yousef Abou El-Neaj et al. “AEDGE: Atomic Experiment for Dark Matter and Gravity Exploration in Space”. In: *EPJ Quant. Technol.* 7 (2020), p. 6. DOI: 10.1140/epjqt/s40507-020-0080-0. arXiv: 1908.00802 [gr-qc].

[90] S. W. Ham, Y. S. Jeong, and S. K. Oh. “Electroweak phase transition in an extension of the standard model with a real Higgs singlet”. In: *J. Phys. G* 31.8 (2005), pp. 857–871. DOI: 10.1088/0954-3899/31/8/017. arXiv: hep-ph/0411352.

[91] Andrew Noble and Maxim Perelstein. “Higgs self-coupling as a probe of electroweak phase transition”. In: *Phys. Rev. D* 78 (2008), p. 063518. DOI: 10.1103/PhysRevD.78.063518. arXiv: 0711.3018 [hep-ph].

[92] David Curtin, Patrick Meade, and Chiu-Tien Yu. “Testing Electroweak Baryogenesis with Future Colliders”. In: *JHEP* 11 (2014), p. 127. DOI: 10.1007/JHEP11(2014)127. arXiv: 1409.0005 [hep-ph].

[93] Stefano Profumo et al. “Singlet-catalyzed electroweak phase transitions and precision Higgs boson studies”. In: *Phys. Rev. D* 91.3 (2015), p. 035018. DOI: 10.1103/PhysRevD.91.035018. arXiv: 1407.5342 [hep-ph].

[94] Ashutosh V. Kotwal et al. “Singlet-catalyzed electroweak phase transitions in the 100 TeV frontier”. In: *Phys. Rev. D* 94.3 (2016), p. 035022. DOI: 10.1103/PhysRevD.94.035022. arXiv: 1605.06123 [hep-ph].

[95] Peisi Huang, Andrew J. Long, and Lian-Tao Wang. “Probing the Electroweak Phase Transition with Higgs Factories and Gravitational Waves”. In: *Phys. Rev. D* 94.7 (2016), p. 075008. DOI: 10.1103/PhysRevD.94.075008. arXiv: 1608.06619 [hep-ph].

[96] Chien-Yi Chen, Jonathan Kozaczuk, and Ian M. Lewis. “Non-resonant Collider Signatures of a Singlet-Driven Electroweak Phase Transition”. In: *JHEP* 08 (2017), p. 096. DOI: 10.1007/JHEP08(2017)096. arXiv: 1704.05844 [hep-ph].

[97] Jeong Han Kim and Ian M. Lewis. “Loop Induced Single Top Partner Production and Decay at the LHC”. In: *JHEP* 05 (2018), p. 095. DOI: 10.1007/JHEP05(2018)095. arXiv: 1803.06351 [hep-ph].

[98] Katsuya Hashino et al. “Selecting models of first-order phase transitions using the synergy between collider and gravitational-wave experiments”. In: *Phys. Rev. D* 99.7 (2019), p. 075011. DOI: 10.1103/PhysRevD.99.075011. arXiv: 1809.04994 [hep-ph].

[99] Michael J. Ramsey-Musolf. “The electroweak phase transition: a collider target”. In: *JHEP* 09 (2020), p. 179. DOI: 10.1007/JHEP09(2020)179. arXiv: 1912.07189 [hep-ph].

[100] Shekhar Adhikari, Ian M. Lewis, and Matthew Sullivan. “Beyond the Standard Model Effective Field Theory: The Singlet Extended Standard Model”. In: (Mar. 2020). arXiv: 2003.10449 [hep-ph].

[101] Subinoy Das et al. “The Dark Side of the Electroweak Phase Transition”. In: *JHEP* 11 (2010), p. 108. DOI: 10.1007/JHEP11(2010)108. arXiv: 0910.1262 [hep-ph].

[102] A. Ashoorioon and T. Konstandin. “Strong electroweak phase transitions without collider traces”. In: *JHEP* 07 (2009), p. 086. DOI: 10.1088/1126-6708/2009/07/086. arXiv: 0904.0353 [hep-ph].

[103] Mitsuru Kakizaki, Shinya Kanemura, and Toshinori Matsui. “Gravitational waves as a probe of extended scalar sectors with the first order electroweak phase transition”. In: *Phys. Rev. D* 92.11 (2015), p. 115007. DOI: 10.1103/PhysRevD.92.115007. arXiv: 1509.08394 [hep-ph].

[104] Katsuya Hashino et al. “Synergy between measurements of gravitational waves and the triple-Higgs coupling in probing the first-order electroweak phase transition”. In: *Phys. Rev. D* 94.1 (2016), p. 015005. DOI: 10.1103/PhysRevD.94.015005. arXiv: 1604.02069 [hep-ph].

[105] Mikael Chala, Germano Nardini, and Ivan Sobolev. “Unified explanation for dark matter and electroweak baryogenesis with direct detection and gravitational wave signatures”. In: *Phys. Rev. D* 94.5 (2016), p. 055006. DOI: 10.1103/PhysRevD.94.055006. arXiv: 1605.08663 [hep-ph].

[106] Tommi Tenkanen, Kimmo Tuominen, and Ville Vaskonen. "A Strong Electroweak Phase Transition from the Inflaton Field". In: *JCAP* 09 (2016), p. 037. DOI: 10.1088/1475-7516/2016/09/037. arXiv: 1606.06063 [hep-ph].

[107] Katsuya Hashino et al. "Gravitational waves and Higgs boson couplings for exploring first order phase transition in the model with a singlet scalar field". In: *Phys. Lett. B* 766 (2017), pp. 49–54. DOI: 10.1016/j.physletb.2016.12.052. arXiv: 1609.00297 [hep-ph].

[108] Amine Ahriche et al. "Gravitational Waves from Phase Transitions in Models with Charged Singlets". In: *Phys. Lett. B* 789 (2019), pp. 119–126. DOI: 10.1016/j.physletb.2018.12.013. arXiv: 1809.09883 [hep-ph].

[109] Stefania De Curtis, Luigi Delle Rose, and Giuliano Panico. "Composite Dynamics in the Early Universe". In: *JHEP* 12 (2019), p. 149. DOI: 10.1007/JHEP12(2019)149. arXiv: 1909.07894 [hep-ph].

[110] Thomas Konstandin and Jose M. No. "Hydrodynamic obstruction to bubble expansion". In: *JCAP* 02 (2011), p. 008. DOI: 10.1088/1475-7516/2011/02/008. arXiv: 1011.3735 [hep-ph].

[111] Stefan Höche et al. "Towards an all-orders calculation of the electroweak bubble wall velocity". In: (July 2020). arXiv: 2007.10343 [hep-ph].

[112] Marc Barroso Mancha, Tomislav Prokopec, and Bogumila Swiezewska. "Field-theoretic derivation of bubble-wall force". In: (May 2020). arXiv: 2005.10875 [hep-th].

[113] Shyam Balaji, Michael Spannowsky, and Carlos Tamarit. "Cosmological bubble friction in local equilibrium". In: (Oct. 2020). arXiv: 2010.08013 [hep-ph].

[114] Aleksandr Azatov and Miguel Vanvlasselaer. "Bubble wall velocity: heavy physics effects". In: *JCAP* 01 (2021), p. 058. DOI: 10.1088/1475-7516/2021/01/058. arXiv: 2010.02590 [hep-ph].

[115] Avi Friedlander et al. "Wall speed and shape in singlet-assisted strong electroweak phase transitions". In: (Sept. 2020). arXiv: 2009.14295 [hep-ph].

[116] Huai-Ke Guo et al. "Phase Transitions in an Expanding Universe: Stochastic Gravitational Waves in Standard and Non-Standard Histories". In: *JCAP* 01 (2021), p. 001. DOI: 10.1088/1475-7516/2021/01/001. arXiv: 2007.08537 [hep-ph].

[117] Mark B. Hindmarsh et al. "Phase transitions in the early universe". In: (Aug. 2020). DOI: 10.21468/SciPostPhysLectNotes.24. arXiv: 2008.09136 [astro-ph.CO].

[118] Wolfgang Waltenberger, André Lessa, and Sabine Kraml. "Artificial Proto-Modelling: Building Precursors of a Next Standard Model from Simplified Model Results". In: (Dec. 2020). arXiv: 2012.12246 [hep-ph].

[119] Jordy de Vries et al. "Electroweak Baryogenesis and the Standard Model Effective Field Theory". In: *JHEP* 01 (2018), p. 089. DOI: 10.1007/JHEP01(2018)089. arXiv: 1710.04061 [hep-ph].

[120] Marieke Postma and Graham White. "Cosmological phase transitions: is effective field theory just a toy?" In: (Dec. 2020). arXiv: 2012.03953 [hep-ph].

[121] James M. Cline and Kimmo Kainulainen. "Electroweak baryogenesis and dark matter from a singlet Higgs". In: *JCAP* 01 (2013), p. 012. DOI: 10.1088/1475-7516/2013/01/012. arXiv: 1210.4196 [hep-ph].

[122] Rajesh R. Parwani. "Resummation in a hot scalar field theory". In: *Phys. Rev. D* 45 (1992). [Erratum: Phys.Rev.D 48, 5965 (1993)], p. 4695. DOI: 10.1103/PhysRevD.45.4695. arXiv: hep-ph/9204216.

[123] Albert M Sirunyan et al. "Combined measurements of Higgs boson couplings in proton–proton collisions at $\sqrt{s} = 13\,\mathrm{TeV}$". In: *Eur. Phys. J.* C79.5 (2019), p. 421. DOI: 10.1140/epjc/s10052-019-6909-y. arXiv: 1809.10733 [hep-ex].

[124] Georges Aad et al. "Combined measurements of Higgs boson production and decay using up to 80 fb^{-1} of proton-proton collision data at $\sqrt{s} = 13$ TeV collected with the ATLAS experiment". In: *Phys. Rev.* D101.1 (2020), p. 012002. DOI: 10.1103/PhysRevD.101.012002. arXiv: 1909.02845 [hep-ex].

[125] Morad Aaboud et al. "Combination of the searches for pair-produced vector-like partners of the third-generation quarks at $\sqrt{s} = 13$ TeV with the ATLAS detector". In: *Phys. Rev. Lett.* 121.21 (2018), p. 211801. DOI: 10.1103/PhysRevLett.121.211801. arXiv: 1808.02343 [hep-ex].

[126] Albert M Sirunyan et al. "Search for vector-like T and B quark pairs in final states with leptons at $\sqrt{s} = 13$ TeV". In: *JHEP* 08 (2018), p. 177. DOI: 10.1007/JHEP08(2018)177. arXiv: 1805.04758 [hep-ex].

[127] G. Brooijmans et al. “Les Houches 2019 Physics at TeV Colliders: New Physics Working Group Report”. In: *11th Les Houches Workshop on Physics at TeV Colliders: PhysTeV Les Houches*. 2019. arXiv: 2002.12220 [hep-ph].

[128] Giacomo Cacciapaglia et al. “Exotic decays of top partners: mind the search gap”. In: *Phys. Lett.* B798 (2019), p. 135015. DOI: 10.1016/j.physletb.2019.135015. arXiv: 1908.07524 [hep-ph].

[129] S. Dawson and E. Furlan. “A Higgs Conundrum with Vector Fermions”. In: *Phys. Rev. D* 86 (2012), p. 015021. DOI: 10.1103/PhysRevD.86.015021. arXiv: 1205.4733 [hep-ph].

[130] M. Tanabashi et al. “Review of Particle Physics”. In: *Phys. Rev.* D98.3 (2018), p. 030001. DOI: 10.1103/PhysRevD.98.030001.

[131] Nathaniel Craig et al. “Shedding Light on Diphoton Resonances”. In: *Phys. Rev.* D93.11 (2016), p. 115023. DOI: 10.1103/PhysRevD.93.115023. arXiv: 1512.07733 [hep-ph].

[132] “Search for resonances decaying to photon pairs in 139 fb^{-1} of pp collisions at $\sqrt{s} = 13$ TeV with the ATLAS detector.” In: (Aug. 2020).

[133] The ATLAS collaboration. “Search for resonances in the 65 to 110 GeV diphoton invariant mass range using 80 fb^{-1} of pp collisions collected at $\sqrt{s} = 13$ TeV with the ATLAS detector”. In: (2018).

[134] Albert M Sirunyan et al. “Search for a standard model-like Higgs boson in the mass range between 70 and 110 GeV in the diphoton final state in proton-proton collisions at $\sqrt{s} = 8$ and 13 TeV”. In: *Phys. Lett.* B793 (2019), pp. 320–347. DOI: 10.1016/j.physletb.2019.03.064. arXiv: 1811.08459 [hep-ex].

[135] Georges Aad et al. “Search for new phenomena in events with two opposite-charge leptons, jets and missing transverse momentum in pp collisions at $\sqrt{s} = 13$ TeV with the ATLAS detector”. In: (Feb. 2021). arXiv: 2102.01444 [hep-ex].

[136] Albert M Sirunyan et al. “Search for top squarks and dark matter particles in opposite-charge dilepton final states at $\sqrt{s} = 13$ TeV”. In: *Phys. Rev. D* 97.3 (2018), p. 032009. DOI: 10.1103/PhysRevD.97.032009. arXiv: 1711.00752 [hep-ex].

[137] K. Enqvist et al. “Nucleation and bubble growth in a first order cosmological electroweak phase transition”. In: *Phys. Rev. D* 45 (1992), pp. 3415–3428. DOI: 10.1103/PhysRevD.45.3415.

[138] Mariano Quiros. “Finite temperature field theory and phase transitions”. In: *Proceedings, Summer School in High-energy physics and cosmology: Trieste, Italy, June 29-July 17, 1998*. 1999, pp. 187–259. arXiv: hep-ph/9901312 [hep-ph].

[139] James M. Cline, Kimmo Kainulainen, and David Tucker-Smith. “Electroweak baryogenesis from a dark sector”. In: *Phys. Rev. D* 95.11 (2017), p. 115006. DOI: 10.1103/PhysRevD.95.115006. arXiv: 1702.08909 [hep-ph].

[140] Sidney R. Coleman. “The Fate of the False Vacuum. 1. Semiclassical Theory”. In: *Phys. Rev. D* 15 (1977). [Erratum: Phys.Rev.D 16, 1248 (1977)], pp. 2929–2936. DOI: 10.1103/PhysRevD.16.1248.

[141] Marc Kamionkowski, Arthur Kosowsky, and Michael S. Turner. “Gravitational radiation from first order phase transitions”. In: *Phys. Rev. D* 49 (1994), pp. 2837–2851. DOI: 10.1103/PhysRevD.49.2837. arXiv: astro-ph/9310044.

[142] Jose R. Espinosa et al. “Energy Budget of Cosmological First-order Phase Transitions”. In: *JCAP* 06 (2010), p. 028. DOI: 10.1088/1475-7516/2010/06/028. arXiv: 1004.4187 [hep-ph].

[143] Stephan J. Huber and Miguel Sopena. “An efficient approach to electroweak bubble velocities”. In: (Feb. 2013). arXiv: 1302.1044 [hep-ph].

[144] Mark Hindmarsh et al. “Shape of the acoustic gravitational wave power spectrum from a first order phase transition”. In: *Phys. Rev. D* 96.10 (2017). [Erratum: Phys.Rev.D 101, 089902 (2020)], p. 103520. DOI: 10.1103/PhysRevD.96.103520. arXiv: 1704.05871 [astro-ph.CO].

[145] Alberto Roper Pol et al. “Numerical simulations of gravitational waves from early-universe turbulence”. In: *Phys. Rev. D* 102.8 (2020), p. 083512. DOI: 10.1103/PhysRevD.102.083512. arXiv: 1903.08585 [astro-ph.CO].

[146] Vincent Corbin and Neil J. Cornish. “Detecting the cosmic gravitational wave background with the big bang observer”. In: *Class. Quant. Grav.* 23 (2006), pp. 2435–2446. DOI: 10.1088/0264-9381/23/7/014. arXiv: gr-qc/0512039.

[147] Eric Thrane and Joseph D. Romano. "Sensitivity curves for searches for gravitational-wave backgrounds". In: *Phys. Rev. D* 88.12 (2013), p. 124032. DOI: 10.1103/PhysRevD.88.124032. arXiv: 1310.5300 [astro-ph.IM].

[148] Moritz Breitbach et al. "Dark, Cold, and Noisy: Constraining Secluded Hidden Sectors with Gravitational Waves". In: *JCAP* 07 (2019), p. 007. DOI: 10.1088/1475-7516/2019/07/007. arXiv: 1811.11175 [hep-ph].

[149] Tommi Alanne et al. "A fresh look at the gravitational-wave signal from cosmological phase transitions". In: *JHEP* 03 (2020), p. 004. DOI: 10.1007/JHEP03(2020)004. arXiv: 1909.11356 [hep-ph].

[150] Kai Schmitz. "New Sensitivity Curves for Gravitational-Wave Signals from Cosmological Phase Transitions". In: *JHEP* 01 (2021), p. 097. DOI: 10.1007/JHEP01(2021)097. arXiv: 2002.04615 [hep-ph].

[151] Kai Schmitz. "LISA Sensitivity to Gravitational Waves from Sound Waves". In: *Symmetry* 12.9 (2020), p. 1477. DOI: 10.3390/sym12091477. arXiv: 2005.10789 [hep-ph].

[152] Eric Thrane and Joseph D. Romano. "Sensitivity curves for searches for gravitational-wave backgrounds". In: *Phys. Rev. D* 88.12 (2013), p. 124032. DOI: 10.1103/PhysRevD.88.124032. arXiv: 1310.5300 [astro-ph.IM].

[153] Michela D'Onofrio, Kari Rummukainen, and Anders Tranberg. "Sphaleron Rate in the Minimal Standard Model". In: *Phys. Rev. Lett.* 113.14 (2014), p. 141602. DOI: 10.1103/PhysRevLett.113.141602. arXiv: 1404.3565 [hep-ph].

[154] James M. Cline, Kimmo Kainulainen, and Michael Trott. "Electroweak Baryogenesis in Two Higgs Doublet Models and B meson anomalies". In: *JHEP* 11 (2011), p. 089. DOI: 10.1007/JHEP11(2011)089. arXiv: 1107.3559 [hep-ph].

[155] Antonio Riotto. "Towards a nonequilibrium quantum field theory approach to electroweak baryogenesis". In: *Phys. Rev.* D53 (1996), pp. 5834–5841. DOI: 10.1103/PhysRevD.53.5834. arXiv: hep-ph/9510271 [hep-ph].

[156] A. Riotto. "Supersymmetric electroweak baryogenesis, nonequilibrium field theory and quantum Boltzmann equations". In: *Nucl. Phys.* B518 (1998), pp. 339–360. DOI: 10.1016/S0550-3213(98)00159-X. arXiv: hep-ph/9712221 [hep-ph].

[157] Kimmo Kainulainen et al. "First principle derivation of semiclassical force for electroweak baryogenesis". In: *JHEP* 06 (2001), p. 031. DOI: 10.1088/1126-6708/2001/06/031. arXiv: hep-ph/0105295 [hep-ph].

[158] Kimmo Kainulainen et al. "Semiclassical force for electroweak baryogenesis: Three-dimensional derivation". In: *Phys. Rev.* D66 (2002), p. 043502. DOI: 10.1103/PhysRevD.66.043502. arXiv: hep-ph/0202177 [hep-ph].

[159] Tomislav Prokopec, Michael G. Schmidt, and Steffen Weinstock. "Transport equations for chiral fermions to order h bar and electroweak baryogenesis. Part 1". In: *Annals Phys.* 314 (2004), pp. 208–265. DOI: 10.1016/j.aop.2004.06.002. arXiv: hep-ph/0312110 [hep-ph].

[160] Tomislav Prokopec, Michael G. Schmidt, and Steffen Weinstock. "Transport equations for chiral fermions to order h-bar and electroweak baryogenesis. Part II". In: *Annals Phys.* 314 (2004), pp. 267–320. DOI: 10.1016/j.aop.2004.06.001. arXiv: hep-ph/0406140 [hep-ph].

[161] Henri Jukkala, Kimmo Kainulainen, and Olli Koskivaara. "Quantum transport and the phase space structure of the Wightman functions". In: *JHEP* 01 (2020), p. 012. DOI: 10.1007/JHEP01(2020)012. arXiv: 1910.10979 [hep-th].

[162] Tomáš Brauner et al. "Dimensional reduction of the Standard Model coupled to a new singlet scalar field". In: *JHEP* 03 (2017), p. 007. DOI: 10.1007/JHEP03(2017)007. arXiv: 1609.06230 [hep-ph].

[163] Kimmo Kainulainen et al. "On the validity of perturbative studies of the electroweak phase transition in the Two Higgs Doublet model". In: *JHEP* 06 (2019), p. 075. DOI: 10.1007/JHEP06(2019)075. arXiv: 1904.01329 [hep-ph].

[164] Djuna Croon et al. "Theoretical uncertainties for cosmological first-order phase transitions". In: (Sept. 2020). arXiv: 2009.10080 [hep-ph].

[165] Daniel Cutting, Mark Hindmarsh, and David J. Weir. "Vorticity, kinetic energy, and suppressed gravitational wave production in strong first order phase transitions". In: *Phys. Rev. Lett.* 125.2 (2020), p. 021302. DOI: 10.1103/PhysRevLett.125.021302. arXiv: 1906.00480 [hep-ph].

[166] Daniel Cutting et al. "Gravitational waves from vacuum first order phase transitions II: from thin to thick walls". In: (May 2020). arXiv: 2005.13537 [astro-ph.CO].

Chapter 4

Conclusions

This thesis has substantially improved the calculation of the BAU and GW spectrum produced during a first-order EWPT. This has been accomplished by rederiving the fluid equations that describe the loss of thermal equilibrium in the wall, which is required to determine the velocity and the shape of the electroweak bubble wall. Using this improved formalism, it is possible to study the electroweak bubble's behaviour without any constraint on the wall velocity, which was previously prohibited by the unphysical singularity of the fluid equations at the speed of sound.

We have applied these new fluid equations to the Z_2-symmetric singlet scalar extension, which has led to a number of surprising results. While the deflagration and hybrid solutions cover a wide range of velocities, all the detonation solutions are ultrarelativistic, with $v_w \approx 1$ ($\gamma > 10$). It is caused by the shock wave's reheating as the wall velocity approaches the speed of sound. This creates a pressure barrier preventing the wall from becoming a detonation, unless the PT is very strong, in which case the wall reaches an ultrarelativistic velocity. This pressure barrier also implies that a large fraction of the walls reaches a terminal velocity close to the speed of sound. Additionally, contrary to the standard expectation, we found a positive correlation between the BAU and the GW signal's strength, at least within the deflagration and hybrid walls. An significant fraction of the models considered is able to reproduce the observed BAU, which indicates that this EWBG scenario is a good candidate to solve the matter-antimatter asymmetry problem. However, only a small fraction of order 1% could produce GW detectable by next-generation space-based detectors.

Although the analysis presented in this thesis represents a clear improvement over the standard treatment, there are still many ways it could be extended further. The collision integrals calculated in Chapter 2 are only good to leading-log accuracy, which is quite imprecise. A next-to-leading-log calculation could substantially improve these terms' accuracy, leading to a more precise determination of the wall velocity. Moreover, we neglected the friction on the wall from the scalar fields, which could also have some effect on the wall velocity. Finally, the formulas to compute the GW spectrum are not expected to be accurate for wall velocities close to the speed of sound. A considerable fraction of our models fall into that range; therefore, we can expect a large error regarding these models' detectability.

The formalism developed in Chapter 2 is very general: it is straightforward to apply it to any model of a first-order EWPT. This thesis has shown that EWBG is a viable option, but it is not limited to the singlet scalar extension considered here. It would be quite interesting to do a survey of some of the most popular models of EWBG and make a thorough comparison between them. In some cases, it would also be possible to predict dark matter, which would have great implications for cosmology. A general better understanding of physics at high energy is possible by further improving the methodology and continuing the work undertaken in this thesis.

Bibliography

[1] Benoit Laurent and James M. Cline. "Fluid equations for fast-moving electroweak bubble walls". In: *Phys. Rev. D* 102.6 (2020), p. 063516. DOI: 10.1103/PhysRevD.102.063516. arXiv: 2007.10935 [hep-ph].

[2] Guy D. Moore and Tomislav Prokopec. "How fast can the wall move? A Study of the electroweak phase transition dynamics". In: *Phys. Rev. D* 52 (1995), pp. 7182–7204. DOI: 10.1103/PhysRevD.52.7182. arXiv: hep-ph/9506475.

[3] James M. Cline and Kimmo Kainulainen. "Electroweak baryogenesis at high bubble wall velocities". In: *Phys. Rev. D* 101.6 (2020), p. 063525. DOI: 10.1103/PhysRevD.101.063525. arXiv: 2001.00568 [hep-ph].

[4] James M. Cline et al. "Baryogenesis and gravity waves from a UV-completed electroweak phase transition". In: (Feb. 2021). arXiv: 2102.12490 [hep-ph].

[5] Pau Amaro-Seoane et al. "Laser Interferometer Space Antenna". In: (Feb. 2017). arXiv: 1702.00786 [astro-ph.IM].

[6] A. I. Bochkarev, S. V. Kuzmin, and M. E. Shaposhnikov. "Electroweak baryogenesis and the Higgs boson mass problem". In: *Phys. Lett.* B244 (1990), pp. 275–278. DOI: 10.1016/0370-2693(90)90069-I.

[7] Andrew G. Cohen, David B. Kaplan, and Ann E. Nelson. "Weak scale baryogenesis". In: *Phys. Lett.* B245 (1990), pp. 561–564. DOI: 10.1016/0370-2693(90)90690-8.

[8] Andrew G. Cohen, David B. Kaplan, and Ann E. Nelson. "Baryogenesis at the weak phase transition". In: *Nucl. Phys.* B349 (1991), pp. 727–742. DOI: 10.1016/0550-3213(91)90395-E.

[9] Neil Turok and John Zadrozny. "Electroweak baryogenesis in the two doublet model". In: *Nucl. Phys.* B358 (1991), pp. 471–493. DOI: 10.1016/0550-3213(91)90356-3.

[10] Ankit Beniwal et al. "Gravitational waves and electroweak baryogenesis in a global study of the extended scalar singlet model". In: *JHEP* 02 (2019), p. 183. DOI: 10.1007/JHEP02(2019)183. arXiv: 1810.02380 [hep-ph].

[11] John Ellis, Marek Lewicki, and Ville Vaskonen. "Updated predictions for gravitational waves produced in a strongly supercooled phase transition". In: (July 2020). arXiv: 2007.15586 [astro-ph.CO].

[12] Tomislav Prokopec, Jonas Rezacek, and Bogumiła Świeżewska. "Gravitational waves from conformal symmetry breaking". In: *JCAP* 02 (2019), p. 009. DOI: 10.1088/1475-7516/2019/02/009. arXiv: 1809.11129 [hep-ph].

[13] Carlo Marzo, Luca Marzola, and Ville Vaskonen. "Phase transition and vacuum stability in the classically conformal B–L model". In: *Eur. Phys. J. C* 79.7 (2019), p. 601. DOI: 10.1140/epjc/s10052-019-7076-x. arXiv: 1811.11169 [hep-ph].

[14] P. S. Bhupal Dev et al. "Gravitational Waves from First-Order Phase Transition in a Simple Axion-Like Particle Model". In: *JCAP* 11 (2019), p. 006. DOI: 10.1088/1475-7516/2019/11/006. arXiv: 1905.00891 [hep-ph].

[15] Ville Vaskonen. "Electroweak baryogenesis and gravitational waves from a real scalar singlet". In: *Phys. Rev. D* 95.12 (2017), p. 123515. DOI: 10.1103/PhysRevD.95.123515. arXiv: 1611.02073 [hep-ph].

[16] Zhaofeng Kang, P. Ko, and Toshinori Matsui. "Strong first order EWPT \& strong gravitational waves in Z_3-symmetric singlet scalar extension". In: *JHEP* 02 (2018), p. 115. DOI: 10.1007/JHEP02(2018)115. arXiv: 1706.09721 [hep-ph].

[17] Ankit Beniwal et al. "Gravitational wave, collider and dark matter signals from a scalar singlet electroweak baryogenesis". In: *JHEP* 08 (2017), p. 108. DOI: 10.1007/JHEP08(2017)108. arXiv: 1702.06124 [hep-ph].

[18] Alexandre Alves et al. "Collider and Gravitational Wave Complementarity in Exploring the Singlet Extension of the Standard Model". In: *JHEP* 04 (2019), p. 052. DOI: 10.1007/JHEP04(2019)052. arXiv: 1812.09333 [hep-ph].

[19] Marcela Carena, Zhen Liu, and Yikun Wang. "Electroweak phase transition with spontaneous Z_2-breaking". In: *JHEP* 08 (2020), p. 107. DOI: 10.1007/JHEP08(2020)107. arXiv: 1911.10206 [hep-ph].

[20] Ke-Pan Xie. "Lepton-mediated electroweak baryogenesis, gravitational waves and the 4τ final state at the collider". In: *JHEP* 02 (2021), p. 090. DOI: 10.1007/JHEP02(2021)090. arXiv: 2011.04821 [hep-ph].

[21] Edward W. Kolb and Michael S. Turner. *The Early Universe*. Vol. 69. 1990. ISBN: 978-0-201-62674-2.

[22] J. I. Kapusta and Charles Gale. *Finite-temperature field theory: Principles and applications*. Cambridge Monographs on Mathematical Physics. Cambridge University Press, 2011. ISBN: 978-0-521-17322-3, 978-0-521-82082-0, 978-0-511-22280-1. DOI: 10.1017/CBO9780511535130.

[23] Andrei D. Linde. "Fate of the False Vacuum at Finite Temperature: Theory and Applications". In: *Phys. Lett.* 100B (1981), pp. 37–40. DOI: 10.1016/0370-2693(81)90281-1.

[24] Carroll L. Wainwright. "CosmoTransitions: Computing Cosmological Phase Transition Temperatures and Bubble Profiles with Multiple Fields". In: *Comput. Phys. Commun.* 183 (2012), pp. 2006–2013. DOI: 10.1016/j.cpc.2012.04.004. arXiv: 1109.4189 [hep-ph].

[25] K. Kajantie et al. "Is there a hot electroweak phase transition at $m_H \geq m_W$?" In: *Phys. Rev. Lett.* 77 (1996), pp. 2887–2890. DOI: 10.1103/PhysRevLett.77.2887. arXiv: hep-ph/9605288.

[26] K. Kajantie et al. "A Nonperturbative analysis of the finite T phase transition in SU(2) x U(1) electroweak theory". In: *Nucl. Phys.* B493 (1997), pp. 413–438. DOI: 10.1016/S0550-3213(97)00164-8. arXiv: hep-lat/9612006 [hep-lat].

[27] K. Rummukainen et al. "The Universality class of the electroweak theory". In: *Nucl. Phys. B* 532 (1998), pp. 283–314. DOI: 10.1016/S0550-3213(98)00494-5. arXiv: hep-lat/9805013.

[28] Greg W. Anderson and Lawrence J. Hall. "The Electroweak phase transition and baryogenesis". In: *Phys. Rev. D* 45 (1992), pp. 2685–2698. DOI: 10.1103/PhysRevD.45.2685.

[29] John McDonald. "Electroweak baryogenesis and dark matter via a gauge singlet scalar". In: *Phys. Lett. B* 323 (1994), pp. 339–346. DOI: 10.1016/0370-2693(94)91229-7.

[30] Jarny Choi and R. R. Volkas. "Real Higgs singlet and the electroweak phase transition in the Standard Model". In: *Phys. Lett. B* 317 (1993), pp. 385–391. DOI: 10.1016/0370-2693(93)91013-D. arXiv: hep-ph/9308234.

[31] Jose Ramon Espinosa and Mariano Quiros. "Novel Effects in Electroweak Breaking from a Hidden Sector". In: *Phys. Rev. D* 76 (2007), p. 076004. DOI: 10.1103/PhysRevD.76.076004. arXiv: hep-ph/0701145.

[32] Stefano Profumo, Michael J. Ramsey-Musolf, and Gabe Shaughnessy. "Singlet Higgs phenomenology and the electroweak phase transition". In: *JHEP* 08 (2007), p. 010. DOI: 10.1088/1126-6708/2007/08/010. arXiv: 0705.2425 [hep-ph].

[33] Jose R. Espinosa, Thomas Konstandin, and Francesco Riva. "Strong Electroweak Phase Transitions in the Standard Model with a Singlet". In: *Nucl. Phys.* B854 (2012), pp. 592–630. DOI: 10.1016/j.nuclphysb.2011.09.010. arXiv: 1107.5441 [hep-ph].

[34] James M. Cline et al. "Update on scalar singlet dark matter". In: *Phys. Rev. D* 88 (2013). [Erratum: Phys.Rev.D 92, 039906 (2015)], p. 055025. DOI: 10.1103/PhysRevD.88.055025. arXiv: 1306.4710 [hep-ph].

[35] P. H. Damgaard et al. "Effective Field Theory and Electroweak Baryogenesis in the Singlet-Extended Standard Model". In: *JHEP* 02 (2016), p. 107. DOI: 10.1007/JHEP02(2016)107. arXiv: 1512.01963 [hep-ph].

[36] Gowri Kurup and Maxim Perelstein. "Dynamics of Electroweak Phase Transition In Singlet-Scalar Extension of the Standard Model". In: *Phys. Rev. D* 96.1 (2017), p. 015036. DOI: 10.1103/PhysRevD.96.015036. arXiv: 1704.03381 [hep-ph].

[37] Cheng-Wei Chiang, Yen-Ting Li, and Eibun Senaha. "Revisiting electroweak phase transition in the standard model with a real singlet scalar". In: *Phys. Lett. B* 789 (2019), pp. 154–159. DOI: 10.1016/j.physletb.2018.12.017. arXiv: 1808.01098 [hep-ph].

[38] N. Aghanim et al. "Planck 2018 results. VI. Cosmological parameters". In: *Astron. Astrophys.* 641 (2020), A6. DOI: 10.1051/0004-6361/201833910. arXiv: 1807.06209 [astro-ph.CO].

[39] Richard H. Cyburt. “Primordial nucleosynthesis for the new cosmology: Determining uncertainties and examining concordance”. In: *Phys. Rev. D* 70 (2004), p. 023505. DOI: 10.1103/PhysRevD.70.023505. arXiv: astro-ph/0401091.

[40] James M. Cline. “Baryogenesis”. In: *Les Houches Summer School - Session 86: Particle Physics and Cosmology: The Fabric of Spacetime.* Sept. 2006. arXiv: hep-ph/0609145.

[41] W. Buchmuller, P. Di Bari, and M. Plumacher. “Leptogenesis for pedestrians”. In: *Annals Phys.* 315 (2005), pp. 305–351. DOI: 10.1016/j.aop.2004.02.003. arXiv: hep-ph/0401240.

[42] W. Buchmuller, P. Di Bari, and M. Plumacher. “Some aspects of thermal leptogenesis”. In: *New J. Phys.* 6 (2004), p. 105. DOI: 10.1088/1367-2630/6/1/105. arXiv: hep-ph/0406014.

[43] W. Buchmuller, R. D. Peccei, and T. Yanagida. “Leptogenesis as the origin of matter”. In: *Ann. Rev. Nucl. Part. Sci.* 55 (2005), pp. 311–355. DOI: 10.1146/annurev.nucl.55.090704.151558. arXiv: hep-ph/0502169.

[44] Mu-Chun Chen. “TASI 2006 Lectures on Leptogenesis”. In: *Theoretical Advanced Study Institute in Elementary Particle Physics: Exploring New Frontiers Using Colliders and Neutrinos.* Mar. 2007, pp. 123–176. arXiv: hep-ph/0703087.

[45] Ian Affleck and Michael Dine. “A New Mechanism for Baryogenesis”. In: *Nucl. Phys. B* 249 (1985), pp. 361–380. DOI: 10.1016/0550-3213(85)90021-5.

[46] A. D. Sakharov. “Violation of CP Invariance, C asymmetry, and baryon asymmetry of the universe”. In: *Pisma Zh. Eksp. Teor. Fiz.* 5 (1967), pp. 32–35. DOI: 10.1070/PU1991v034n05ABEH002497.

[47] Gerard ’t Hooft. “Symmetry Breaking Through Bell-Jackiw Anomalies”. In: *Phys. Rev. Lett.* 37 (1976). Ed. by Mikhail A. Shifman, pp. 8–11. DOI: 10.1103/PhysRevLett.37.8.

[48] Sidney R. Coleman. “The Uses of Instantons”. In: *Subnucl. Ser.* 15 (1979). Ed. by Mikhail A. Shifman, p. 805.

[49] V. A. Kuzmin, V. A. Rubakov, and M. E. Shaposhnikov. “On the Anomalous Electroweak Baryon Number Nonconservation in the Early Universe”. In: *Phys. Lett. B* 155 (1985), p. 36. DOI: 10.1016/0370-2693(85)91028-7.

[50] D. Bodeker, Guy D. Moore, and K. Rummukainen. “Chern-Simons number diffusion and hard thermal loops on the lattice”. In: *Phys. Rev. D* 61 (2000), p. 056003. DOI: 10.1103/PhysRevD.61.056003. arXiv: hep-ph/9907545.

[51] Guy D. Moore. “Measuring the broken phase sphaleron rate nonperturbatively”. In: *Phys. Rev. D* 59 (1999), p. 014503. DOI: 10.1103/PhysRevD.59.014503. arXiv: hep-ph/9805264.

[52] Kaori Fuyuto and Eibun Senaha. “Improved sphaleron decoupling condition and the Higgs coupling constants in the real singlet-extended standard model”. In: *Phys. Rev. D* 90.1 (2014), p. 015015. DOI: 10.1103/PhysRevD.90.015015. arXiv: 1406.0433 [hep-ph].

[53] Hiren H. Patel and Michael J. Ramsey-Musolf. “Baryon Washout, Electroweak Phase Transition, and Perturbation Theory”. In: *JHEP* 07 (2011), p. 029. DOI: 10.1007/JHEP07(2011)029. arXiv: 1101.4665 [hep-ph].

[54] J. H. Christenson et al. “Evidence for the 2π Decay of the K_2^0 Meson”. In: *Phys. Rev. Lett.* 13 (1964), pp. 138–140. DOI: 10.1103/PhysRevLett.13.138.

[55] Bernard Aubert et al. “Observation of CP violation in the B^0 meson system”. In: *Phys. Rev. Lett.* 87 (2001), p. 091801. DOI: 10.1103/PhysRevLett.87.091801. arXiv: hep-ex/0107013.

[56] Roel Aaij et al. “Observation of CP Violation in Charm Decays”. In: *Phys. Rev. Lett.* 122.21 (2019), p. 211803. DOI: 10.1103/PhysRevLett.122.211803. arXiv: 1903.08726 [hep-ex].

[57] Jose R. Espinosa et al. “Electroweak Baryogenesis in Non-minimal Composite Higgs Models”. In: *JCAP* 01 (2012), p. 012. DOI: 10.1088/1475-7516/2012/01/012. arXiv: 1110.2876 [hep-ph].

[58] Björn Garbrecht. “Why is there more matter than antimatter? Calculational methods for leptogenesis and electroweak baryogenesis”. In: *Prog. Part. Nucl. Phys.* 110 (2020), p. 103727. DOI: 10.1016/j.ppnp.2019.103727. arXiv: 1812.02651 [hep-ph].

[59] David E. Morrissey and Michael J. Ramsey-Musolf. “Electroweak baryogenesis”. In: *New J. Phys.* 14 (2012), p. 125003. DOI: 10.1088/1367-2630/14/12/125003. arXiv: 1206.2942 [hep-ph].

[60] K. Kajantie et al. “The Electroweak phase transition: A Nonperturbative analysis”. In: *Nucl. Phys. B* 466 (1996), pp. 189–258. DOI: 10.1016/0550-3213(96)00052-1. arXiv: hep-lat/9510020.

[61] Mark Trodden. "Electroweak baryogenesis". In: *Rev. Mod. Phys.* 71 (1999), pp. 1463–1500. DOI: 10.1103/RevModPhys.71.1463. arXiv: hep-ph/9803479.

[62] Chiara Caprini et al. "Science with the space-based interferometer eLISA. II: Gravitational waves from cosmological phase transitions". In: *JCAP* 04 (2016), p. 001. DOI: 10.1088/1475-7516/2016/04/001. arXiv: 1512.06239 [astro-ph.CO].

[63] Chiara Caprini et al. "Detecting gravitational waves from cosmological phase transitions with LISA: an update". In: *JCAP* 03 (2020), p. 024. DOI: 10.1088/1475-7516/2020/03/024. arXiv: 1910.13125 [astro-ph.CO].

[64] Jose R. Espinosa et al. "Energy Budget of Cosmological First-order Phase Transitions". In: *JCAP* 06 (2010), p. 028. DOI: 10.1088/1475-7516/2010/06/028. arXiv: 1004.4187 [hep-ph].

[65] Thomas Konstandin, Germano Nardini, and Ingo Rues. "From Boltzmann equations to steady wall velocities". In: *JCAP* 09 (2014), p. 028. DOI: 10.1088/1475-7516/2014/09/028. arXiv: 1407.3132 [hep-ph].

[66] Stephan J. Huber and Miguel Sopena. "An efficient approach to electroweak bubble velocities". In: (2013). arXiv: 1302.1044 [hep-ph].

[67] Ariel Mégevand and Alejandro D. Sánchez. "Velocity of electroweak bubble walls". In: *Nuclear Physics B* 825 (2010), p. 151. ISSN: 0550-3213. DOI: 10.1016/j.nuclphysb.2009.09.019. arXiv: 0908.3663 [hep-ph].

[68] Jonathan Kozaczuk. "Bubble Expansion and the Viability of Singlet-Driven Electroweak Baryogenesis". In: *JHEP* 10 (2015), p. 135. DOI: 10.1007/JHEP10(2015)135. arXiv: 1506.04741 [hep-ph].

[69] Dietrich Bodeker and Guy D. Moore. "Can electroweak bubble walls run away?" In: *JCAP* 05 (2009), p. 009. DOI: 10.1088/1475-7516/2009/05/009. arXiv: 0903.4099 [hep-ph].

[70] Dietrich Bodeker and Guy D. Moore. "Electroweak Bubble Wall Speed Limit". In: *JCAP* 05 (2017), p. 025. DOI: 10.1088/1475-7516/2017/05/025. arXiv: 1703.08215 [hep-ph].

[71] Ariel Mégevand. "Friction forces on phase transition fronts". In: *JCAP* 07 (2013), p. 045. DOI: 10.1088/1475-7516/2013/07/045. arXiv: 1303.4233 [astro-ph.CO].

[72] Guy D. Moore and Tomislav Prokopec. "Bubble wall velocity in a first order electroweak phase transition". In: *Phys. Rev. Lett.* 75 (1995), pp. 777–780. DOI: 10.1103/PhysRevLett.75.777. arXiv: hep-ph/9503296.

[73] P. John and M.G. Schmidt. "Do stops slow down electroweak bubble walls?" In: *Nucl. Phys. B* 598 (2001). [Erratum: Nucl.Phys.B 648, 449–452 (2003)], pp. 291–305. DOI: 10.1016/S0550-3213(00)00768-9. arXiv: hep-ph/0002050.

[74] Stephan J. Huber and Miguel Sopena. "The bubble wall velocity in the minimal supersymmetric light stop scenario". In: *Phys. Rev. D* 85 (2012), p. 103507. DOI: 10.1103/PhysRevD.85.103507. arXiv: 1112.1888 [hep-ph].

[75] Glauber C. Dorsch, Stephan J. Huber, and Thomas Konstandin. "Bubble wall velocities in the Standard Model and beyond". In: *JCAP* 12 (2018), p. 034. DOI: 10.1088/1475-7516/2018/12/034. arXiv: 1809.04907 [hep-ph].

[76] Michael Joyce, Tomislav Prokopec, and Neil Turok. "Nonlocal electroweak baryogenesis. Part 2: The Classical regime". In: *Phys. Rev. D* 53 (1996), pp. 2958–2980. DOI: 10.1103/PhysRevD.53.2958. arXiv: hep-ph/9410282.

[77] James M. Cline, Michael Joyce, and Kimmo Kainulainen. "Supersymmetric electroweak baryogenesis". In: *JHEP* 07 (2000), p. 018. DOI: 10.1088/1126-6708/2000/07/018. arXiv: hep-ph/0006119.

[78] Lars Fromme, Stephan J. Huber, and Michael Seniuch. "Baryogenesis in the two-Higgs doublet model". In: *JHEP* 11 (2006), p. 038. DOI: 10.1088/1126-6708/2006/11/038. arXiv: hep-ph/0605242.

[79] Lars Fromme and Stephan J. Huber. "Top transport in electroweak baryogenesis". In: *JHEP* 03 (2007), p. 049. DOI: 10.1088/1126-6708/2007/03/049. arXiv: hep-ph/0604159.

[80] Peter Arnold, Guy David Moore, and Laurence G Yaffe. "Transport coefficients in high temperature gauge theories (I): leading-log results". In: *JHEP* 0011 (2000), p. 001. DOI: 10.1088/1126-6708/2000/11/001. arXiv: hep-ph/0010177 [hep-ph].

[81] H. Arthur Weldon. "Effective Fermion Masses of Order gT in High Temperature Gauge Theories with Exact Chiral Invariance". In: *Phys. Rev. D* 26 (1982), p. 2789. DOI: 10.1103/PhysRevD.26.2789.

[82] Peter Arnold, Guy D Moore, and Laurence G Yaffe. "Transport coefficients in high temperature gauge theories: (II) Beyond leading log". In: *Journal of High Energy Physics* 0305 (2003), p. 051. DOI: 10.1088/1126-6708/2003/05/051. arXiv: hep-ph/0302165 [hep-ph].

[83] Guy D Moore. "Transport coefficients in large Nf gauge theory: testing hard thermal loops". In: *Journal of High Energy Physics* 0105 (2001), p. 039. ISSN: 1029-8479. DOI: 10.1088/1126-6708/2001/05/039. arXiv: hep-ph/0104121 [hep-ph].

[84] Andrew J. Long, Andrea Tesi, and Lian-Tao Wang. "Baryogenesis at a Lepton-Number-Breaking Phase Transition". In: *JHEP* 10 (2017), p. 095. DOI: 10.1007/JHEP10(2017)095. arXiv: 1703.04902 [hep-ph].

[85] Chiara Caprini et al. "Science with the space-based interferometer eLISA. II: Gravitational waves from cosmological phase transitions". In: *JCAP* 04 (2016), p. 001. DOI: 10.1088/1475-7516/2016/04/001. arXiv: 1512.06239 [astro-ph.CO].

[86] Jeff Crowder and Neil J. Cornish. "Beyond LISA: Exploring future gravitational wave missions". In: *Phys. Rev. D* 72 (2005), p. 083005. DOI: 10.1103/PhysRevD.72.083005. arXiv: gr-qc/0506015.

[87] Naoki Seto, Seiji Kawamura, and Takashi Nakamura. "Possibility of direct measurement of the acceleration of the universe using 0.1-Hz band laser interferometer gravitational wave antenna in space". In: *Phys. Rev. Lett.* 87 (2001), p. 221103. DOI: 10.1103/PhysRevLett.87.221103. arXiv: astro-ph/0108011.

[88] Shuichi Sato et al. "The status of DECIGO". In: *J. Phys. Conf. Ser.* 840.1 (2017). Ed. by Domencio Giardini and Philippe Jetzer, p. 012010. DOI: 10.1088/1742-6596/840/1/012010.

[89] Yousef Abou El-Neaj et al. "AEDGE: Atomic Experiment for Dark Matter and Gravity Exploration in Space". In: *EPJ Quant. Technol.* 7 (2020), p. 6. DOI: 10.1140/epjqt/s40507-020-0080-0. arXiv: 1908.00802 [gr-qc].

[90] S. W. Ham, Y. S. Jeong, and S. K. Oh. "Electroweak phase transition in an extension of the standard model with a real Higgs singlet". In: *J. Phys. G* 31.8 (2005), pp. 857–871. DOI: 10.1088/0954-3899/31/8/017. arXiv: hep-ph/0411352.

[91] Andrew Noble and Maxim Perelstein. "Higgs self-coupling as a probe of electroweak phase transition". In: *Phys. Rev. D* 78 (2008), p. 063518. DOI: 10.1103/PhysRevD.78.063518. arXiv: 0711.3018 [hep-ph].

[92] David Curtin, Patrick Meade, and Chiu-Tien Yu. "Testing Electroweak Baryogenesis with Future Colliders". In: *JHEP* 11 (2014), p. 127. DOI: 10.1007/JHEP11(2014)127. arXiv: 1409.0005 [hep-ph].

[93] Stefano Profumo et al. "Singlet-catalyzed electroweak phase transitions and precision Higgs boson studies". In: *Phys. Rev. D* 91.3 (2015), p. 035018. DOI: 10.1103/PhysRevD.91.035018. arXiv: 1407.5342 [hep-ph].

[94] Ashutosh V. Kotwal et al. "Singlet-catalyzed electroweak phase transitions in the 100 TeV frontier". In: *Phys. Rev. D* 94.3 (2016), p. 035022. DOI: 10.1103/PhysRevD.94.035022. arXiv: 1605.06123 [hep-ph].

[95] Peisi Huang, Andrew J. Long, and Lian-Tao Wang. "Probing the Electroweak Phase Transition with Higgs Factories and Gravitational Waves". In: *Phys. Rev. D* 94.7 (2016), p. 075008. DOI: 10.1103/PhysRevD.94.075008. arXiv: 1608.06619 [hep-ph].

[96] Chien-Yi Chen, Jonathan Kozaczuk, and Ian M. Lewis. "Non-resonant Collider Signatures of a Singlet-Driven Electroweak Phase Transition". In: *JHEP* 08 (2017), p. 096. DOI: 10.1007/JHEP08(2017)096. arXiv: 1704.05844 [hep-ph].

[97] Jeong Han Kim and Ian M. Lewis. "Loop Induced Single Top Partner Production and Decay at the LHC". In: *JHEP* 05 (2018), p. 095. DOI: 10.1007/JHEP05(2018)095. arXiv: 1803.06351 [hep-ph].

[98] Katsuya Hashino et al. "Selecting models of first-order phase transitions using the synergy between collider and gravitational-wave experiments". In: *Phys. Rev. D* 99.7 (2019), p. 075011. DOI: 10.1103/PhysRevD.99.075011. arXiv: 1809.04994 [hep-ph].

[99] Michael J. Ramsey-Musolf. "The electroweak phase transition: a collider target". In: *JHEP* 09 (2020), p. 179. DOI: 10.1007/JHEP09(2020)179. arXiv: 1912.07189 [hep-ph].

[100] Shekhar Adhikari, Ian M. Lewis, and Matthew Sullivan. "Beyond the Standard Model Effective Field Theory: The Singlet Extended Standard Model". In: (Mar. 2020). arXiv: 2003.10449 [hep-ph].

[101] Subinoy Das et al. "The Dark Side of the Electroweak Phase Transition". In: *JHEP* 11 (2010), p. 108. DOI: 10.1007/JHEP11(2010)108. arXiv: 0910.1262 [hep-ph].

[102] A. Ashoorioon and T. Konstandin. "Strong electroweak phase transitions without collider traces". In: *JHEP* 07 (2009), p. 086. DOI: 10.1088/1126-6708/2009/07/086. arXiv: 0904.0353 [hep-ph].

[103] Mitsuru Kakizaki, Shinya Kanemura, and Toshinori Matsui. “Gravitational waves as a probe of extended scalar sectors with the first order electroweak phase transition”. In: *Phys. Rev. D* 92.11 (2015), p. 115007. DOI: 10.1103/PhysRevD.92.115007. arXiv: 1509.08394 [hep-ph].

[104] Katsuya Hashino et al. “Synergy between measurements of gravitational waves and the triple-Higgs coupling in probing the first-order electroweak phase transition”. In: *Phys. Rev. D* 94.1 (2016), p. 015005. DOI: 10.1103/PhysRevD.94.015005. arXiv: 1604.02069 [hep-ph].

[105] Mikael Chala, Germano Nardini, and Ivan Sobolev. “Unified explanation for dark matter and electroweak baryogenesis with direct detection and gravitational wave signatures”. In: *Phys. Rev. D* 94.5 (2016), p. 055006. DOI: 10.1103/PhysRevD.94.055006. arXiv: 1605.08663 [hep-ph].

[106] Tommi Tenkanen, Kimmo Tuominen, and Ville Vaskonen. “A Strong Electroweak Phase Transition from the Inflaton Field”. In: *JCAP* 09 (2016), p. 037. DOI: 10.1088/1475-7516/2016/09/037. arXiv: 1606.06063 [hep-ph].

[107] Katsuya Hashino et al. “Gravitational waves and Higgs boson couplings for exploring first order phase transition in the model with a singlet scalar field”. In: *Phys. Lett. B* 766 (2017), pp. 49–54. DOI: 10.1016/j.physletb.2016.12.052. arXiv: 1609.00297 [hep-ph].

[108] Amine Ahriche et al. “Gravitational Waves from Phase Transitions in Models with Charged Singlets”. In: *Phys. Lett. B* 789 (2019), pp. 119–126. DOI: 10.1016/j.physletb.2018.12.013. arXiv: 1809.09883 [hep-ph].

[109] Stefania De Curtis, Luigi Delle Rose, and Giuliano Panico. “Composite Dynamics in the Early Universe”. In: *JHEP* 12 (2019), p. 149. DOI: 10.1007/JHEP12(2019)149. arXiv: 1909.07894 [hep-ph].

[110] Thomas Konstandin and Jose M. No. “Hydrodynamic obstruction to bubble expansion”. In: *JCAP* 02 (2011), p. 008. DOI: 10.1088/1475-7516/2011/02/008. arXiv: 1011.3735 [hep-ph].

[111] Stefan Höche et al. “Towards an all-orders calculation of the electroweak bubble wall velocity”. In: (July 2020). arXiv: 2007.10343 [hep-ph].

[112] Marc Barroso Mancha, Tomislav Prokopec, and Bogumila Swiezewska. “Field-theoretic derivation of bubble-wall force”. In: (May 2020). arXiv: 2005.10875 [hep-th].

[113] Shyam Balaji, Michael Spannowsky, and Carlos Tamarit. “Cosmological bubble friction in local equilibrium”. In: (Oct. 2020). arXiv: 2010.08013 [hep-ph].

[114] Aleksandr Azatov and Miguel Vanvlasselaer. “Bubble wall velocity: heavy physics effects”. In: *JCAP* 01 (2021), p. 058. DOI: 10.1088/1475-7516/2021/01/058. arXiv: 2010.02590 [hep-ph].

[115] Avi Friedlander et al. “Wall speed and shape in singlet-assisted strong electroweak phase transitions”. In: (Sept. 2020). arXiv: 2009.14295 [hep-ph].

[116] Huai-Ke Guo et al. “Phase Transitions in an Expanding Universe: Stochastic Gravitational Waves in Standard and Non-Standard Histories”. In: *JCAP* 01 (2021), p. 001. DOI: 10.1088/1475-7516/2021/01/001. arXiv: 2007.08537 [hep-ph].

[117] Mark B. Hindmarsh et al. “Phase transitions in the early universe”. In: (Aug. 2020). DOI: 10.21468/SciPostPhysLectNotes.24. arXiv: 2008.09136 [astro-ph.CO].

[118] Wolfgang Waltenberger, André Lessa, and Sabine Kraml. “Artificial Proto-Modelling: Building Precursors of a Next Standard Model from Simplified Model Results”. In: (Dec. 2020). arXiv: 2012.12246 [hep-ph].

[119] Jordy de Vries et al. “Electroweak Baryogenesis and the Standard Model Effective Field Theory”. In: *JHEP* 01 (2018), p. 089. DOI: 10.1007/JHEP01(2018)089. arXiv: 1710.04061 [hep-ph].

[120] Marieke Postma and Graham White. “Cosmological phase transitions: is effective field theory just a toy?” In: (Dec. 2020). arXiv: 2012.03953 [hep-ph].

[121] James M. Cline and Kimmo Kainulainen. “Electroweak baryogenesis and dark matter from a singlet Higgs”. In: *JCAP* 01 (2013), p. 012. DOI: 10.1088/1475-7516/2013/01/012. arXiv: 1210.4196 [hep-ph].

[122] Rajesh R. Parwani. “Resummation in a hot scalar field theory”. In: *Phys. Rev. D* 45 (1992). [Erratum: Phys.Rev.D 48, 5965 (1993)], p. 4695. DOI: 10.1103/PhysRevD.45.4695. arXiv: hep-ph/9204216.

[123] Albert M Sirunyan et al. “Combined measurements of Higgs boson couplings in proton–proton collisions at $\sqrt{s} = 13\,\text{TeV}$”. In: *Eur. Phys. J.* C79.5 (2019), p. 421. DOI: 10.1140/epjc/s10052-019-6909-y. arXiv: 1809.10733 [hep-ex].

[124] Georges Aad et al. "Combined measurements of Higgs boson production and decay using up to 80 fb^{-1} of proton-proton collision data at $\sqrt{s} = 13$ TeV collected with the ATLAS experiment". In: *Phys. Rev.* D101.1 (2020), p. 012002. DOI: 10.1103/PhysRevD.101.012002. arXiv: 1909.02845 [hep-ex].

[125] Morad Aaboud et al. "Combination of the searches for pair-produced vector-like partners of the third-generation quarks at $\sqrt{s} = 13$ TeV with the ATLAS detector". In: *Phys. Rev. Lett.* 121.21 (2018), p. 211801. DOI: 10.1103/PhysRevLett.121.211801. arXiv: 1808.02343 [hep-ex].

[126] Albert M Sirunyan et al. "Search for vector-like T and B quark pairs in final states with leptons at $\sqrt{s} = 13$ TeV". In: *JHEP* 08 (2018), p. 177. DOI: 10.1007/JHEP08(2018)177. arXiv: 1805.04758 [hep-ex].

[127] G. Brooijmans et al. "Les Houches 2019 Physics at TeV Colliders: New Physics Working Group Report". In: *11th Les Houches Workshop on Physics at TeV Colliders: PhysTeV Les Houches*. 2019. arXiv: 2002.12220 [hep-ph].

[128] Giacomo Cacciapaglia et al. "Exotic decays of top partners: mind the search gap". In: *Phys. Lett.* B798 (2019), p. 135015. DOI: 10.1016/j.physletb.2019.135015. arXiv: 1908.07524 [hep-ph].

[129] S. Dawson and E. Furlan. "A Higgs Conundrum with Vector Fermions". In: *Phys. Rev. D* 86 (2012), p. 015021. DOI: 10.1103/PhysRevD.86.015021. arXiv: 1205.4733 [hep-ph].

[130] M. Tanabashi et al. "Review of Particle Physics". In: *Phys. Rev.* D98.3 (2018), p. 030001. DOI: 10.1103/PhysRevD.98.030001.

[131] Nathaniel Craig et al. "Shedding Light on Diphoton Resonances". In: *Phys. Rev.* D93.11 (2016), p. 115023. DOI: 10.1103/PhysRevD.93.115023. arXiv: 1512.07733 [hep-ph].

[132] "Search for resonances decaying to photon pairs in 139 fb^{-1} of *pp* collisions at $\sqrt{s} = 13$ TeV with the ATLAS detector." In: (Aug. 2020).

[133] The ATLAS collaboration. "Search for resonances in the 65 to 110 GeV diphoton invariant mass range using 80 fb^{-1} of *pp* collisions collected at $\sqrt{s} = 13$ TeV with the ATLAS detector". In: (2018).

[134] Albert M Sirunyan et al. "Search for a standard model-like Higgs boson in the mass range between 70 and 110 GeV in the diphoton final state in proton-proton collisions at $\sqrt{s} = 8$ and 13 TeV". In: *Phys. Lett.* B793 (2019), pp. 320–347. DOI: 10.1016/j.physletb.2019.03.064. arXiv: 1811.08459 [hep-ex].

[135] Georges Aad et al. "Search for new phenomena in events with two opposite-charge leptons, jets and missing transverse momentum in *pp* collisions at $\sqrt{s} = 13$ TeV with the ATLAS detector". In: (Feb. 2021). arXiv: 2102.01444 [hep-ex].

[136] Albert M Sirunyan et al. "Search for top squarks and dark matter particles in opposite-charge dilepton final states at $\sqrt{s} = 13$ TeV". In: *Phys. Rev. D* 97.3 (2018), p. 032009. DOI: 10.1103/PhysRevD.97.032009. arXiv: 1711.00752 [hep-ex].

[137] K. Enqvist et al. "Nucleation and bubble growth in a first order cosmological electroweak phase transition". In: *Phys. Rev. D* 45 (1992), pp. 3415–3428. DOI: 10.1103/PhysRevD.45.3415.

[138] Mariano Quiros. "Finite temperature field theory and phase transitions". In: *Proceedings, Summer School in High-energy physics and cosmology: Trieste, Italy, June 29-July 17, 1998*. 1999, pp. 187–259. arXiv: hep-ph/9901312 [hep-ph].

[139] James M. Cline, Kimmo Kainulainen, and David Tucker-Smith. "Electroweak baryogenesis from a dark sector". In: *Phys. Rev. D* 95.11 (2017), p. 115006. DOI: 10.1103/PhysRevD.95.115006. arXiv: 1702.08909 [hep-ph].

[140] Sidney R. Coleman. "The Fate of the False Vacuum. 1. Semiclassical Theory". In: *Phys. Rev. D* 15 (1977). [Erratum: Phys.Rev.D 16, 1248 (1977)], pp. 2929–2936. DOI: 10.1103/PhysRevD.16.1248.

[141] Marc Kamionkowski, Arthur Kosowsky, and Michael S. Turner. "Gravitational radiation from first order phase transitions". In: *Phys. Rev. D* 49 (1994), pp. 2837–2851. DOI: 10.1103/PhysRevD.49.2837. arXiv: astro-ph/9310044.

[142] Jose R. Espinosa et al. "Energy Budget of Cosmological First-order Phase Transitions". In: *JCAP* 06 (2010), p. 028. DOI: 10.1088/1475-7516/2010/06/028. arXiv: 1004.4187 [hep-ph].

[143] Stephan J. Huber and Miguel Sopena. "An efficient approach to electroweak bubble velocities". In: (Feb. 2013). arXiv: 1302.1044 [hep-ph].

[144] Mark Hindmarsh et al. “Shape of the acoustic gravitational wave power spectrum from a first order phase transition”. In: *Phys. Rev. D* 96.10 (2017). [Erratum: Phys.Rev.D 101, 089902 (2020)], p. 103520. DOI: 10.1103/PhysRevD.96.103520. arXiv: 1704.05871 [astro-ph.CO].

[145] Alberto Roper Pol et al. “Numerical simulations of gravitational waves from early-universe turbulence”. In: *Phys. Rev. D* 102.8 (2020), p. 083512. DOI: 10.1103/PhysRevD.102.083512. arXiv: 1903.08585 [astro-ph.CO].

[146] Vincent Corbin and Neil J. Cornish. “Detecting the cosmic gravitational wave background with the big bang observer”. In: *Class. Quant. Grav.* 23 (2006), pp. 2435–2446. DOI: 10.1088/0264-9381/23/7/014. arXiv: gr-qc/0512039.

[147] Eric Thrane and Joseph D. Romano. “Sensitivity curves for searches for gravitational-wave backgrounds”. In: *Phys. Rev. D* 88.12 (2013), p. 124032. DOI: 10.1103/PhysRevD.88.124032. arXiv: 1310.5300 [astro-ph.IM].

[148] Moritz Breitbach et al. “Dark, Cold, and Noisy: Constraining Secluded Hidden Sectors with Gravitational Waves”. In: *JCAP* 07 (2019), p. 007. DOI: 10.1088/1475-7516/2019/07/007. arXiv: 1811.11175 [hep-ph].

[149] Tommi Alanne et al. “A fresh look at the gravitational-wave signal from cosmological phase transitions”. In: *JHEP* 03 (2020), p. 004. DOI: 10.1007/JHEP03(2020)004. arXiv: 1909.11356 [hep-ph].

[150] Kai Schmitz. “New Sensitivity Curves for Gravitational-Wave Signals from Cosmological Phase Transitions”. In: *JHEP* 01 (2021), p. 097. DOI: 10.1007/JHEP01(2021)097. arXiv: 2002.04615 [hep-ph].

[151] Kai Schmitz. “LISA Sensitivity to Gravitational Waves from Sound Waves”. In: *Symmetry* 12.9 (2020), p. 1477. DOI: 10.3390/sym12091477. arXiv: 2005.10789 [hep-ph].

[152] Eric Thrane and Joseph D. Romano. “Sensitivity curves for searches for gravitational-wave backgrounds”. In: *Phys. Rev. D* 88.12 (2013), p. 124032. DOI: 10.1103/PhysRevD.88.124032. arXiv: 1310.5300 [astro-ph.IM].

[153] Michela D’Onofrio, Kari Rummukainen, and Anders Tranberg. “Sphaleron Rate in the Minimal Standard Model”. In: *Phys. Rev. Lett.* 113.14 (2014), p. 141602. DOI: 10.1103/PhysRevLett.113.141602. arXiv: 1404.3565 [hep-ph].

[154] James M. Cline, Kimmo Kainulainen, and Michael Trott. “Electroweak Baryogenesis in Two Higgs Doublet Models and B meson anomalies”. In: *JHEP* 11 (2011), p. 089. DOI: 10.1007/JHEP11(2011)089. arXiv: 1107.3559 [hep-ph].

[155] Antonio Riotto. “Towards a nonequilibrium quantum field theory approach to electroweak baryogenesis”. In: *Phys. Rev.* D53 (1996), pp. 5834–5841. DOI: 10.1103/PhysRevD.53.5834. arXiv: hep-ph/9510271 [hep-ph].

[156] A. Riotto. “Supersymmetric electroweak baryogenesis, nonequilibrium field theory and quantum Boltzmann equations”. In: *Nucl. Phys.* B518 (1998), pp. 339–360. DOI: 10.1016/S0550-3213(98)00159-X. arXiv: hep-ph/9712221 [hep-ph].

[157] Kimmo Kainulainen et al. “First principle derivation of semiclassical force for electroweak baryogenesis”. In: *JHEP* 06 (2001), p. 031. DOI: 10.1088/1126-6708/2001/06/031. arXiv: hep-ph/0105295 [hep-ph].

[158] Kimmo Kainulainen et al. “Semiclassical force for electroweak baryogenesis: Three-dimensional derivation”. In: *Phys. Rev.* D66 (2002), p. 043502. DOI: 10.1103/PhysRevD.66.043502. arXiv: hep-ph/0202177 [hep-ph].

[159] Tomislav Prokopec, Michael G. Schmidt, and Steffen Weinstock. “Transport equations for chiral fermions to order h bar and electroweak baryogenesis. Part 1”. In: *Annals Phys.* 314 (2004), pp. 208–265. DOI: 10.1016/j.aop.2004.06.002. arXiv: hep-ph/0312110 [hep-ph].

[160] Tomislav Prokopec, Michael G. Schmidt, and Steffen Weinstock. “Transport equations for chiral fermions to order h-bar and electroweak baryogenesis. Part II”. In: *Annals Phys.* 314 (2004), pp. 267–320. DOI: 10.1016/j.aop.2004.06.001. arXiv: hep-ph/0406140 [hep-ph].

[161] Henri Jukkala, Kimmo Kainulainen, and Olli Koskivaara. “Quantum transport and the phase space structure of the Wightman functions”. In: *JHEP* 01 (2020), p. 012. DOI: 10.1007/JHEP01(2020)012. arXiv: 1910.10979 [hep-th].

[162] Tomáš Brauner et al. “Dimensional reduction of the Standard Model coupled to a new singlet scalar field”. In: *JHEP* 03 (2017), p. 007. DOI: 10.1007/JHEP03(2017)007. arXiv: 1609.06230 [hep-ph].

[163] Kimmo Kainulainen et al. “On the validity of perturbative studies of the electroweak phase transition in the Two Higgs Doublet model”. In: *JHEP* 06 (2019), p. 075. DOI: 10.1007/JHEP06(2019)075. arXiv: 1904.01329 [hep-ph].

[164] Djuna Croon et al. “Theoretical uncertainties for cosmological first-order phase transitions”. In: (Sept. 2020). arXiv: 2009.10080 [hep-ph].

[165] Daniel Cutting, Mark Hindmarsh, and David J. Weir. “Vorticity, kinetic energy, and suppressed gravitational wave production in strong first order phase transitions”. In: *Phys. Rev. Lett.* 125.2 (2020), p. 021302. DOI: 10.1103/PhysRevLett.125.021302. arXiv: 1906.00480 [hep-ph].

[166] Daniel Cutting et al. “Gravitational waves from vacuum first order phase transitions II: from thin to thick walls”. In: (May 2020). arXiv: 2005.13537 [astro-ph.CO].